Trends in sediment geochemistry along the fluvial to marine transition of the Waihou River, Aotearoa New Zealand

A thesis

submitted in partial fulfilment

of the requirements for the degree

of

Master Of Science (Research) in Earth Science

at

The University of Waikato

by

Nicole Greaves

THE UNIVERSITY OF
WAIKATO
Te Whare Wānanga o Waikato

Year of submission

2025

Abstract

The nuances of the dynamic changes in the water chemistry and sediment deposition within the fluvial to marine transition zone (FMTZ) are difficult and time consuming to capture within water samples as due to the constantly changing nature. Marine water intrusion up rivers changes along short time scales of minutes, hours, and days to months and years. To be able to accurately capture the extent and changes that occur along the FMTZ would provide vital environmental and depositional information regarding river health, temporal variations and forming depositional environments. The use of geochemical sediment proxies as a measure of marine water intrusion upstream is an ongoing topic of research with many potential proxies investigated throughout literature. However, the identification of proxies that represent not only the general movement from fresh to brackish to marine conditions but can also be used to distinguish a gradient along river position as recording the finer changes in water chemistry have yet to be demonstrated within literature. This study aims to identify whether the dynamics of marine water intrusion are recorded through sediment geochemistry or physical properties along a gradient and to assess the uses for the proxies identified, creating an assemblage of proxies to be utilised within future study. Sediment proxies of grainsize, percentage mud (%mud), loss on ignition (LOI), strontium and barium ratios (Sr/Ba), carbon isotopes of delta thirteen carbon ($\delta^{13}C$) and carbon and nitrogen ratios (C/N), X-Ray diffraction (XRD) minerology, and X-ray fluorescence (XRF) elements, will be investigated as potential proxies for marine water intrusion up the FMTZ of the lower Waihou River, Aotearoa, New Zealand. This research finds that whilst varying levels of success were demonstrated within literature, many of the tested proxies fail to identify the fluvial to marine transition let alone distinguish a gradient of change through river position. Strontium/Barium ratios are the only proxy to identify a clear relationship with river distance, presenting with a weak to moderate relationship, finding a lack of small scale precision but the larger scale transition was observed. The carbon isotope results presented a negligible relationship but indicated it may have potential use as a proxy, which prompts the need for further study of the usage of this method as a proxy for marine water intrusion. Whilst this study does not claim to disregard the usefulness of these proxies nor their potential for identifying the

hydrodynamics of the FMTZ within the sediment, it does stand that little evidence of it has been found within this research and prompts the thorough investigation of the potential held by these proxies both within the Waihou River and various other river systems of varying size and type where processes vary. Consideration to the type of river environments literature seems to focus on is also prompted as to whether these proxies may only be viable under certain conditions.

Acknowledgements

Whilst there are many people to thank for their amazing contributions and support, I want to thank my supervisor Andrew LaCroix for all the guidance he has given me, his incredible patience, and his continuous support throughout this difficult process which kept me working towards the end goal and gave me the ability to find ways around the obstacles that occurred along the way.

The sample collection and data analysis for this project required a lot of time and effort, I would like to thank all of the University of Waikato staff and students that helped me with this process. Thank you to Annette Rogers and Kirsty Vincent who went above and beyond by teaching and helping me prepare samples, run analyses and process my data. I would also like to thank Holly Fergurson and Bonnie Lewis who acted as skippers, got up early and made themselves readily available so that my fieldwork was possible. Fellow Masters student Charlotte Blackler also deserves a thank you for the help and company given during fieldwork and continuous support and friendship throughout my masters.

Another massive thanks goes out to Sarah Bury, Josette Delgado, Olle Kerr-Hislop and Graeme Moss, from NIWA Wellington who prepped and ran the analysis for my Carbon isotope data, and also to Aihua Wang and team in China who processed my samples for strontium/ barium analysis.

Chris Eager and all members of the Waikato Regional Council who collected my control marine and fluvial samples (27 and 28) from the Firth of Thames and upriver near Te Aroha require a special thank you for their willingness to retrieve them, providing a baseline for all other results. Another thank you is directed to the Thame/Coromandel Council who provided a research grant to support me in the study I was undertaking.

Last but not least, I would like to thank my family and friends for their support and encouragement during this part of my life. Thank you to my parents, Jeanine and Stuart Greaves, who always supported me and showed me comfort and encouragement, providing me with the best conditions in which I could succeed. I will also thank my sister Dana who always had a side comment but would often stay up with me during

long writing sessions. To all of my friends who provided both support and understanding over thesis struggles as well as an escape from the stresses of studying, thank you for all the fun that broke up the seriousness.

Table of Contents

List of Figures

List of Tables

Chapter 1
Introduction and Literature Review

1.1 Introduction

The fluvial to marine transition (FMTZ) is located in the lower reaches of rivers flowing into the sea. This is one of the most complex sedimentary environments on earth, due to the interactions between river flow, waves, and tides, and their impact on sedimentation. It is important to understand these parts of sedimentary systems because their physico-chemical environmental conditions affect aquatic ecosystems (Dalrymple and Choi, 2007; Shchepetkina, 2019), deposit strata with economic importance (i.e., McMurray Formation, Canada; Mungaroo Fm, Australia) (La Croix et al., 2019; Jablonski & Dalrymple, 2016; Martinius et al., 2017), and control the geomorphic conditions along the world's coastlines (Dalrymple and Choi, 2007). Yet despite the vast number of studies investigating the physical (La Croix et al., 2015: La Croix et al., 2014), chemical (Dashtgard et al., 2022; Wang et al., 2021; Czarnecki et al., 2014; Coffey et al., 1997), and biological characteristics (Gringas et al., 2012; La Croix et al., 2015; Pospelova et al., 2008), our understanding of how sedimentary deposits link with position along the FMTZ remain in their infancy.

Dashtgard et al. (2022) carried out a study on the FMTZ of the Fraser River Delta, Canada, where proxies of strontium/barium ratios extracted with acetic acid (Sr/Ba-Hac) and ammonium acetate (Sr/Ba-NH_4Ac), delta thirteen carbon isotopic ratios ($\delta^{13}C_{org}$), carbon/nitrogen ratios (C/N) and relative and absolute abundances of dinocysts were measured and compared to distance extended up river from the river mouth (river km), and salinity. La Croix et al., (2015), also studied the Fraser River Delta in Canada, where proxies of $\delta^{13}C_{org}$ and neoichnology. Wang et al. (2021), outlined the Sr/Ba ratios as a proxy for marine water intrusion, as needing consideration regarding where the Sr and Ba is sourced from, and identified the importance of separating Sr/Ba through Sr/Ba-NH_4Ac or Sr/Ba-Hac rather than as an accumulation of all Sr and Ba

present. Though certain proxies are promising and there is a vast number of potential proxies (Czarnecki et al., 2014; Dashtgard et al., 2022, & Wang et al., 2021) further investigation is required to assess the suitability of the proxies for tracking marine water intrusion across the fluvial marine transition. Furthermore, a direct comparison between the proxies is needed to assess which proxy best represents the active marine water intrusion and how it interacts in a system with lower river flow and area.

Whilst these studies have looked at the differing array of options for potential proxies for marine water intrusion, no study attempts to use the proxies to identify whether the dynamics of marine water intrusion up a river is captured through the deposited sediment along the river gradient. In this study geochemical proxies of $\delta^{13}C_{org}$, C/N, X-ray diffraction (XRD) and X-ray fluorescence (XRF) and Sr/Ba, and physical property of grainsize and percent mud will be compared against distance and salinity within the lower portion of the Waihou river, New Zealand.

The goals of this study include:

1. To determine if marine water intrusion is recorded in the physical or geochemical characteristics of sediments across the gradient of the fluvial to marine transition zone of the lower Waihou River.
2. To test the application and range of usefulness of common proxies in a river environment to establish an assemblage of valuable proxies for future works to utilise and expand upon.

1.2 Processes in the FMTZ

1.2.1 Hydrodynamics of the Fluvial Marine Transition

The fluvial to marine transition zone (FMTZ) of deltas and estuaries has three major physical processes that affect sedimentation: tidal currents, river currents and waves (Dalrymple & Choi 2007). Tidal currents extend from the marine shelf landwards and increase in energy as a result of the narrowing and reduction of cross-channel area up-stream causing flow convergence. This amplification of tidal energy increases inland to

the point of the tidal maximum (Figure 1), the area of highest tidal current velocity, within the estuary or delta plain (Dalrymple and Choi, 2007). Beyond the tidal maximum, tidal energy wanes as a result of friction decreasing the tidal current speeds. The maximum extent of the tidal current inland is called the tidal limit (Dalrymple & Choi, 2007). Inland of the tidal limit the sedimentary environments are fluvial and there are no current variations from tides. In the seaward region of the FMTZ waves can contribute to the energy present in the delta/estuary though the influence is often minimal. Wave energy increases as the water depth decreases and is the highest at the mouth, moving landwards. The influence of waves reduces as friction increases within the seaward region of the estuary or delta (Dalrymple &Choi, 2007). Tidally influenced rivers can experience flow reversal during periods of higher tidal influence (flood tides) or periods of low river discharge, where the direction of flow moves from seaward in the fluvial portion to becoming landward in the brackish ones (Dalrymple &Choi, 2007). In the fluvial dominant section of the river the net direction of flow and sediment transport is seaward, however in the lower portion of the transition zone flow can vary in direction depending on the strength of tidal and fluvial currents. Due to the narrowing of tidal currents and waves increasing the landward directed energy the tidal section often has a landward movement of bedload sediment (Dalrymple & Choi, 2007). This results in bedload convergence between the seaward and landward moving bedloads, for deltas this tends to be nearer to the river mouth due to higher fluvial output compared to estuaries where it is often found near the middle of the estuary.

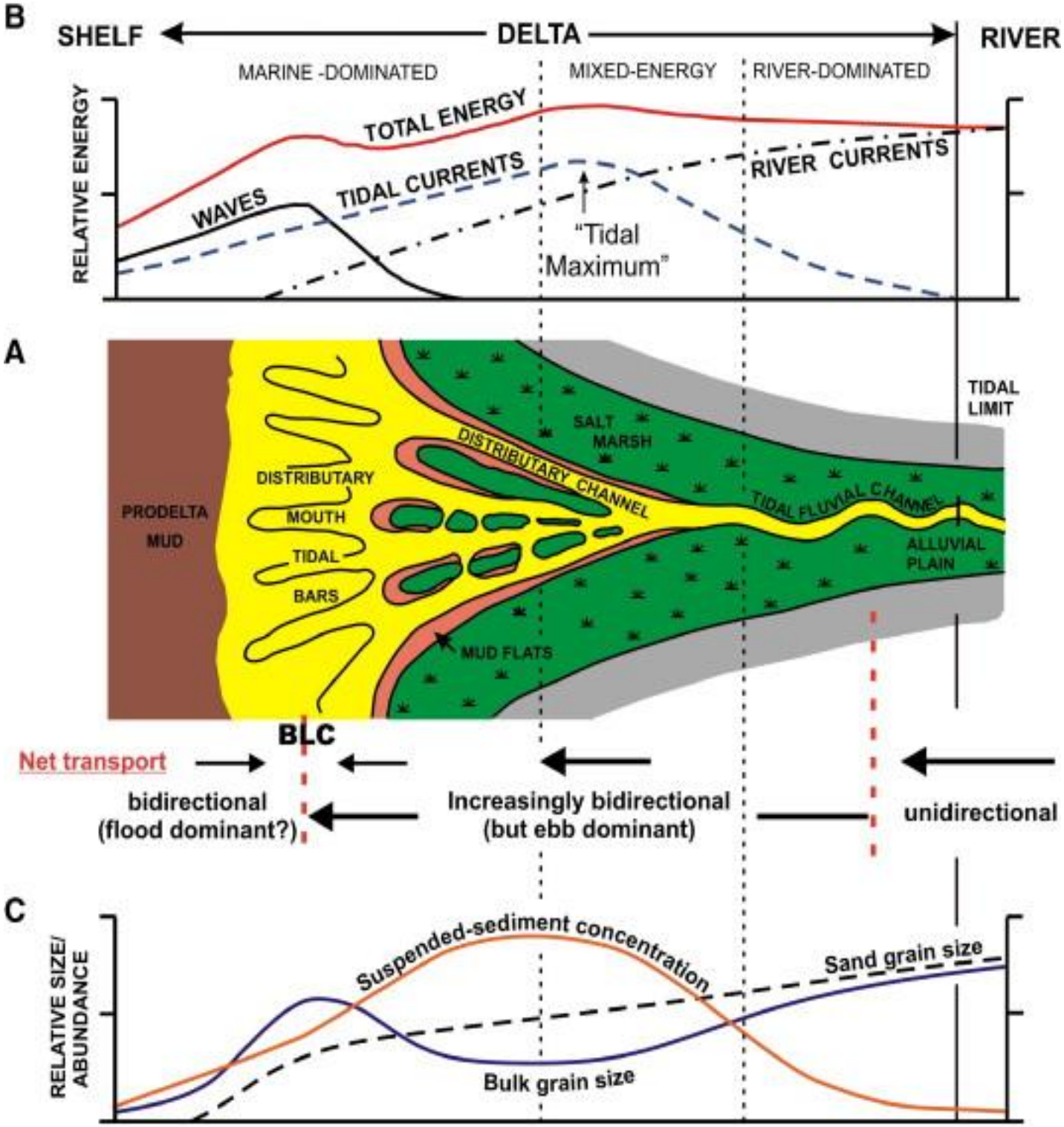

Figure 1.Processes across a tide dominated delta system. (A) Diagram of FMTZ geomorphology. (B) Energy distribution through the FMTZ as well as energy patterns of the tidal currents, river currents and waves. (C) Grainsize distribution across the FMTZ. (Cited from Dalrymple &Choi, 2007.

Due to mixing between fresh seaward flowing river currents and salty/marine landward flowing tidal currents a mixing zone is formed, referred to as the turbidity maximum zone (TMZ) (Dalrymple &Choi, 2007). The TMZ is a dynamic area characterised by an increase in suspended sediment concentration located within the zone of mixing in the FMTZ, positioned in the central region of the transition. The location of the TMZ can vary along a single delta or estuary, during periods of high river discharge the TMZ moves seaward through the estuary or delta (Dalrymple &Choi, 2007). Suspended sediment within the TMZ experiences high levels of flocculation as a result of ions in the water bonding with the suspended sediment. Flocculation increases in brackish water at salinity levels between 1-10‰ but can occur at any location between the tidal limit and a salinity of 20‰. The flocs of sediment proceed to settle in the turbid areas of mixing, which increases the deposition of finer gained sediments within this zone (Dalrymple &Choi, 2007). During periods of higher flow rates, the flocs are less likely to settle and have higher chance at being separated by the current. Lower flow rates fail to suspend the flocs and result in the deposition of the finer grained sediment within the turbidity maximum zone whist the courser grained sediment is less predominant (Dalrymple &Choi, 2007). Spring tides produce higher tidal currents and resultantly increase the mud particles in suspension creating increased flocculation and once currents decrease, higher floc deposition. It has been documented that the presence of a turbidity maximum can be dependent on the spring tides in certain systems (Wolanski et al., 1995).

As a result of the mixing of fresh and marine water, in addition to the seaward to landward horizontal gradient observed, the interaction also influences the vertical gradient in the water column. Often, vertical variation within the zone of brackish water is homogenised in tidally dominated systems due to high turbulence from high river and tidal currents (Dalrymple & Choi, 2007). The mixing of saltwater and freshwater depends on the proportion of salt water compared to the amount of fresh water that is present. If the river currents are higher and tidal currents are lower, density stratification can develop in the water column resulting in the surface containing seaward flowing fresh water and flow at the bed containing landward flowing salt water. This forms the presence of a salt wedge (Dalrymple & Choi, 2007; Geyer & Farmer, 1989; McKeon et.

al., 2020). The intrusion distance of the salt wedge decreases with increased river current volume but stratification between salinities will increase (Dalrymple & Choi, 2007; McKeon et. al., 2020).

1.2.2 Deposits

Due to the dynamic and complex nature of the FMTZ a variety of deposits can be identified as a product of the interaction between fluvial and marine water. The energy gradient across the FMTZ (Figure 1) results in various depositional environments which may produce varied deposits and structures. Finer grainsizes are often carried as suspended sediment within the water column whereas the courser material is transported as the bedload, as a result the sand grainsizes are transported via the bedload opposed to the finer suspended silt and clay grainsizes (Dalrymple &Choi, 2007). The increase in energy and brackish conditions initiating flocculation in the TMZ lends the zone to mud deposition from the suspended sediment rather than sand from the bedload, producing central FMTZ mud deposits (Dalrymple &Choi, 2007; La Croix and Dashtgard, 2014). The sand is deposited in the less brackish, fluvially dominant and tidally dominant zones upstream and downstream of the TMZ from the bedload (Dalrymple &Choi, 2007). La Croix and Dashtgard (2014) found that in the Fraser River, Canada, upriver samples near the tidal limit had 100% sand present but had the percentage of mud present gradually increase as the samples were taken down stream to a maximum of 88%, 28km from the river mouth. From the maximum, the mud percentage gradually decreased seaward dropping to 14% at the most seaward sample at river kilometre 10 (La Croix and Dashtgard, 2014).

1.3 Proxies for marine intrusion across the FMTZ

Various methods of determining a proxy for sediment deposition across the fluvial to marine transition that accurately depicts the environmental conditions at the time of deposition have been proposed in literature. The methods include biological, chemical and physical components as a basis for accurately representing the complex environment. Biological methods include neoichnology/ichnology, dinoflagellate cyst abundance (Gingras et al., 2012; La Croix et al., 2015; Czarnecki et al., 2014; Dashtgard et al., 2022). Chemical proxies investigated include $\delta^{13}C_{org}$ (carbon isotopes), carbon

nitrogen ratios (C/N), Strontium Barium ratios (Ba/Sr), which look at the geochemical properties of the deposited sediments (Czarnecki et al., 2014, Wang et al., 2021, & Dashtgard et al. 2022).

1.3.1 Biological Proxies

The array of trace fossils presents, and the various defining features such as fossil size, type and diversity observed can allude to the depositional position in the FMTZ and to the presence of brackish water (Gringas et al., 2012). La Croix et al. (2015) found that in the Fraser River Delta, Canada, neoichnology revealed basic trends through the major zones of the FMTZ. The study found that on a regional scale the abundance of bioturbation is high in brackish water influenced settings, with the highest bioturbation in the most seaward parts of the delta. The intensity and abundance of bioturbation decrease as the FMTZ becomes more fresh water, the highest abundance is in the marine section of the study area and also spikes for a short distance of the turbidity maximum (La Croix et al., 2015). In the fully freshwater section bioturbation was low in abundance, intensity and variability. The burrow distribution also decreased with decreasing salinity (La Croix et al., 2015).

1.3.2 Chemical Proxies

Thornton & McManus (1994), Czarneki et al. (2014), and Dashtgard et al. (2022) used geochemistry as an indicator of depositional position along a FMTZ. These three studies used the carbon stable isotopes of organic matter within the transition zone to link deposits with the FMTZ. The organics based geochemical proxies for depositional position include $\delta^{13}C$ (Thornton & Mcmanus,1994; Czarneki et al., 2014 & Dashtgard et al., 2022), C/N (carbon nitrogen ratio) (Thornton & Mcmanus,1994 & Dashtgard et al., 2022) and $\delta^{15}N$ ratios. The $\delta^{13}C$ values are used to identify the sources of the carbon detected which can as a result potentially provide insight on marine water intrusion. Terrestrial carbon sources have two common categories C4 plants and C3 plants, C4 plants are usually grasses whereas C3 plants include most tree styled vegetation e.g.

Mangrove leaves or pine needles (Meyers, 1994). Marine sources of carbon tend to come from algae and phytoplankton, which produces differing values. Higher values of $\delta^{13}C$, -10 to -15 ‰ indicates the organic matter originated from terrestrial C4 plants, values around -18‰ to-22‰ indicate a marine source of organic matter, around -27‰ or a range of -23‰ to -34‰ is for C3 plants (Meyers, 1994; Czarneki et al., 2014; Han et al., 2020). A high C/N ratio indicates a terrestrial origin, and a low suggests marine carbon sources (Meyers, 1994). The C/N ratio from Thornton & McManus, (1994) had multiple inconsistencies with the $\delta^{13}C$ results and indicated potential occurrence of diagenetic alteration which influenced the results in an unreliable way so the C/N results could not be used to establish positions in the FMTZ (Thornton & Mcmanus,1994). A similar situation occurred with the $\delta^{15}N$ ratios as the results were seemingly influenced by diagenetic alteration (Thornton & Mcmanus,1994). The $\delta^{15}N$ proxies need to be blank corrected as when analysed, atmospheric N_2 can interfere and produce less reliable results (Langel & Dyckmans, 2017). Both $\delta^{15}N$ and C/N ratios have potential value for identifying depositional position in the FMTZ however they may not be the best suited as the measures record both organic matter and any diagenetic alterations that can occur. Dashtgard et al. (2022), found no significant variation or correlation in the C/N ratio with depositional position or salinity. Regardless of the lack of significant results from the C/N and $\delta^{15}N$, the $\delta^{13}C$ ratios showed an increase in value from the minimum of -26.55‰ upstream of the Fraser River, Canada, to the maximum -21.08‰ in the Strait of Georgia (Czarneki et al., 2014). Terrestrial sources of organic material were dominant over the marine sources with the entire river classified as deriving from a terrestrial source (Czarneki et al., 2014). Thornton & McManus (1994) also experienced a seaward increase in $\delta^{13}C$ values as Czarneki et al. (2014) did, and found the upstream section of the Tay Estuary defined by terrestrial organic matter which decreased downstream within the FMZT, and marine organic matter increased in the lower estuary. Dashtgard et al. (2022), also shows an increase in $\delta^{13}C$ towards the delta from upstream with a large rapid increase at ~60km upstream, however there is low correlation in the river portion and negligible correlation in the delta. Salinity has a trend with $\delta^{13}C$ in sections SG1- 5 but not in SG6.

Barium has a wide ionic radius and is a cation with as +2 charge which makes it less mobile and more susceptible to ionic exchange reactions. As a result, Ba^{+2} in the environment will be absorbed by organic matter, clays, and minerals found in riverine or terrestrial environments, and so is found less in marine environments (Wang et al., 2021). When entering the mixing zone, fluvial water with barium bonded particles interacts with the increased salinity resulting in the barium dispersing back into the water as the bonds with the particles separate (Coffey, et al., 1997). When barium comes into contact with marine salt water, the sulphate (SO_4^{-2}) anions draw the barium into forming an ionic bond, creating barium sulphate ($BaSO_4$) which is an insoluble salt and so it does not dissolve in water and instead it precipitates out leaving little barium present in marine settings. Strontium, however, is more mobile and has a smaller ionic radius, therefore it doesn't form the ionic bonds as readily as barium and can be transported to and be abundant in marine water. This creates a high marine strontium level compared to barium which is low in marine water yet higher in fresh water. So, the ratio between strontium and barium indicates the proportion of marine water and salinity, to freshwater present. (Wang et al., 2021, Sharma et al., 2025).

Sr/Ba ratios as a proxy for depositional position was proposed and showed promising results when extracted with acetic acid (Hac) or ammonium acetate (NH_4Ac). Dashtgard et al (2022), used this method of Sr/Ba ratio for depositional position along the Fraser River. The Sr/Ba ratios correlate well with salinity, with the acetic acid Sr/Ba ratio the best across the FMTZ and was the most accurate proxy tested (Dashtgard et al., 2022). However, with the Sr/Ba proxy it is important to confirm lower values are correct and not the result of the proxy being influenced by other sediment factors (Dashtgard et al., 2022). While these studies have identified and assessed the proxy's' ability to discern saltwater intrusion across FMTZs, the information regarding whether sediment geochemical proxies can record the details of rapidly changing dynamics of marine water intrusion along the FMTZ gradient is still lacking.

1.4 Waihou River

1.4.1. Hauraki Rift and Regional Setting

Waihou River flows through the 200 – 250km long active Hauraki Rift, which consists of the Hauraki depression, the Firth of Thames and the Gulf of Hauraki. The Hauraki Rift system is approximately 25km wide and extends from the edge of the Hauraki Gulf inland to the Taupō Volcanic Zone (Figure 2) (Hochstein & Nixon, 1979, Hochstein et al., 1986, De Lange, & Lowe,1991, Persaud, et al., 2016). Within the rift is a half graben, median horst and a fault angled depression in sequence from east to west, as well as containing two major normal faults of the Kerepehi Fault and Hauraki Faults which both strike in a NNW direction. The Hauraki Fault is no longer active and is located along the eastern side at the base of the Kaimai Ranges. The Kerepehi fault is still considered active and is located more centrally to the rift depression (Figure 3). There are various other faults within the rift, including one of note, the Thames Fault which is a minor hinge fault that extends down the western edge of the Hauraki Rift (Figure 3) (Hochstein & Nixon, 1979, De Lange, & Lowe,1991, Persaud, et. al., 2016).

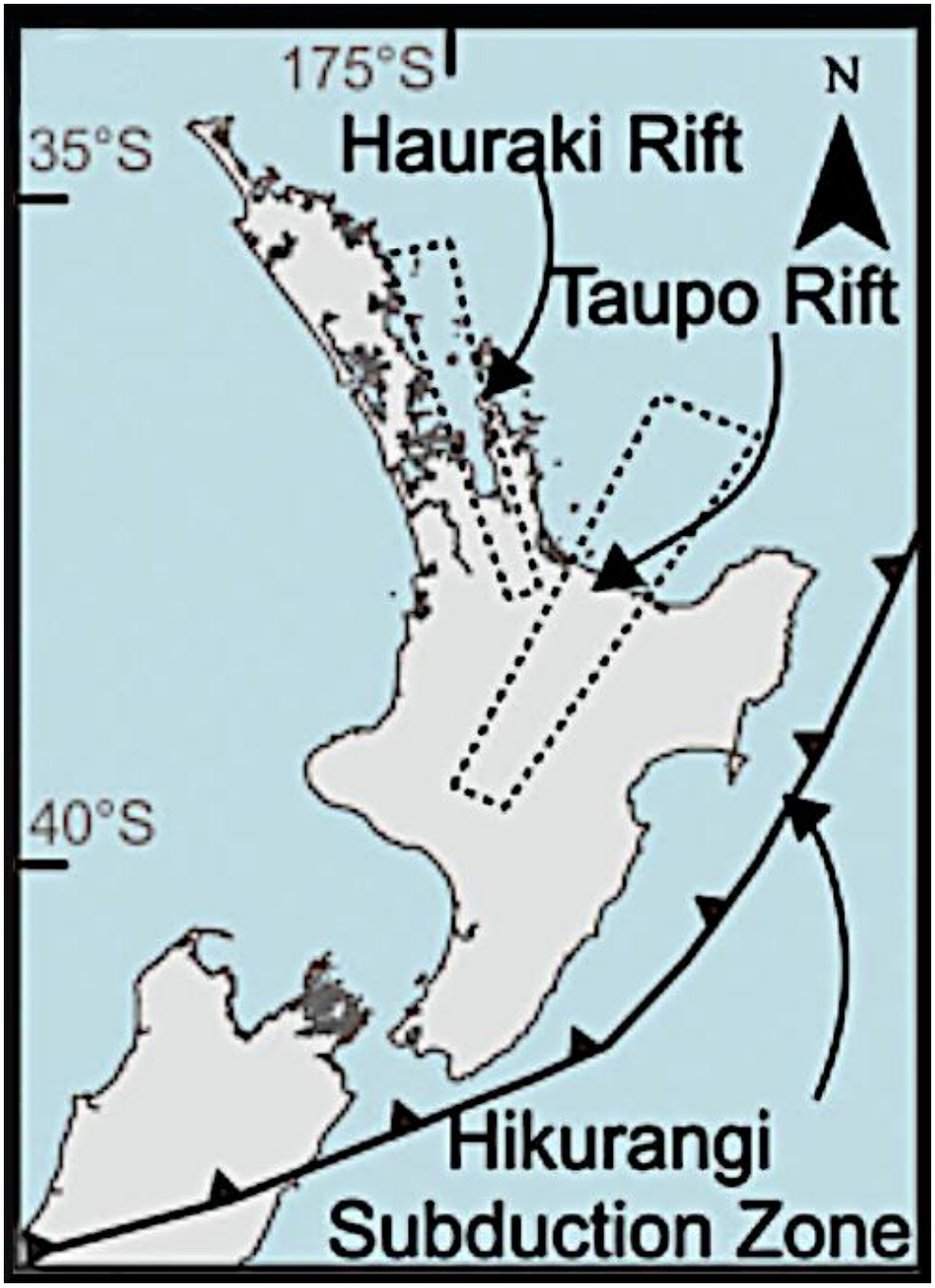

Figure 2.Hauraki Rift location and approximate area, image sourced from Persaud et. al, 2016.

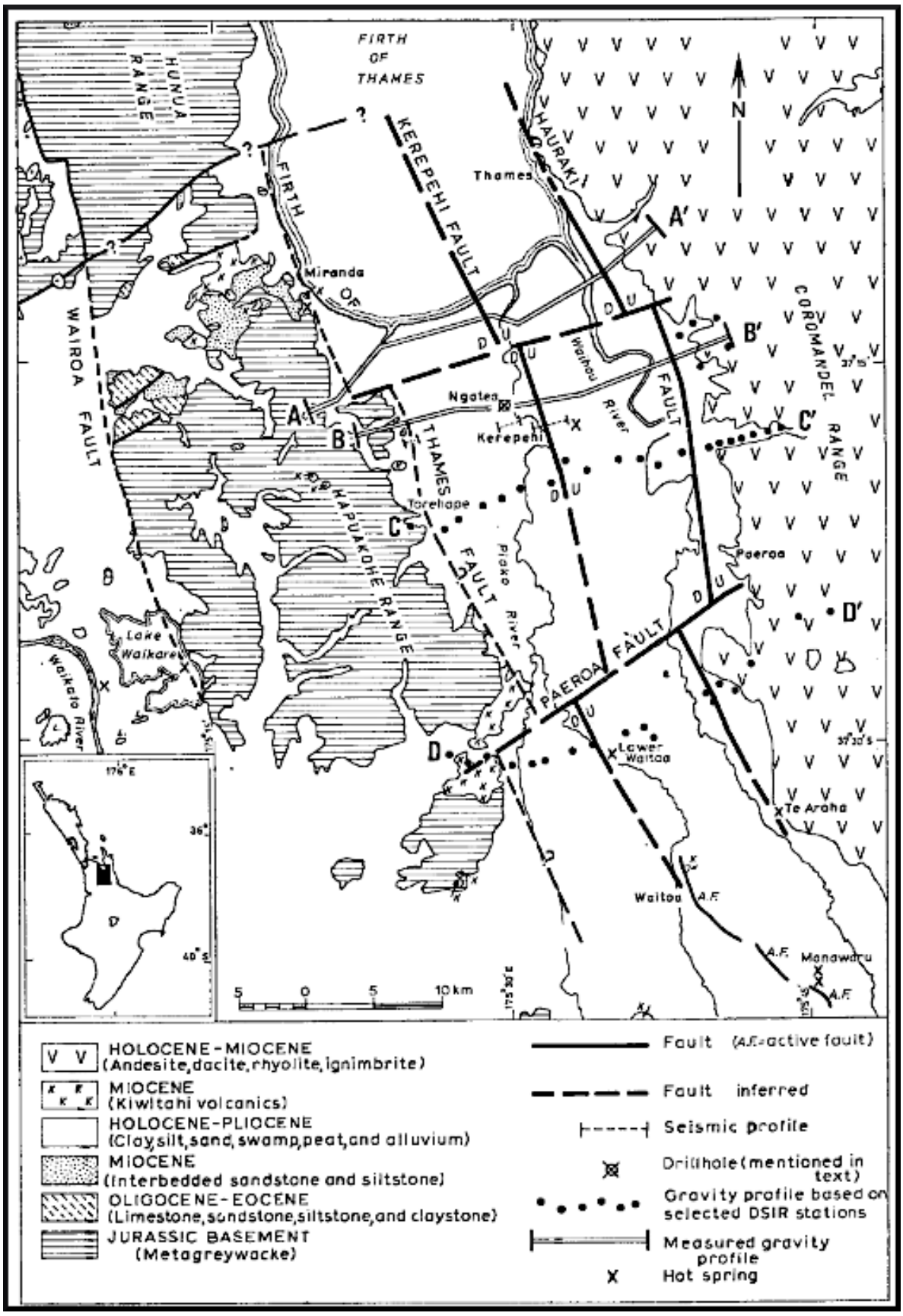

Figure 3. Geology and major faults of the Hauraki Rift, image sourced from Hochstein & Nixon, 1979.

The Hauraki Rift is confined by Jurassic metagreywacke in the Hunua Range and Hapuakohe Range to the west and Miocene andesite/dacite in the Coromandel Ranges to the east (Figure 3). Tertiary and Quaternary sediment from terrestrial origin has infilled the rift structure up to 3km and 0.7km in depth, respectively (Hochstein et al. 1986; Hochstein & Nixon, 1979; De Lange, & Lowe,1991; Persaud, et. al., 2016; Naish et al. 1993). In the Pleistocene, ignimbrites such as the Mamaku Plateau Formation/Mamaku Ignimbrite were deposited in the surrounding ranges and over the southern edge of the Hauraki Rift system (Hochstein & Ballance 1993; Leonard et. al., 2010; Persaud, et. al., 2016). The latest deposited Tertiary-Quaternary sediments in the rift system comprise the Hinuera Formation (volcanoclastic alluvium), estuarine/deltaic sediment and reworked local sediments (De Lange, & Lowe,1991; Hochstein & Nixon, 1979). Recent sediment deposition in the Hauraki Rift has been largely from alluvial and marine sources depositing during the Holocene as a result of the river systems throughout the rift and through marine transgression as sea level increased in relation to the land (Newnham et. al., 1995). Marine transgression occurred in the mid Holocene which was followed by progradation due to volcanoclastic mud deposition from the Waihou, Waitoa and Piako rivers (Newnham et al., 1995; Naish et al., 1993). The shoreline of the Hauraki plains increased 13km north into the Firth of Thames (Naish et al., 1993).

1.4.2 The Firth of Thames and the Waihou River

The Firth of Thames (FOT) is positioned within a central portion of the Hauraki Rift Valley and is the end destination for a large portion of the Hauraki catchment (McLeod et al. 2011). The FOT is a shallow marine meso-tidal estuarine embayment that has depths up to 35m, with an area of ~800km^2 and a total catchment area of 4194km^2 (Land Air Water Aotearoa, n.d-a; McLeod et al. 2011; Swales et al, 2007; Naish et al., 1993). Rivers such as the Waihou, Kauaeranga and Piako outlet into the southern Firth of Thames. The main body of the Waihou River runs from the western edge of the Mamaku Plateau, west of the Kaimai Ranges and through the Hauraki Plains as it flows northwest to its outlet into the Firth of Thames (Land Air Water Aotearoa, n.d-a). The Waihou River is 186 km in

length (Land Air Water Aotearoa, n.d-b) and stretches from its source of the Blue Springs in New Zealand's central North Island to its outlet in the Firth of Thames. The Blue Springs is located near to the township of Putaruru and the Waihou, travels past many towns such as Te Aroha, Paeroa, Turua and Thames. The catchment area of the Waihou River is 1977 km^2 (Land Air Water Aotearoa, n.d-b) and contains land uses of mainly pasture and areas of forest, both native and plantation. The catchment topography ranges from steep slopes to flat plains, with some tributaries moving through the Kaimai Ranges before entering the Waihou River (Land Air Water Aotearoa, n.d-c). The Waihou River has many tributaries which have an accumulated length of 2945km (Land Air Water Aotearoa, n.d-b). Some tributaries include the Ohinemuri River, the largest tributary, Tui Stream (Webster 1995), Puriri River, Hikutaia River and Kamata River (Speirs, 2001).

The Firth of Thames had ~10 m of mud deposited within the Holocene (Naish et al., 1993; Swales et al., 2007). Naish et al. (1993) collected sediment cores from the Firth of Thames and found that the offshore cores contained massive clayey silt/silty clay muds with occasional shell layers with bioturbation evident. Cores taken closer to shore showed similar properties with massive muds but had more established interbedded shell and sand layers and coarsened upwards in the top layers, with sand/gravel present (Naish et al., 1993). The muds were primarily halloysite, smectite and volcanic glass, with quarts, feldspars, carbonates, volcanic rock fragments, organic material and allophane also present in smaller quantities (Naish et al., 1993). The volcanic rock fragments were composed of andesite, ignimbrite and rhyolite, which has similarities to the surrounding geology of the region. Naish et al. (1993) also compared the surface sediments 0-0.2m from the Firth of Thames to sediments collected up stream of the major rivers outletting into the FOT (Figure 4). The river sediments consisted of volcanic glass, ignimbrite, rhyolite and andesite rock fragments, quarts, feldspar, pumice and clay minerals (allophane and halloysite). The averaged Firth of Thames samples showed similar compositions with the addition of skeletal carbonates present (Figure 4). Naish et al (1993) acknowledged similarities between the current surface sediments and the massive mud cores composition.

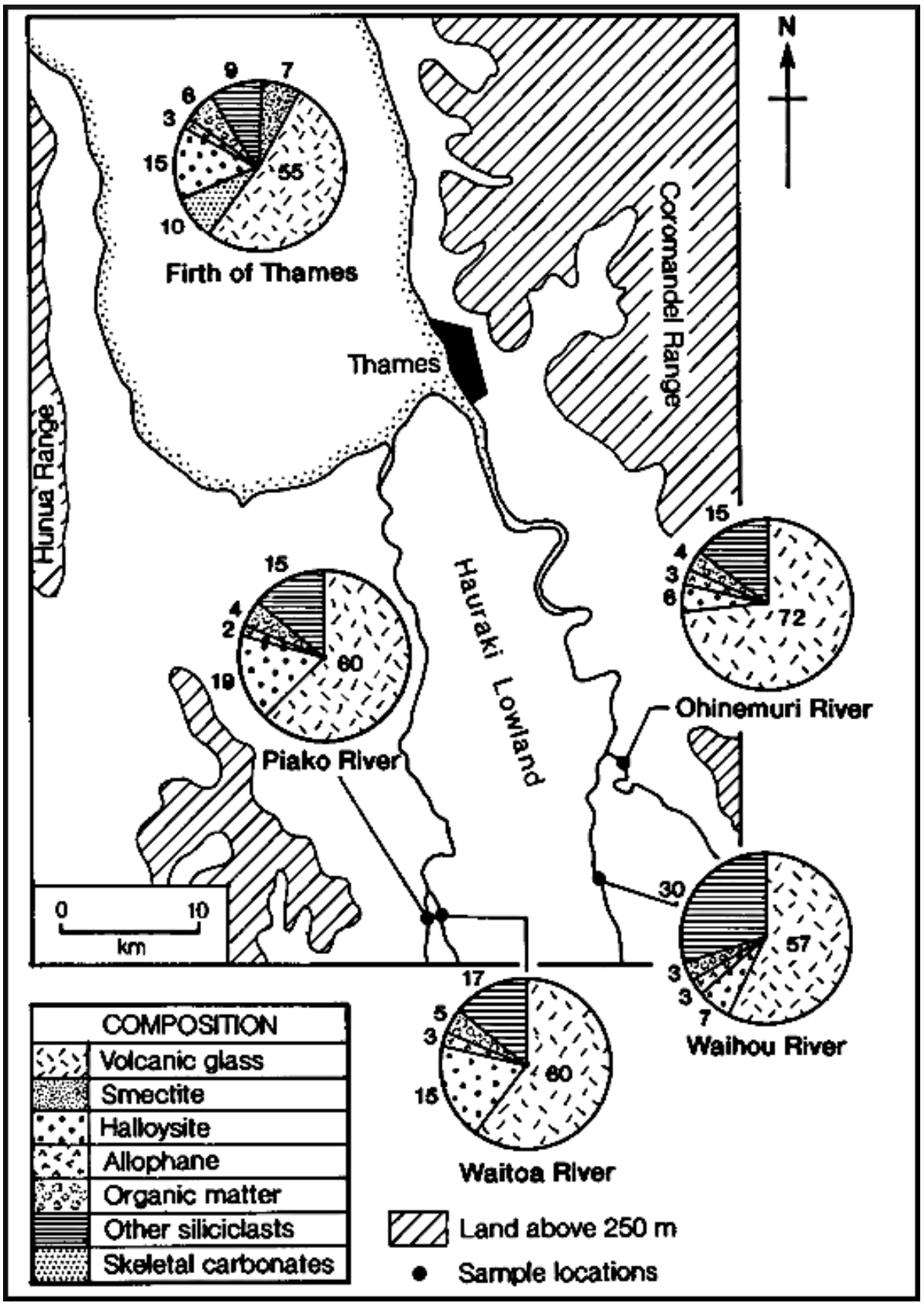

Figure 4. Bulk sediment composition of the Waihou, Piako, Ohinemuri and Waitoa rivers upstream of marine influence and averaged sediment composition of Firth of Thames (Cited from Naish et al., 1993).

Roche (2022) explored the deposition of mud within the lower Waihou river. Five sites were established along the FMTZ, both surface sediment and sediment cores were collected. Samples of surface mud deposits were collected using a ponar style grab sampler. Results indicated that 3 of the 5 sites had a significant proportion of mud and that the majority of mud deposits followed along either side of the channel with some deposits extending into the middle of the channel (Figure5). A mean proportion of mud was calculated for each site area, the proportions were 44.65%, 47.87%, 50.48%, 36.49% and 34.93% for sites 1,2,3,4, and 5 respectively (Roche, 2022). A total of seven sedimentary packages were identified across the fluvial to marine transition zone, 2 sand facies, both of which occurred in all sediment cores, one cross bedded and deposited in turbulent flow conditions and the other a structureless sand deposited during a period of rapidly decreasing flow. (Roche, 2022). Five mud facies were identified, a thin structureless mud, a thick structureless mud, normally graded mud facies, a cross-laminated mud with muddy ripples and a cross laminated mud with sandy laminations (Roche, 2022). Site 3 is the only site where the core had all 5 mud facies present, the cores proceeded to decrease in muds present both seaward and landward. The mud deposition across the FMTZ in the Waihou River was highest in the middle of the study area at site 3. Roche (2022) estimated the TMZ to be positioned in the vicinity of site 3 (approximately 8-9 km from the river mouth).

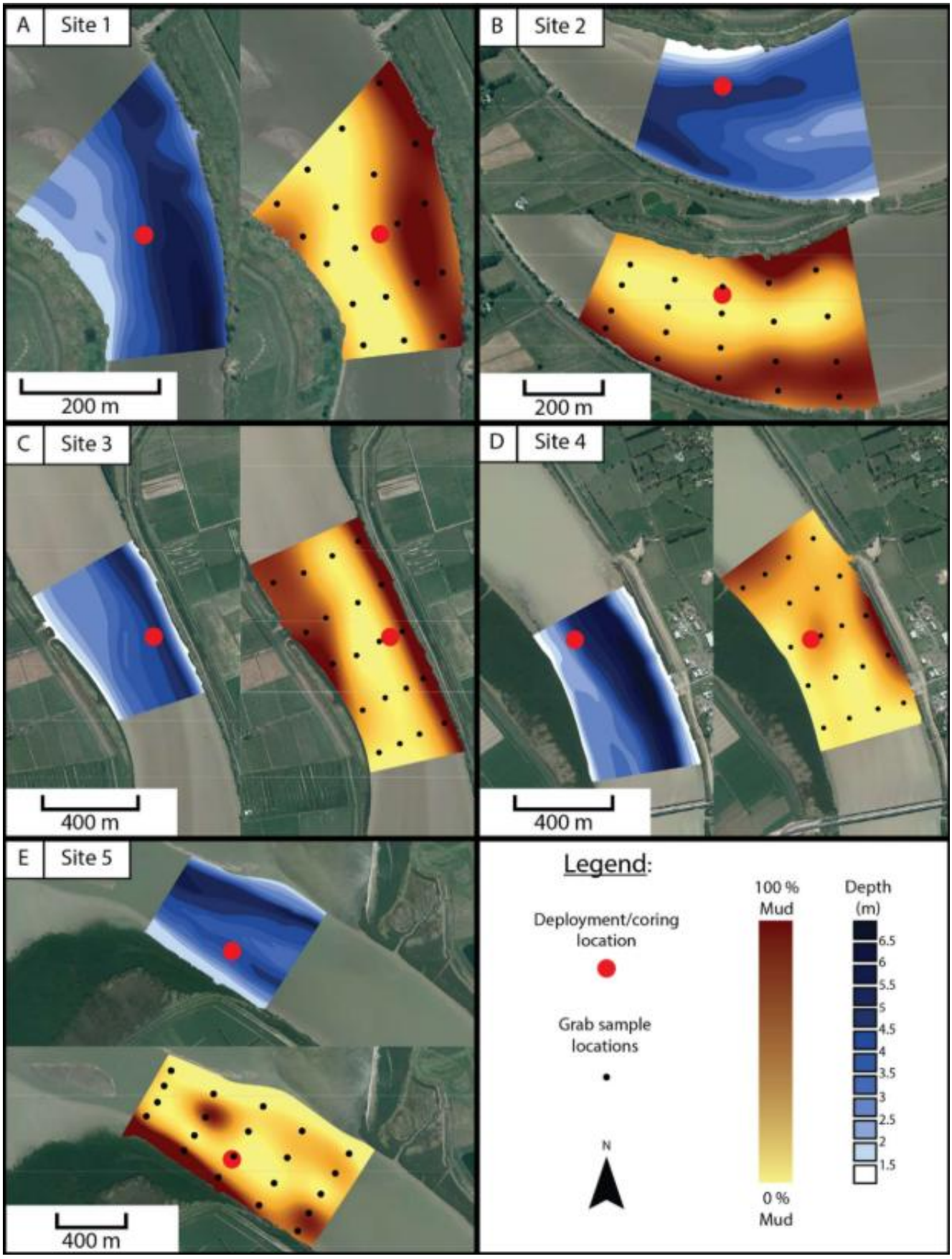

Figure 5. Distribution of mud proportion and bathymetry across 5 sites along the Waihou river FMTZ (Cited from Roche, 2022).

1.4.4 Mining history in the Waihou River catchment

In the 1850's the presence of alluvial gold was detected in the Coromandel region resulting in a gold rush which led to the identification of quartz reef gold in Thames and Coromandel. Coromandel and Thames goldfields were founded in 1862 and 1867 respectively (Clement et al., 2017), and contain bonanza grade gold which is high in the ratio of silver to gold (Simpson et al., 2011). Further expansion of the goldfields occurred in 1875 when the Ohinemuri River goldfield was opened leading to another gold rush in the area with hundreds seeking claims (Clement et al., 2017). Once again there was a lack of alluvial gold in the region, but reef gold was discovered in Waitekauri Valley, Owharoa, Waihi, and Karangahake (Clement et al., 2017). In 1899, due to the difficulty of extracting the gold it led to a method which uses cyanide to separate the gold from the rock which became used in Karangahake (Clement et al., 2017).

The Waihou River tributaries of the Ohinemuri River and Tui Stream have been largely contaminated by past mining activities and tailing remains resulting in high amounts of trace metals in the water. Water samples from near the upper Tui Stream tailings dam had high acidity and metals such as lead, zinc, copper, iron, manganese and arsenic present in excess, with amounts reducing towards the join with the Waihou River (Webster, 1995). The Ohinemuri River was also found to have detectable manganese, copper and zinc with no detectable lead and a neutral pH. Water in the lower Waihou River within the estuary found reasonably high levels of acid-soluble particulate metals including iron, manganese, copper, lead, and zinc as well as dissolved arsenic (Webster, 1995). High levels were also detected beyond the river estuary in sea water from neighbouring Tararu Beach with most metal concentrations the same as or slightly less than levels within the lower Waihou River (Webster, 1995).

Further metal or elemental analysis of the Waihou River has been limited since the study by Webster, (1995), and there are also gaps in information regarding the current river sediments being deposited and if they are influenced by past mining activity. High levels of metals within the water could be of interest for this study as XRF analysis will be undertaken as a means of identifying proxies. There are limited examples of using element abundance without comparisons, such as Sr/Ba, as potential proxies for marine water intrusion however that does not eliminate the possibility of a correlation.

The levels of elements found within the Waihou river sediment will also be reported within this study to provide a comparative figure to what Webster (1995) found, to investigate if the riverbed sediment shows similar results to provide a record for potential use in environmental monitoring or ecological health in further studies.

1.5 References

Clement, A. J. H., Nováková, T., Hudson-Edwards, K. A., Fuller, I. C., Macklin, M. G., Fox, E. G., & Zapico, I. (2017). The environmental and geomorphological impacts of historical gold mining in the Ohinemuri and Waihou river catchments, Coromandel, New Zealand. *Geomorphology*, *295*. https://doi.org/10.1016/j.geomorph.2017.06.011

Coffey, M., Dehairs, F., Collette, O., Luther, G., Church, T. and Jickells, T. (1997). The Behaviour of Dissolved Barium in Estuaries. *Estuarine, Coastal and Shelf Science. 45*, 113-121.

Czarnecki, J. M., Dashtgard, S. E., Pospelova, V., Mathewes, R. W., & MacEachern, J. A. (2014). Palynology and geochemistry of channel-margin sediments across the tidal-fluvial transition, lower Fraser River, Canada: Implications for the rock record. *Marine and Petroleum Geology*, *51*, 152-166. https://doi.org/10.1016/j.marpetgeo.2013.12.008

Dalrymple, R. W., & Choi, K. (2007). Morphologic and facies trends through the fluvial-marine transition in tide-dominated depositional systems: A schematic framework for environmental and sequence-stratigraphic interpretation. *Earth-Science Reviews*, *81*(3–4). https://doi.org/10.1016/j.earscirev.2006.10.002

Dashtgard, S. E., Wang, A., Pospelova, V., Wang, P.L., La Croix, A. & Ayranci, K. (2022). Salinity indicators in sediment through the fluvial-to-marine transition (Fraser River, Canada). Scientific Reports, 12. https://doi.org/10.1038/s41598-022-18466-4

De Lange, P. J. & Lowe, D. (1991). History of vertical displacement of Kerepehi Fault at Kopouatai bog, Hauraki Lowlands, New Zealand, since c.10 700 years ago. *New Zealand Journal of Geology and Geophysics*. *33*, 277-283. 10.1080/00288306.1990.10425685.

Geyer, W. R., & Farmer, D. M. (1989). Tide-Induced Variation of the Dynamics of a Salt Wedge Estuary. *Journal of Physical Oceanography*, *19*(8). https://doi.org/10.1175/1520-0485(1989)019<1060:tivotd>2.0.co;2

Gingras, M.K., MacEachern, J.A., Dashtgard, S.E., Zonneveld, J.-P., Schoengut, J., Ranger, M.J. and Pemberton, S.G., 2012. Estuaries. In: D. Knaust and R.G. Bromley (Editors), Trace Fossils as Indicators of Sedimentary Environments Elsevier, New York, pp. 463-505.

Hochstein, M. P. & Ballance, P.F. (1993). Hauraki Rift: A young, active, intra-continental rift in a back-arc setting. *South Pacific Sedimentary Basins*, *2*, 295-305.

Hochstein, M. P., & Nixon, M. (1979). Geophysical study of the Hauraki Depression, North Island, New Zealand. NZ. *Journal of Geology and Geophysics, 22*(1), 1-19.

Hochstein, M., Tearney, K., Rawson, S., Davey, F., Davidge, S., Henrys, S., & Backshall, D. (1986). Structure of the Hauraki Rift (New Zealand). Royal society of New Zealand bulletin, 24, 333-348.

Jablonski, B.V.J. & Dalrymple, R.W. (2016). Recognition of strong seasonality and climatic cyclicity in an ancient, fluvially dominated, tidally influenced point bar: middle McMurray Formation, Lower Steepbank River, north-eastern Alberta, Canada. Sedimentology, 63, 552-585.

La Croix, A. D., & Dashtgard, S. E. (2014). Of sand and mud: Sedimentological criteria for identifying the turbidity maximum zone in a tidally influenced river. *Sedimentology*, *61*(7), 1961-1981. https://doi.org/10.1111/sed.12126

La Croix, A. D., & Dashtgard, S. E. (2015). A synthesis of depositional trends in intertidal and upper subtidal sediments across the tidal-fluvial transition in the Fraser River, Canada. *Journal of Sedimentary Research*, *85*(6), 683-698. https://doi.org/10.2110/jsr.2015.47

La Croix, A. D., Dashtgard, S. E., & MacEachern, J. A. (2019). Using a modern analogue to interpret depositional position in ancient fluvial-tidal channels: Examples from the McMurray Formation, Canada. *Geoscience Frontiers*, *10*, 2219 – 2238.

Land Air Water Aotearoa. (n.d-a). *Firth of Thames*. *https://www.lawa.org.nz/explore-data/waikato-region/estuaries/firth-of-thames*

Land Air Water Aotearoa. (n.d-b). *Waihou River*. https://www.lawa.org.nz/explore-data/waikato-region/river-quality/waihou-river

Land Air Water Aotearoa. (n.d-c). *Waikato Region – Surface water zone: Waihou River at mouth*. https://www.lawa.org.nz/explore-data/waikato-region/water-quantity/surface-water-zones/waihou-river-at-mouth

Langel, R., Dyckmans, J. (2017) A closer look into the nitrogen blank in elemental analyser/isotope ratio mass spectrometry measurements. Rapid Communications in *Mass Spectrometry*, *31*(23): 2051-2055.

Leonard, G., Begg, J., Wilson, C., & Leonard, G. (2010). *Geology of the Rotorua area*. Institute of Geological & Nuclear Sciences 1:250 000 Geological Map 5.

Martinius, A. W., Fustic, M., Garner, D. L., Jablonski, B. V. J., Strobl, R. S., MacEachern, J. A., & Dashtgard, S. E. (2017). Reservoir characterisation and multiscale heterogeneity modelling of inclined heterolithic strata for bitumen-production forecasting, McMurray Formation, Corner, Alberta, Canada. *Marine and Petroleum Geology*, *82*, 336 – 361.

McKeon, M. A., Horner-Devine, A. R., & Giddings, S. N. (2020). Seasonal changes in structure and dynamics in an urbanized salt wedge estuary. *Estuaries and Coasts*, *44*, 589–607. https://doi.org/10.1007/s12237-020-00788-z

McLeod, I. M., Parsons, D. M., Morrison, M. A., Le Port, A., & Taylor, R. B. (2011). Factors affecting the recovery of soft-sediment mussel reefs in the Firth of Thames, New Zealand. *Marine and Freshwater Research*, *63*(1), 78. https://doi.org/10.1071/mf11083

Naish, T.R., Nelson, C. S. and Hodder, A. P. W. (1993). Evolution of Holocene sedimentary bentonite in a shallow marine embayment, Firth of Thames, New Zealand. *Marine Geology*, *109* (1993) 267-278.

Newnham, R. M., Delange, P. J., & Lowe, D. J. (1995). Holocene vegetation, climate and history of a raised bog complex, northern New-Zealand based on palynology, plant macrofossils and tephrochronology. *Holocene*, *5(*3), 267-282.

Persaud, M., Villamor, P., Berryman, K., Ries, W., Cousins, J., Litchfield, N., & Alloway, B. (2016). The Kerepehi Fault, Hauraki Rift, North Island, New Zealand: active fault characterisation and hazard. *New Zealand Journal of Geology and Geophysics*, *59*(1), 117–135. https://doi.org/10.1080/00288306.2015.1127826

Pospelova, V., de Vernal, A. and Pedersen, T.F. (2008). Distribution of Dinoflagellate Cysts in Surface Sediments from the Northeastern Pacific Ocean (43–25°N) in Relation to Sea-Surface Temperature, Salinity, Productivity and Coastal Upwelling. *Marine Micropaleontology*, *68*(1-2), 21-48.

Roche, B. (2022). Sedimentologic and hydrodynamic trends along a modern fluvial to marine transition zone: Mud deposition in the Lower Waihou River, Aotearoa-New Zealand [MSc Thesis]. https://hdl.handle.net/10289/15607

Sharma, S., Bolan, S., Mukherjee, S., Guilherme, L. R. G., Gomes Viana, D., Ferreira, A. D., Myrvang, M. B., Almås, A. R., Gjengedal, E. L. F., Cappuyns, V., Bueno Guerra, M. B., de Oliveira, C., Lamb, D., Siddique, K. H. M., & Bolan, N. (2025). Barium distribution, dynamics and fate in terrestrial and aquatic environments. *Environmental Research*, *287*. https://doi.org/10.1016/j.envres.2025.123059

Shchepetkina, A., Gingras, M. K., Mángano, M. G., & Buatois, L. A. (2019). Fluvio-tidal transition zone: Terminology, sedimentological and ichnological characteristics, and significance. *Earth-Science Reviews 192*, 214-235. https://doi.org/10.1016/j.earscirev.2019.03.001

Simpson, M., Mauk, J., & Merchant, R. (2011). *Bonanza-grade epithermal veins from the Coromandel and Thames districts, Hauraki Goldfield*.

Speirs, D. (2001). *The Diversity and Distribution of Freshwater Fish and their Habitat in the Major Rivers of the Waikato Region*. Environmental Waikato Technical Report, # 635256.

Thornton, S. F., & McManus, J. (1994). Application of organic-carbon and nitrogen stable-isotope and C/N ratios as source indicators of organic-matter provenance in estuarine systems – evidence from the Tay estuary, Scotland. *Estuarine Coastal and Shelf Science*, *38*(3), 219-233. https://doi.org/10.1006/ecss.1994.1015

Wang, A. H., Wang, Z. H., Liu, J. K., Xu, N., & Li, H. L. (2021). The Sr/Ba ratio response to salinity in clastic sediments of the Yangtze River Delta. *Chemical Geology*, *559*, Article 119923. https://doi.org/10.1016/j.chemgeo.2020.119923

Webster, J. G. (1995). Chemical processes affecting trace metal transport in the Waihou River and estuary, New Zealand. *New Zealand Journal of Marine and Freshwater Research*, *29*:4, 539-553.

Wolanski, E., King, K., and Galloway, D. (1995). Dynamics of the Turbidity Maximum in the Fly River Estuary, Papua New Guinea. *Estuarine, Coastal and Shelf Science, 40*, 321-337

Chapter 2

Research Study

2.1 Introduction

The fluvial to marine transition zone (FMTZ) has a dynamic mix of hydrodynamics, geochemistry and sedimentation. The study of the complex environments of the FMTZ provides insights to the geological and sea level variations of past and present shorelines over Earth's history and provide explanation to deposits produced in the FMTZ which are known stores of important natural resources (Gugliotta et al., 2016; Richards & Bhattacharya, 2018; Jablonski & Darlymple, 2016; La Croix et al., 2019). The sediment and water dynamics within the FMTZ vary greatly across the gradient producing a range of habitable environments for organisms vital to the local ecosystems. Understanding the relevant changes and variations in these zones gives insight to conditions which organisms can exist in while carrying out vital ecosystem services and show how these changes may influence the ecosystems, flora and fauna which exist in the FMTZ (Levin et al., 2001; Haque & Reza, 2017).

Mixing of marine and fresh water within reaches of estuaries and deltas produces highly dynamic environments such as the turbidity maximum where water movement, chemistry and stratification can vary significantly based on tidal forcing and river flow (Dalrymple and Choi, 2007). Sediment deposition, therefore, has the potential to record these dynamics (Roche, 2022) and the potential to be used as a source of proxies for the rapidly changing hydrodynamics of the FMTZ (Gringas et al., 2012; La Croix et al., 2015: La Croix et al., 2014; Thornton & Mcmanus,1994; Dashtgard et al., 2022; Wang et al., 2021; Czarnecki et al., 2014; Chmura & Aharon, 1995).

Physical (La Croix et al., 2015: La Croix et al. 2014), chemical (Dashtgard et al., 2022; Wang et al., 2021; Czarnecki et al., 2014; Thornton & Mcmanus,1994) and biological (La Croix et al., 2015; Gringas et al., 2012; Czarnecki et al., 2014), proxies such as grainsize, bed thickness distributions, sand to mud ratios (La Croix et al. 2014), strontium/barium ratios extracted from the sediment samples with acetic acid (Sr/Ba-Hac) and

ammonium acetate (Sr/Ba-NH_4Ac) (Wang et al., 2021), delta thirteen carbon isotopic ratio ($\delta^{13}C_{org}$), carbon/nitrogen ratios (C/N), relative and absolute abundance of dinoflagellate cysts, dinoflagellate cyst concentration (Dashtgard et al., 2022), have been considered in the past as proxies for depositional position within the FMTZ with varying levels of effectiveness.

To have the ability to measure and monitor gradual changes in marine water intrusion in the ranges and extent to which is its present upstream will provide vital information for sediment deposition and ecological variations which may impact organisms, such as mangroves (Haque & Reza, 2017), within the FMTZ. Proxies of $\delta^{13}C_{org}$, C/N, Sr/Ba-Hac (Sr/Ba), grainsize, percentage mud (%mud), x-ray diffraction minerology (XRD) and X-ray florescence elements (XRF), will be used within this study to assess marine water intrusion within the lower Waihou River, Aotearoa New Zealand. The goals of this study are to investigate whether sediment properties record the dynamics of marine water intrusion through physical or geochemical attributes across the upstream gradient of the lower Waihou River and identify the extent of usefulness of each proxy for this application and create an assemblage of viable proxies for further studies to apply. A look into the ability to identify marine water intrusion via river position across the FMTZ gradient through the use of these proxies will aid to provide insights currently lacking from literature.

2.2 Study Area

Located on New Zealand's North Island, the Waihou River extends 186 km up the eastern side of the Waikato region, from the Blue Springs headwaters east of Putaruru to its outlet into the Firth of Thames (Figure 6) (Land Air Water Aotearoa, n.d-b). The Waihou River has a catchment area of 1977 km^2 which consists of flat plains such as the Hauraki Plains, to steep slopes from the surrounding Kaimai, Hanau, and Coromandel ranges, and land use is dominated by pasture and native and planted forests (Land Air Water Aotearoa, n.d-b; Land Air Water Aotearoa, n.d-c). The Waihou River runs through the Hauraki Rift which is 200-250 km in length and 25km wide. The

three sections of the Rift include the Hauraki plains/depression, Firth of Thames and the Hauraki Gulf (Hochstein & Nixon, 1979). As a NNW flowing river, the Waihou outlets into the Firth of Thames. Roche (2022) identified evidence of the turbidity maximum zone (TMZ) at ~9km upriver.

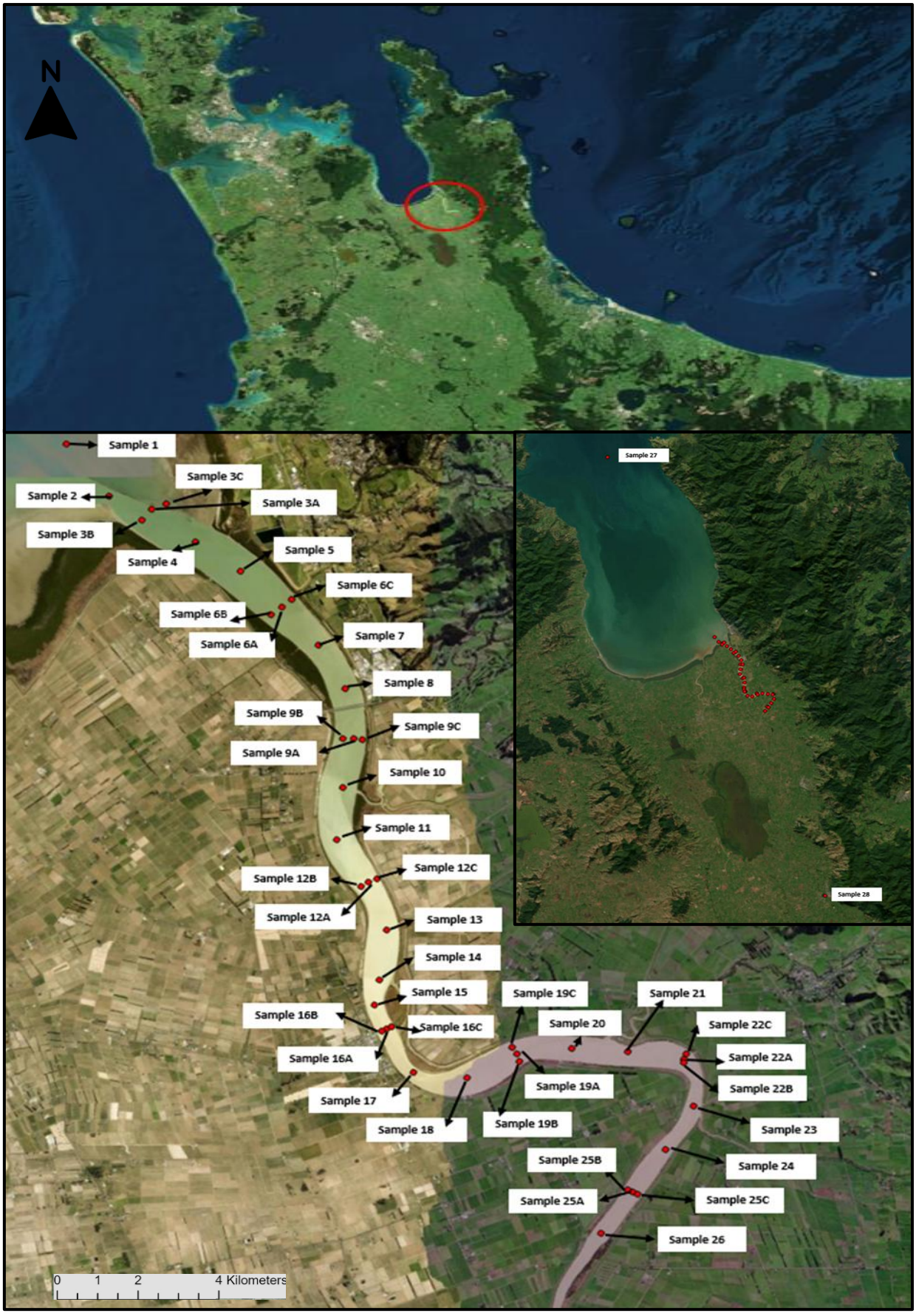

Figure 6.Location of Waihou River New Zealand with labelled samples sites along the lower Waihou River.

The range of salinities measured by James, (2024), along the lower Waihou River has measurements taken during September, December, January, March and April. Field measurements recorded a maximum of 20 PSU recorded at 4.7 km upstream (Figure 7). The furthest measured salinity was 0.1 PSU at 12.5 km upstream (James, 2024). The range in salinity decreases upstream rapidly over a few kilometres, with the maximum 20 PSU decreasing to 1 PSU within 6 km. From 7.7 km the lowest salinity value of the range is 0.1 PSU.

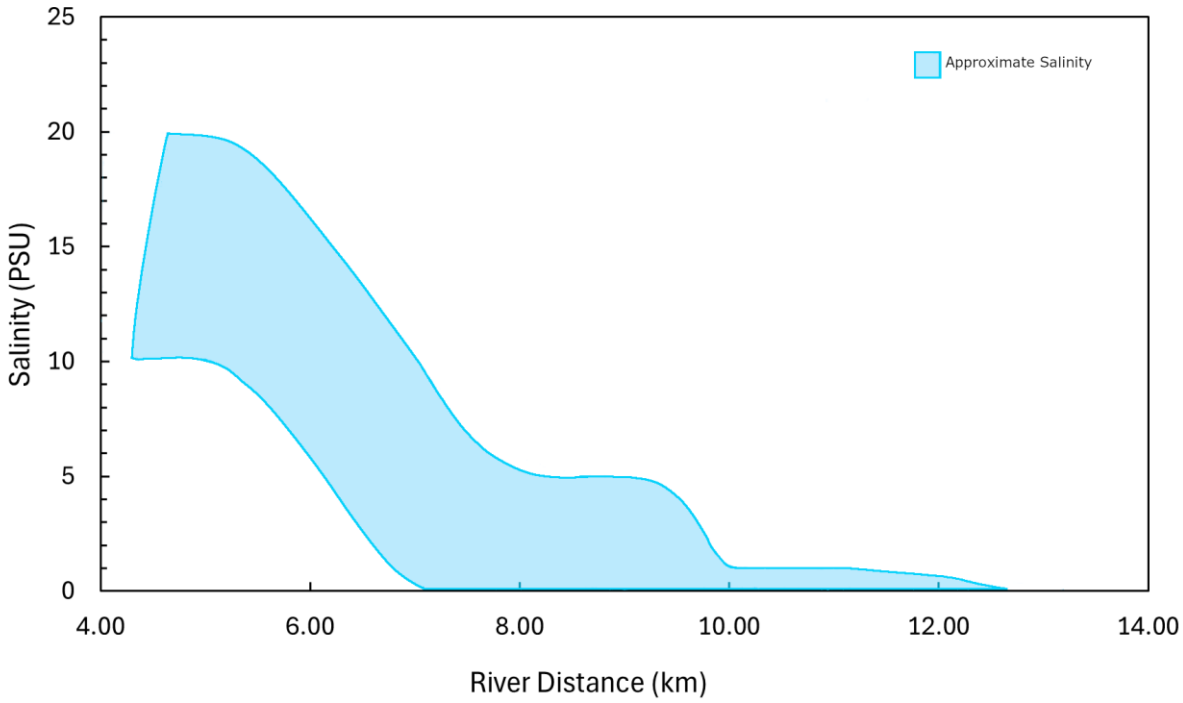

Figure 7.Approximate range of salinities in the Waihou River using data measured by James, (2024). The highest and lowest detected salinities over the study period of 5 months were used to produce a range detected along the lower Waihou River.

2.3 Methodology

On the 24th and 25th of August 2023, 42 sediment samples were collected from the lower Waihou River using a boat. A further 2 samples were collected later by members of the Waikato Regional Council from a purely marine source in the Firth of Thames (sample 27), and a purely fluvial source from 88km upstream near Te Aroha (Sample 28).

Geochemical and physical analyses of grainsize, loss on ignition (LOI), carbon isotope, strontium (Sr) and barium (Ba) ratio, X-ray diffraction (XRD) and X-ray fluorescence (XRF) were completed to determine sediment properties of the river profile along the FMTZ.

Pathways created by James (2024) were followed whilst measuring distances upstream (pathway 1) and out to sea (pathway 2), with the river mouth as the start of each pathway (0 km), the upstream distances are positive values and out to sea distances are negative values. The upstream and out to sea distances of samples 1 through 26 were determined using ArcGIS Pro and Google Earth software to indicate the equivalent position along the pathways used by James (2024). The distances from the river mouth for Samples 27 and 28 were extrapolated using ArcGIS Pro software.

2.3.1. Sample Collection

There is a semi-diurnal tidal system, sample collection occurred during the flood and slack tide during the morning and early afternoon (Figure 8). High tides marked the end of the collection periods due to the Waihou being strongly influenced by the tides. The boat had to be retrieved from the water via the boat ramp during the slack tide, as the outgoing tide posed potential safety risks with boat extraction. The weather was overcast with short clear intervals and light winds.

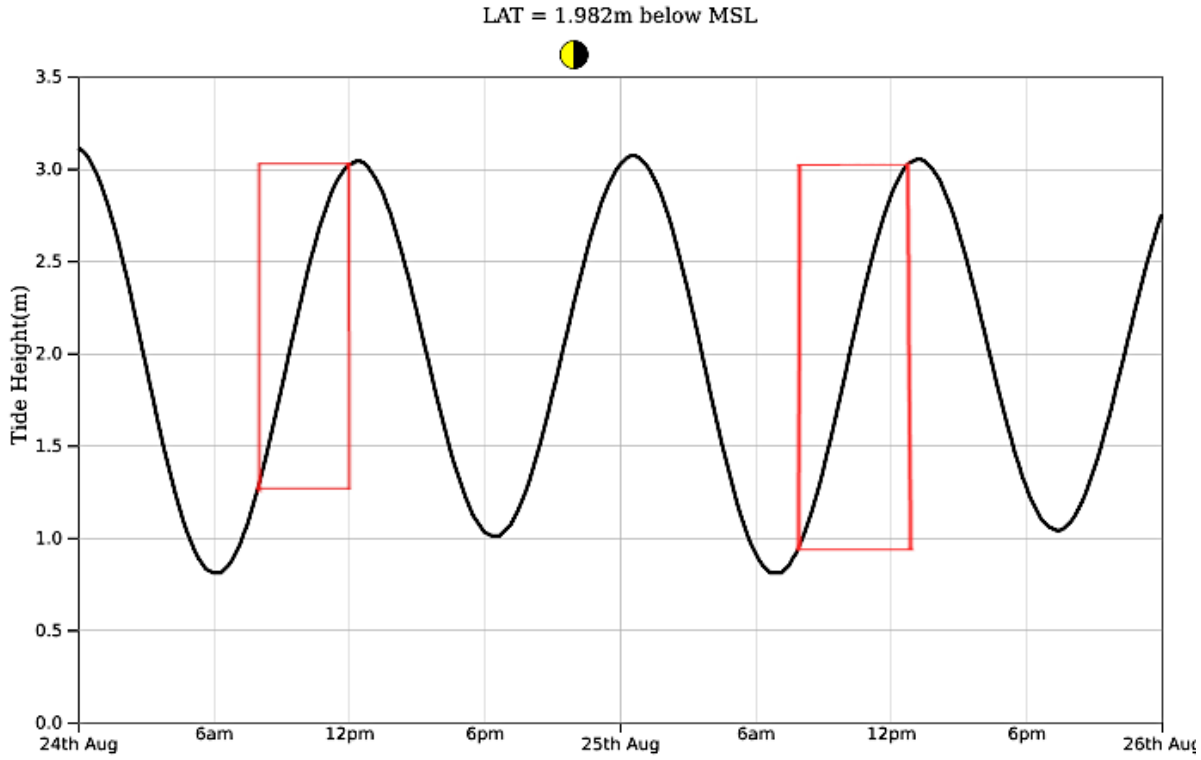

Figure 8. Tidal elevation as per the lowest astronomical tide (LAT) at Kopu Bridge (-37.191, 175.563), Waihou River for the 24th and 25th of August 2023. The red boxes indicate the periods of sample collection. Modified tidal predictions from https://tides.niwa.co.nz.

Sediment samples were collected every ~1000m for the main 26 central samples that followed the deeper channel (excluding sample 15), 16 cross section samples, B and C, were collected, with a cross section every ~3km (Figure 6). Samples 27 (Firth of Thames, 46km from river mouth) and 28 (Te Aroha, 88km from river mouth) were taken as controls and are out of the main study area. Sediment was collected using a ponar grab sampler (Figure 9C), the sampler was lowered into the river and collected the top ~30 cm of surface river sediment.

Figure 9. Machinery and equipment used to collect and analyse data. ***A.*** *Mastersizer 2000 particle sizer used for grain size analysis.* ***B.*** *Panalytical Empyrean Series 2 XRD used in XRD analysis.* ***C****. Ponar grab sampler used for sediment sampling the FMTZ of the Waihou River.* ***D****. Furnace used for loss on ignition analysis.* ***E****. The Neo Fluxer Furnace used to create the fusion beads for XRF major element analysis.* ***F****. Bruker S8 Tiger used in XRF major and trace element analysis.*

3.3.2 Sample Analysis

Wet sediment samples were stored in individual plastic zip lock bags. Samples were divided in half. The first half was frozen, and the other half was refrigerated. All analysis was done using the refrigerated samples which were subsampled and dried at 30°C until samples were fully dry.

2.3.3. Grainsize Analysis

Dried samples were sieved through a 1mm sieve. Approximately 1g of sample was added to a beaker and treated with 30% H_2O_2 to remove organics. If samples reacted strongly to the 30%, a 10% H_2O_2 (hydrogen peroxide) solution was added until reactions

calmed and 30% could be added without the sample overflowing. H_2O_2 was added until reactions slowed sufficiently or ceased. To each sample, 2ml of 0.5% Sodium Hexametaphosphate was added as a dispersion agent and left for 24 hours. Pretreated samples were placed within an ultrasonic bath. Sample grain size was analysed with a Mastersizer 2000 particle sizer (Figure 9A). The data was analysed with GRADISTAT software (Blott and Pye) and then classified according to Folk and Ward (1957).

2.3.4 Loss on Ignition

A set of fresh sediment samples were placed in an oven at 30°C until dried and transferred to an oven at 150°C for 24 hours to remove all moisture from the samples. The dried samples were weighed, and Initial dry weight was recorded. Dried samples were placed in a furnace (Figure 9D) at 550°C for 4 hours in batches of 9-10 samples. From the furnace the samples were measured again, and post furnace weight was recorded. The difference is weight between samples was calculated as the loss of organic material that occurred and percentage of LOI was calculated in an excel spreadsheet.

2.3.5 Strontium and Barium Ratio

The wet samples were placed in small aluminium tins and oven dried at 30°C until samples appeared fully dried. The dried samples presented as pellets which were then broken using a wooden mallet. The broken samples were added to a mortar and pestle, crushed then sieved to <200µm. Mortar and pestle were cleaned in between samples using acetone and paper towels and sieves were brushed out between samples. From each crushed sample 10-20g of powder <200µm in size was added into clean sample bags. In a centrifuge tube, 0.5g of sample and 50ml of 10% acetic acid were combined and mixed for 2 hours at 20-30°C. The mixed samples were left for 24 hours undisturbed before removing 5ml of the solution and adding 18ml of ultrapure water and added to

the Agilent 7900 ICP-MS for Sr/Ba-Hac analysis. Analysis was undertaken at the Nanjing Hongchuang Geological Exploration Technology Service Co. Ltd., China.

2.3.6 Carbon Isotope and Nitrogen Analysis

Samples were dried at 30°C until completely dried and then were broken using a wooden mallet. The samples were then sieved to 63µm to extract the finer fraction of sediment. Cleaning the sieve and mallet in-between samples. Samples of 0.4-3g in weight were added to clean sample bags. Samples were acidified and analysed by the NIWA Environmental and Ecological Stable Isotope Facility in Wellington, New Zealand. The analysis for stable isotopes was completed using a DELTA V Plus continuous flow isotope ratio mass spectrometer which was connected to a Flash 2000 elemental analyser. The elemental analyser used a MAS 200 R autosampler. If $\delta^{15}N$ results for Ampl28 were <1800mV then the samples were blank corrected via the subtraction method (Langel & Dyckmans, 2017; Ohlsson, 2013). Both $\delta^{13}C$ and $\delta^{15}N$ analyses were two points normalised using the NIST 8573 USGS40 L-glutamic acid from the daily stable isotopic data, $\delta^{13}C$ also used L-Valine #2 USGS74, and $\delta^{15}N$ used NIST 8548 IAEA-N2 ammonium sulphate. The $^{13}C_{org}$ value is the product of equation:

$$\delta 13Corg\ (‰) = (Rsample - Rstandard) / (Rstandard) \times 1000$$

Which uses the Pee Dee Belemnite (PDB) to produce $^{13}C_{org}$ from R ($^{13}C/^{12}C$).

2.3.7 X-Ray Diffraction

The dried samples were pulverised using a tungsten-carbide ring mill and stored in plastic zip lock bags. The dry powdered sediment was placed into the XRD mould using a glass plane to smoothly compact the sediment into the mould and placed into the rack for analysis. Samples were completed in batches of 10 and were placed in the Panalytical Empyrean Series 2 XRD (Figure 9B) for 5-80 °2θ, at 50s per step to assess the

mineral composition within the samples. The results were analysed using the HighScore and Data Viewer software.

2.3.8 X-Ray Fluorescence

Dried samples were pulverised by a tungsten-carbide ring mill for 45 seconds to a fine powder and stored within plastic zip lock bags. Samples were analysed for both major and trace elements, loss on ignition was also analysed to account for the loss of organics which occurred during the preparation of the majors. The LOI was completed using ceramic crucibles which were weighed, 2g of the pulverised sediment was added to the crucible and reweighed before being placed in the muffle furnace (Figure 9D) at 1100°C for 1 hour. The crucibles were placed in the desiccator until room temperature and reweighed as the after weight. Loss on ignition was calculated as the difference between before and after the furnace weights.

The major element analysis preparation used metal crucibles. In the crucible, between 7.9990-8.0030g of 12:22 Flux was added. An amount of 0.7990-0.8030g of sample was then measured in a plastic boat and added to the flux, weighing the boat before and after the sample was added to the crucible to get the actual weight of the sample. Between 0.1 - 0.2g of ammonium iodide was mixed gently with the sample and flux in the crucible. The crucible was then placed within the Neo Fluxer furnace (Figure 9E) for 27 minutes where the sample was melted at 1050°C and poured into a mould to produce a fused bead. Glass fused beads were then added to the Burker S8 Tiger (Figure 9F) at the University of Waikato to be analysed.

The trace elements were prepped using a metal piston and hydraulic press. A mixture of ~8g of sample and 17-20 drops of pipetted PVA binder were combined in a paper cup with a wooden stirrer. Sample and PVA were mixed until a crumbly consistency and added to an aluminium cup in a mounded shape. The aluminium cup was placed on the base of the die unit and had the die unit cylinder fitted over the top smooth side up. The plunger was then added to the centre of the cylinder on top of the sample. The Die Unit

was then placed in a hydraulic press and pumped to 200 bar, released slightly, brought back to 200 bar, then released completely. The compressed pellets were removed from the piston and placed ready for analysis. The die unit was cleaned using acetone and a paper towel. The pellets were added to the Burker S8 Tiger (Figure 9F) and tested for trace elements.

2.4 Results

2.4.1 Grainsize

The grainsizes measured along the lower Waihou river had a range of sizes, ranging from medium silt to coarse sand (Figure 10A). The highest mean grainsize is 690.11µm coarse sand is present in Sample 12B at 8.05km and the lowest mean grainsize is 8.66µm medium silt in Sample 12C at 8.07km. When cross section samples B and C are excluded the highest and lowest grainsizes are 593.28µm and 10.96µm in samples 26 (coarse sand) and 11 (medium silt)). The mean grainsize for all samples is 246.8 µm which is a medium sand

The highest proportion of mud was 90.1% in Sample 12C (S12C), followed by 86.8% in S6B which are 8km and 2km from the river mouth, respectively. The lowest measured mud percentage was S28 (2.3%) followed by S5 and S8 (3.1%). Sample 27 had a value of 61.1%. When only considering the central samples and excluding the cross sections the highest %mud becomes 79.3% at Sample 11. The mean percentage of mud for all samples is 26.6% and the median value is 10.2%. There is a large range of values present with most lower values (Figure 10B)

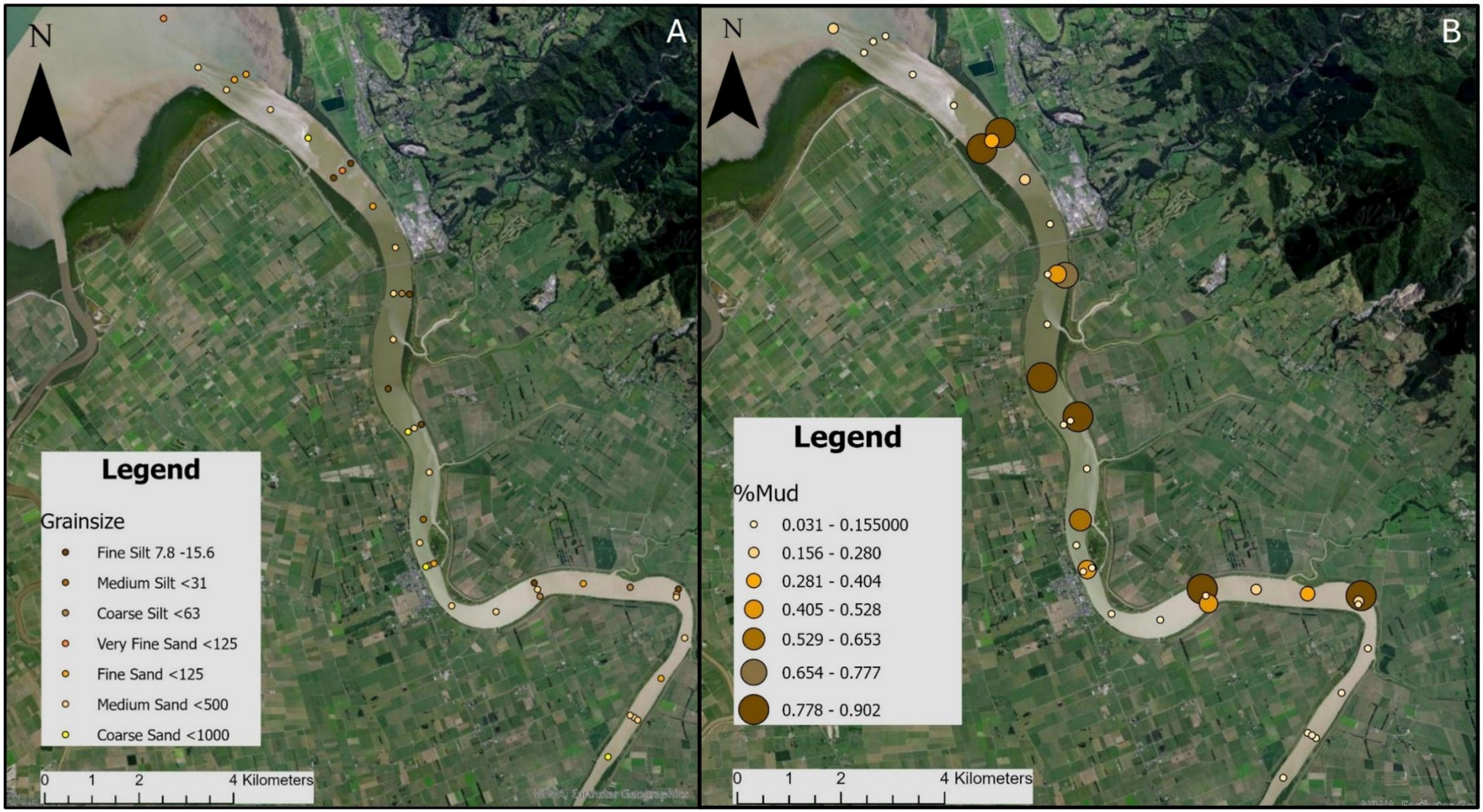

Figure 10.Maps of sediment grainsize and %mud using colour and/or scale as representation. A. Mean grainsize for samples along the lower Waihou River with Grainsize represented by colour. B. percentage mud recorded along the lower Waihou River with variation in size proportional to the proportion of mud in each sample.

2.4.2 Loss On Ignition

Loss on ignition was conducted on all samples, the majority range between 1-6% LOI and 8 samples between 6-11% LOI. Sample 6B had the highest LOI (10.17 %) and S28 had the lowest (1.28 %) with an overall range of 8.89%. The mean LOI for all samples was 3.99% and the median LOI was 3.31% which are both towards the lower range of values.

2.4.3 Strontium Barium Ratio

The highest value is 49.80 in Sample 27 (S27) and is closely matched by Sample 1 at 37.15 which occurs near the river mouth (Figure 11). The lowest two samples are 28 with 0.08 and 26 with 0.09 located upstream. Majority of samples range between 1.5 and 0. The mean of all samples is 3.70 however when samples 27 and 28 are removed the mean drops to 2.69. The median value is 0.80 when all values are considered. The larger values are found in samples 1, 2 3C, 6B and 6C (Figure 11).

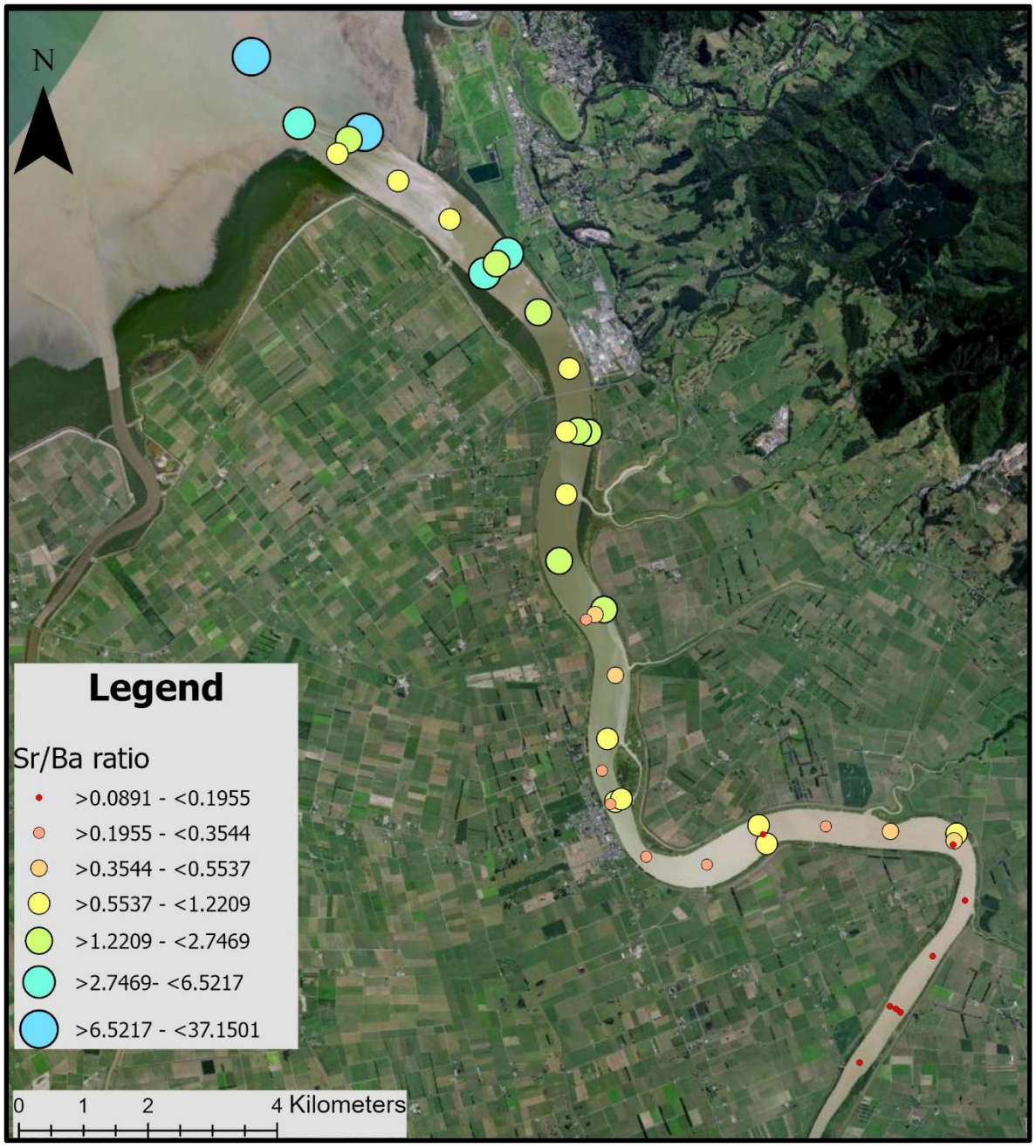

Figure 11. Map of Lower Waihou River with Sr/Ba displayed via colour and size.

2.4.4 Carbon Isotopes

The highest $\delta^{13}C$ value -21.76‰ is located in Sample 27, followed by Sample 25B, -23.45‰, and the lowest values of -27.45‰ (S24) and -27.14‰ (S18). The majority of samples (22 of 32) range between -24‰ and -26‰, 4 over -24‰ and 6 under -26‰

(Figure 12). When the cross section samples B and C are removed the highest and lowest values remain the same except S25B, replaced by Sample 2 (-23.95‰). Carbon/nitrogen ratios highest value is 11.03 (S24) followed by 10.69 (S18) and lowest value is 7.31 (S27) then 7.40 (S2) (Figure 13). The highest and lowest values remained the same.

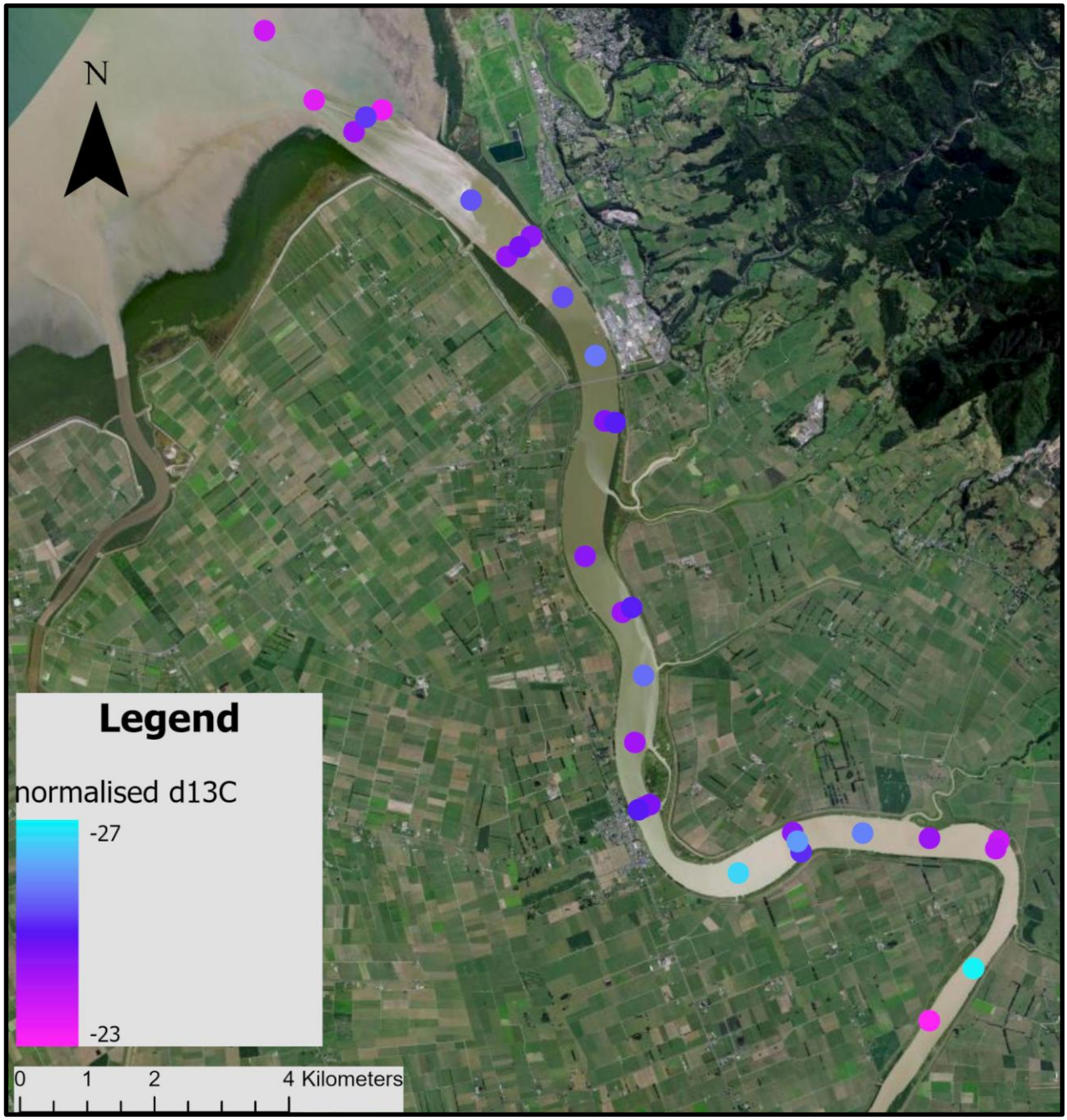

Figure 12. Map of 13Corg along the lower Waihou River identified by colour.

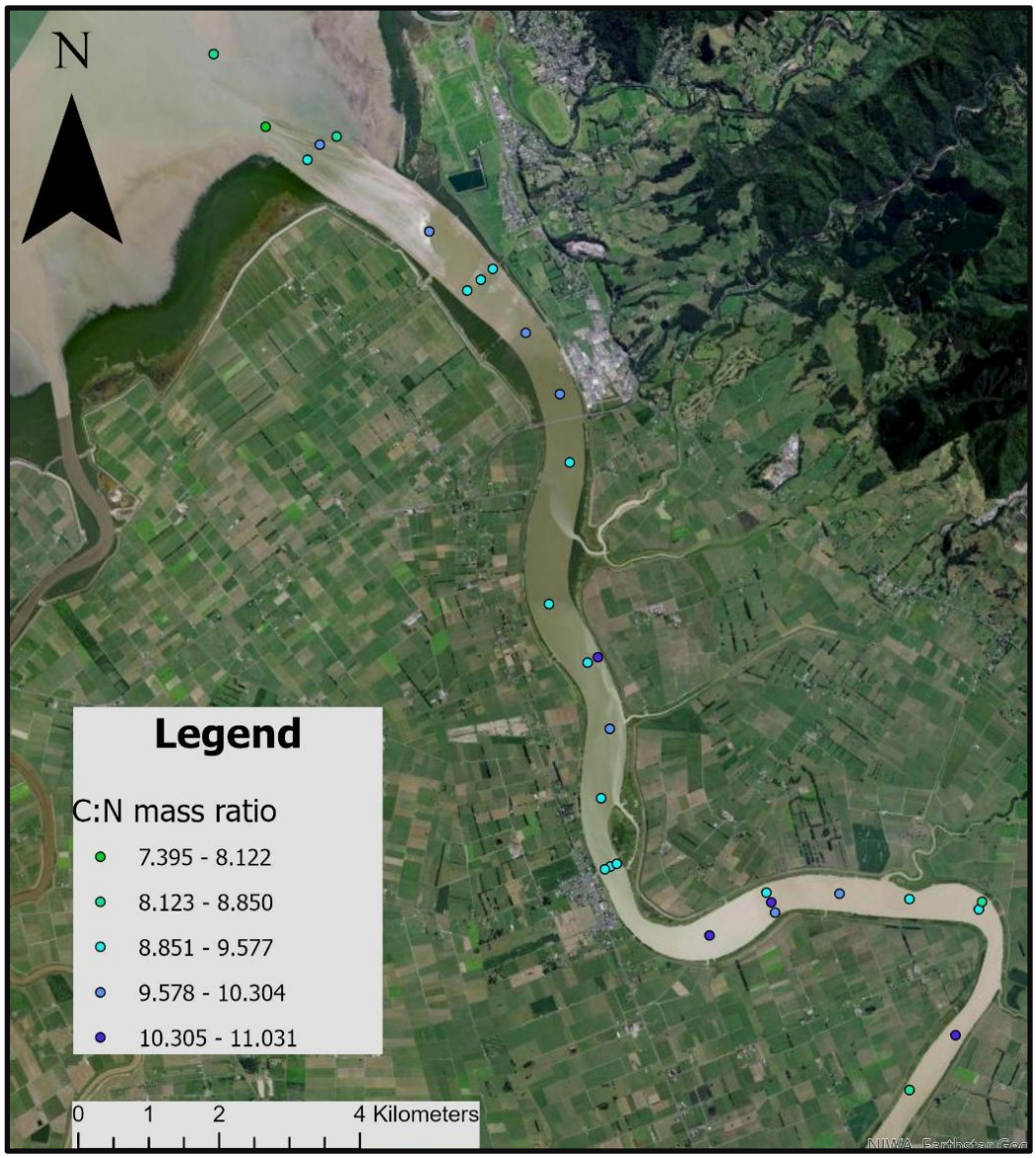

Figure 13. Map displaying C/N along the Waihou River through colour coding.

2.4.5 XRD

XRD analysis has identified peaks which correspond with mineral composition within the sediments. Of the many peaks identified, ones that are consistent with all samples are the d-spacings 3.345Å peak at 26.7° and the d-spacing 4.257Å peak at 20.9°, which both correspond with quartz, as well as 1.816Å. The quartz peaks range in intensity across samples (Figure 14). D-spacing 4.046Å, 3.183Å and 3.211Å correspond with plagioclase. All samples have quartz and plagioclase present

regardless of river position (Figure 14, Table 1). However, three other minerals are present occasionally including aragonite, calcite and halite (Table 1). D-spacings 3.274Å and 1.980Å correspond to aragonite, d-spacing 3.307Å corresponds with calcite and d-spacings 2.812Å and 1.195Å relates to halite. The additional minerals are only found on the marine end with the furthest upriver at 2.6km from the river mouth, Sample 6C. Small peaks can be acknowledged near 10° and 7° these peaks are theorised to suggest clays within the sample however clay analysis was not completed so it cannot be confirmed (Figure 14).

.

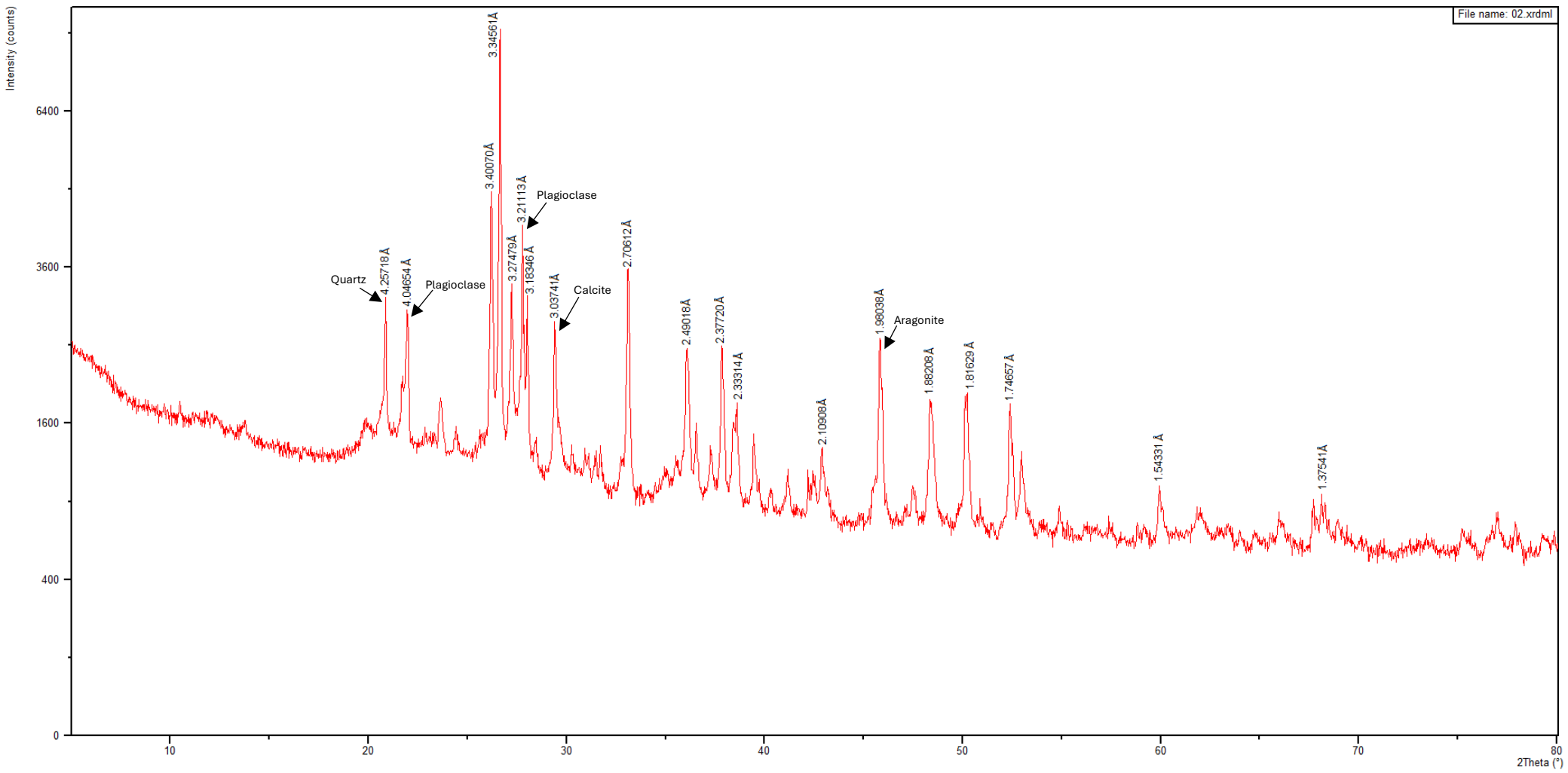

Figure 14. XRD analysis of peaks for sample 2 with labelled peaks.

Table 1.Minerals present within samples through XRD analysis, summarised. All samples include 1-26, 27 and 28 including cross section B and C samples. Green is present in the sample; Grey is not applicable as covered by all samples and blank/white is not present in the sample. D-spacings are from sample 2 excluding halite where D-spacing are from sample 27.

Minerals	D-Spacing (Å (2θ))	Mineral present in all samples	27	1	2	3C	6B	6C
Quartz	4.257 (20.0) 3.345 (26.7) 1.816 (50.1)							
Plagioclase	4.046 (21.9) 3.183 (28.0) 3.211 (27.7)							
Aragonite	3.274 (27.2) 1.980 (45.9)							
Calcite	3.037 (29.4)							
Halite	2.821 (31.7) 1.195 (45.5)							

2.4.6 XRF

The major elements assessed with XRF are calculated as a percentage of the sample, with silicon (Si), aluminium (Al), titanium (Ti), manganese (Mn), iron (Fe), magnesium (Mg), calcium (Ca), sodium (Na), potassium (K), phosphorus (P), sulphur (S) and carbon dioxide (CO_2). Of the major elements Si was consistently highest ranging between 50 – 70% across all samples except in Sample 2 where Si was only 39.12% (Figure 15). Sample 2 was also recorded to have higher Ca at 22.05% than the other samples which had Ca values under 5% excluding S1 and S3A which had 11.57% and 8.15% respectively. The next highest percentages were either Aluminium or CO_2 for all samples (Figure 15). Sample 2 also had the highest CO_2 value of 23.01%. The major element composition of the samples seems rather consistent regardless of river position with the exclusion of Sample 2. The major elements also contained strontium and barium which were not considered a percentage but as parts per million (PPM). The analysis above in section 2.4.3 looks at Sr/Ba as a ratio and so it will not be addressed in this section.

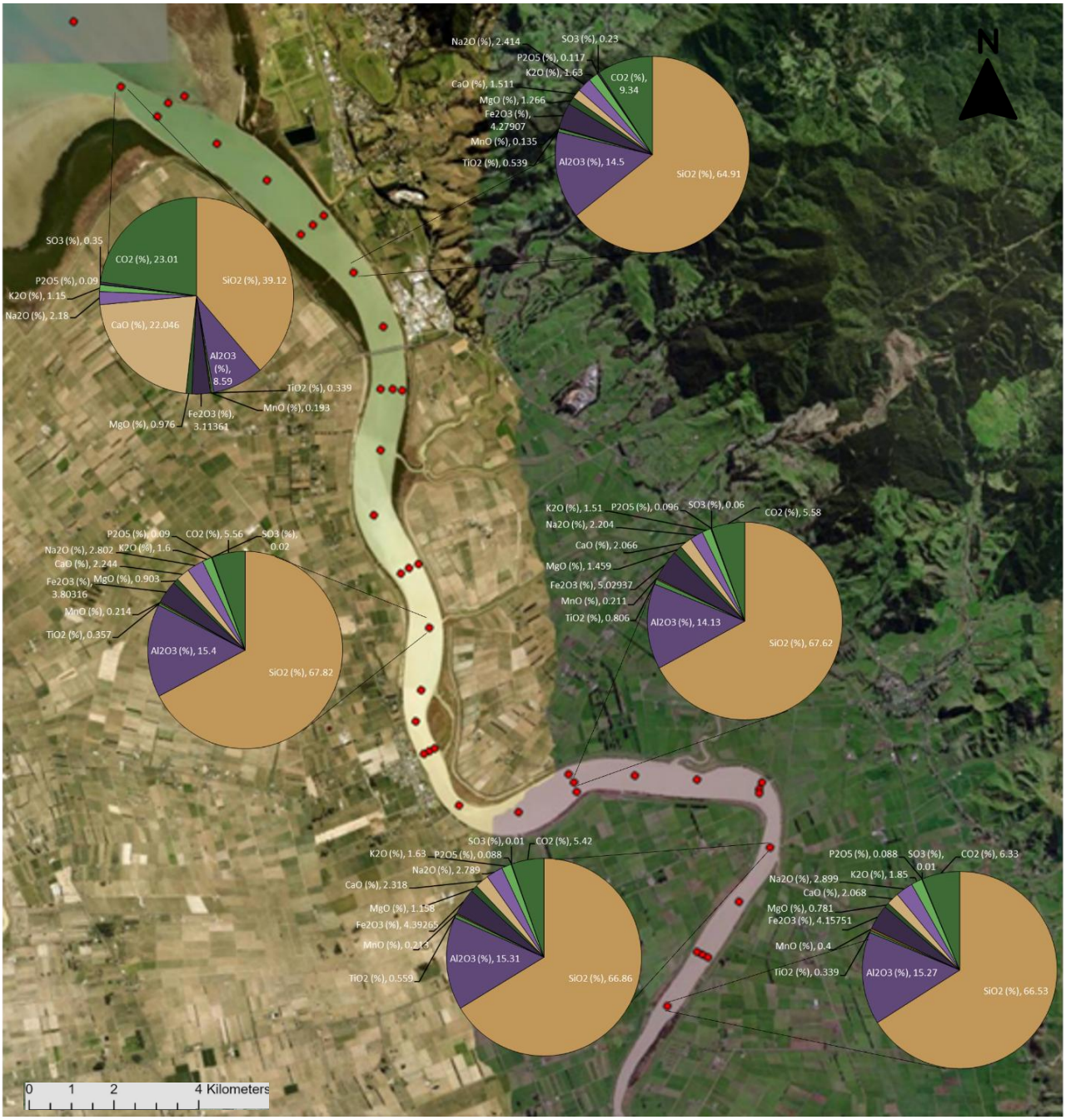

Figure 15.XRF major elements and CO2 by percentage as shown for 6 samples, S2, S7, S13, S19A, S23 and S26, to show composition along the river.

From the trace element analyses various elements were identified in small quantities, measured in PPM. Most trace elements showed no noticeable change in quantity with river distance and contained similar values throughout the samples. Lead (Pb) had a range of values of 0 – 53 PPM in all samples except for samples 20 and 12A which had 227 and 212 PPM respectively Sample 20 has an elevated antimony (Sb) of 18 PPM

much higher than other samples. For highest nickel value it was 23 PPM (S26), and lowest of 6 PPM (S27).

2.5 Discussion

The goals of this study are to investigate whether evidence of the extent of marine water intrusion up the lower Waihou River is identifiable through geochemical and physical sediment proxies. Subsequently, the aims assess the levels of success shown by each proxy to establish a toolbox to be utilised by further studies in these topics. As such, I will discuss river position as demonstrated by the proxies and compare the findings with past research. Finally, considerations regarding further study required on the subject will be explored.

2.5.1 Trends in proxies in the lower Waihou River

The range of salinity measured by James (2024) in the lower Waihou River show that as distance up the river increases, the salinity decreases. The values recorded at each location up the river vary in the range of salinities observed, with the range in salinity decreasing upstream as tidal influence lessens.

There is no clear relationship with mud content/proportion and river position when all samples, 1-26 and cross section B and C samples, are included (Figure 16A). There was no consistent increase or decreases in mud content from river mouth to upstream samples (Figure 16A). The low R^2 value (0.0098) demonstrates the lack of relationship. When cross section samples B and C are excluded, there is still no clear change in %mud with river position, the R^2 value increases but remains insignificant (Figure 16B). Central river samples, (not including B and C samples), 20 of 28 samples, have under 30% mud and 6 samples are between 30 – 60%, with sample 27 and 11 over 60%.

The R^2 values are very low for grainsize regardless of whether the B and C samples were included. The R^2 value (0.0057) for grainsize suggests a lack of relationship between river position and mean grainsize (Figure 16C). A similar result came from the %mud analysis, the R^2 values were very low when all samples were compared to distance and when B and C samples were removed, though the R^2 value increased there was still no correlation. There is a negligible relationship between river position and grainsize without the cross section samples, R^2 value 0.0025 (Figure 16D).

Both %mud and grainsize analyses offered no distinct patterning upstream, values measured sample to sample fluctuated significantly. Samples a kilometre apart varied from high mud content to very low mud and coarse to fine grainsize with constant variation in the level found. The lack of relationship with distance stands as an indicator for a lack of relationship with salinity as the salinity from James (2024) is shown to decrease with the increase in river distance (Figure 7).

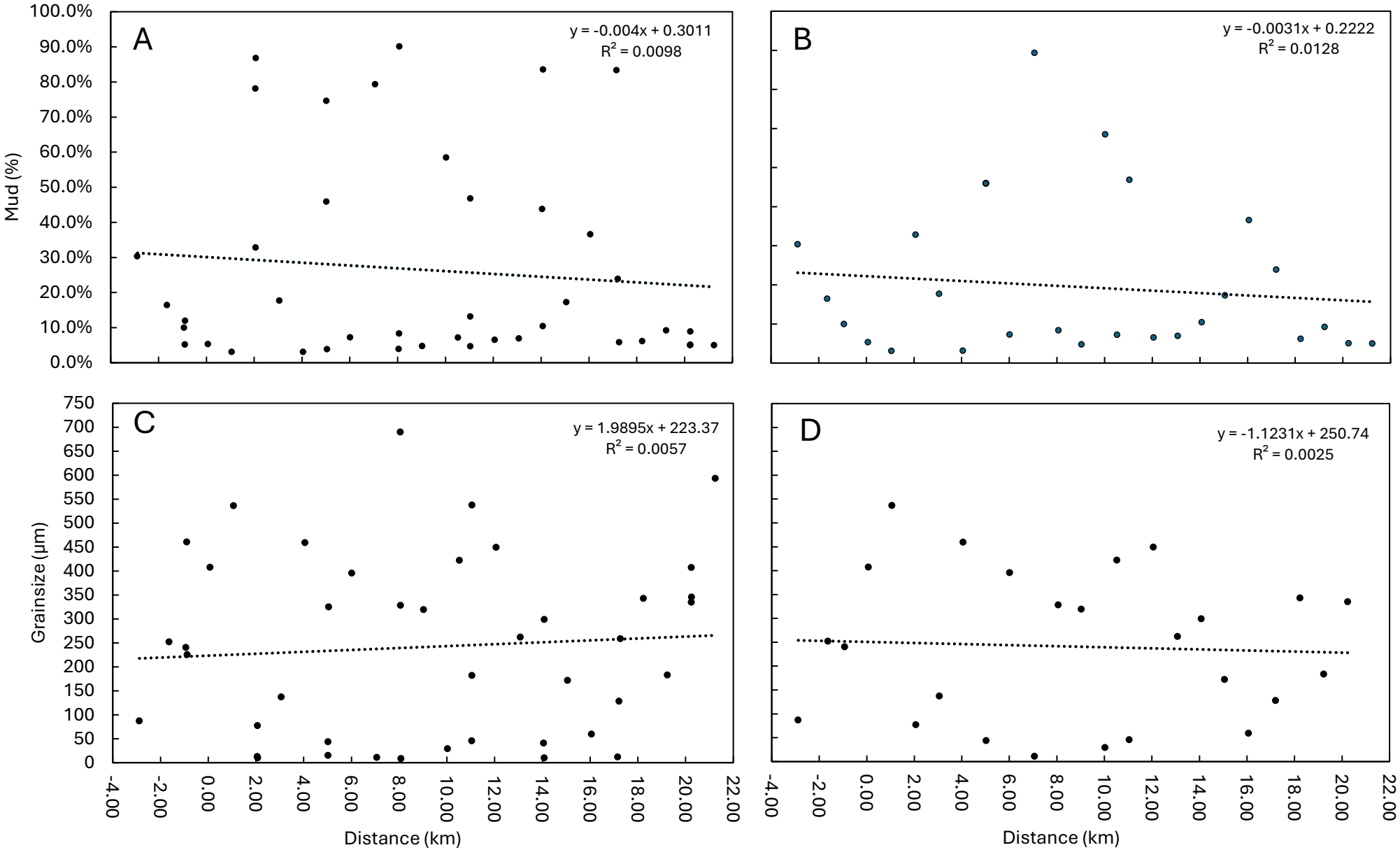

*Figure 16. Graphs comparing grainsizes and %mud with distance along the lower Waihou River. **A**. Percentage of mud present in sediment samples 1-26 along the lower Waihou River. Samples 27 and 28 are excluded from this graph with 61.1% and 2.3% mud respectively. **B**. Percentage mud along the Waihou River samples 1-26 excluding cross section samples B and C. **C**. Mean sediment grainsizes of samples 1-26 inclusive of cross section samples along the Waihou River. Samples 27 (23.19 µm) and 28 (673.1 µm) are out of bounds of this graph. **D**. Mean sediment Grainsize of samples 1 -26 excluding cross section samples B and C. Samples 27 and 28 are excluded as they extend beyond the depicted range.*

Values varied significantly with some samples recording an LOI over 10%. Loss on ignition also showed no correlation with distance up the river, has a negligible relationship (R^2: 0.0528) and no discernible trend is apparent (Figure 17). Lower LOI values are present across the whole study area compared to the higher range values which only occur between 2 – 15 km. There is high variation in the LOI between samples and the variation is not consistent with the distance they were collected up the Waihou River. The high variation in the LOI between samples indicates large amounts of organic matter, volatiles or carbonates are present in inflated quantities within some sediments but minimal in others. Potential reason for these variations may be the presence of organisms such as shellfish, changing dynamics of the main river channel and sand banks, or the function of the grab sampler.

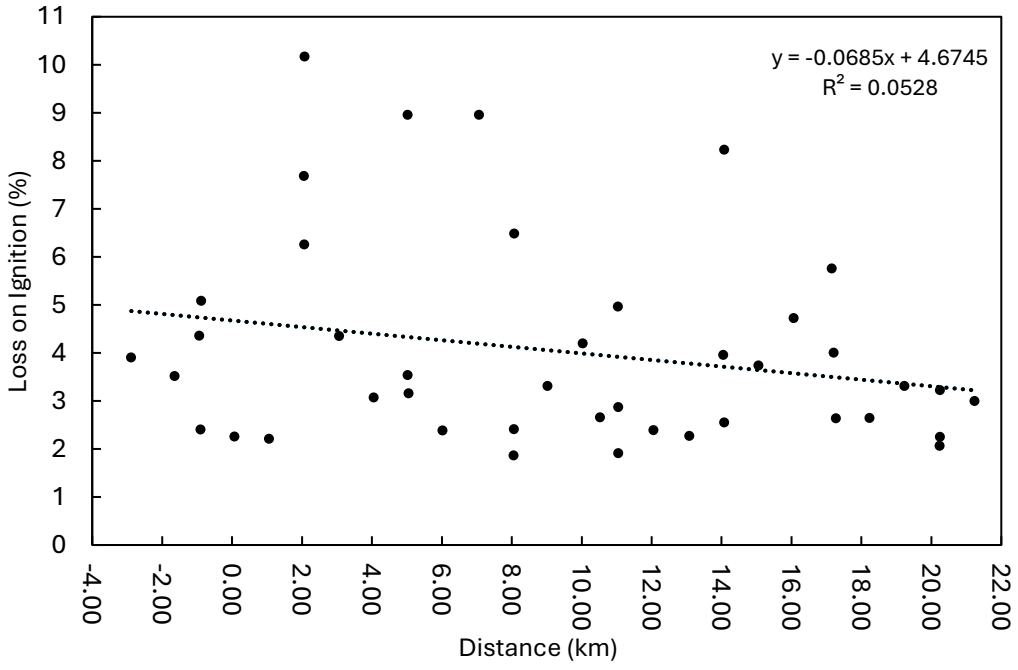

Figure 17.Loss on ignition along river position, samples 1 - 26 including cross section variables B and C. Samples 27 (8.55%) and 28 (1.28%) are excluded.

For Sr/Ba the cross section at S12 identifies S12A and B as values of 0.43 and 0.35 respectively and S12C as 2.72 which is higher than the other 12, 11 and 13 sample values. Sample 3C has a value of 31.55 which is potentially an outlier based on the

samples close in proximity to it ranging between 6.52 and 1.08, however it has not been removed from the dataset. The Sr/BA ratio has a R^2 value of 0.3964 and a moderate relationship with river position across all samples, excluding 27 and 28 (Figure 18A). When cross section samples are removed the R^2 value increases slightly (0.4071) but the relationship remains moderate (Figure 18B). The highest and lowest samples remain the same as they are from the central river samples.

Strontium/Barium ratios presented a correlation with river distance, presenting with a weak-moderate relationship, as per a similar relationship/correlation classification standard to Dashtgard et al. (2022). The variance in values explained by the R^2 values were near 40% for Sr/Ba, both including and excluding the B and C samples collected in cross section. A decrease can be observed in overall Sr/Ba values against river distance (Figure 18A, Figure 18B), if the distance is considered in 5 km zones, results show the highest of each zone and lowest of each zone would fall lower in value than the previous zone as it moves upstream with little exception. Salinity shows a rather rapid decrease in the ranges observed between 4 km and 7 km, decreasing from 20-10 PSU to 10-0.1 PSU (Figure 7). However, within this range, though the gradual Sr/Ba ratios are decreasing across the full study area, there is no rapid or distinguishable drop in values that follow that of the salinity ranges (Figure 18A, Figure 18B). The same can be said for the salinity plateau between 8-10km and for the drop from10-12 km, with no clear drop in Sr/Ba in the samples taken within those distances. Due to the variance in the Sr/Ba ratios being rather low it can be said that having only a few samples over the distances where salinity drops may not be able to capture the finer differences that could be present and instead may require many more samples in a smaller area to represent it accurately. Salinities being a constantly changing variable based on tides, depth and river flow may also make finer definition of location upstream elusive and encourages potential zonation of rivers as a means of estimating marine water intrusion location through the Sr/Ba proxy. Barium is a function of salinity through the Ba^{+2} forming an ionic bond with the sulphate (SO_4^{-2}) in marine water causing barium sulphate to form and precipitate out of the water column leaving little barium in marine environments. Thus, more targeted zonation and clustered samples around long term patterns of rapid changes in salinity may better represent the gradient of how the barium precipitates

with the presence of marine water and capture the fluvial to marine transition better on a smaller scale.

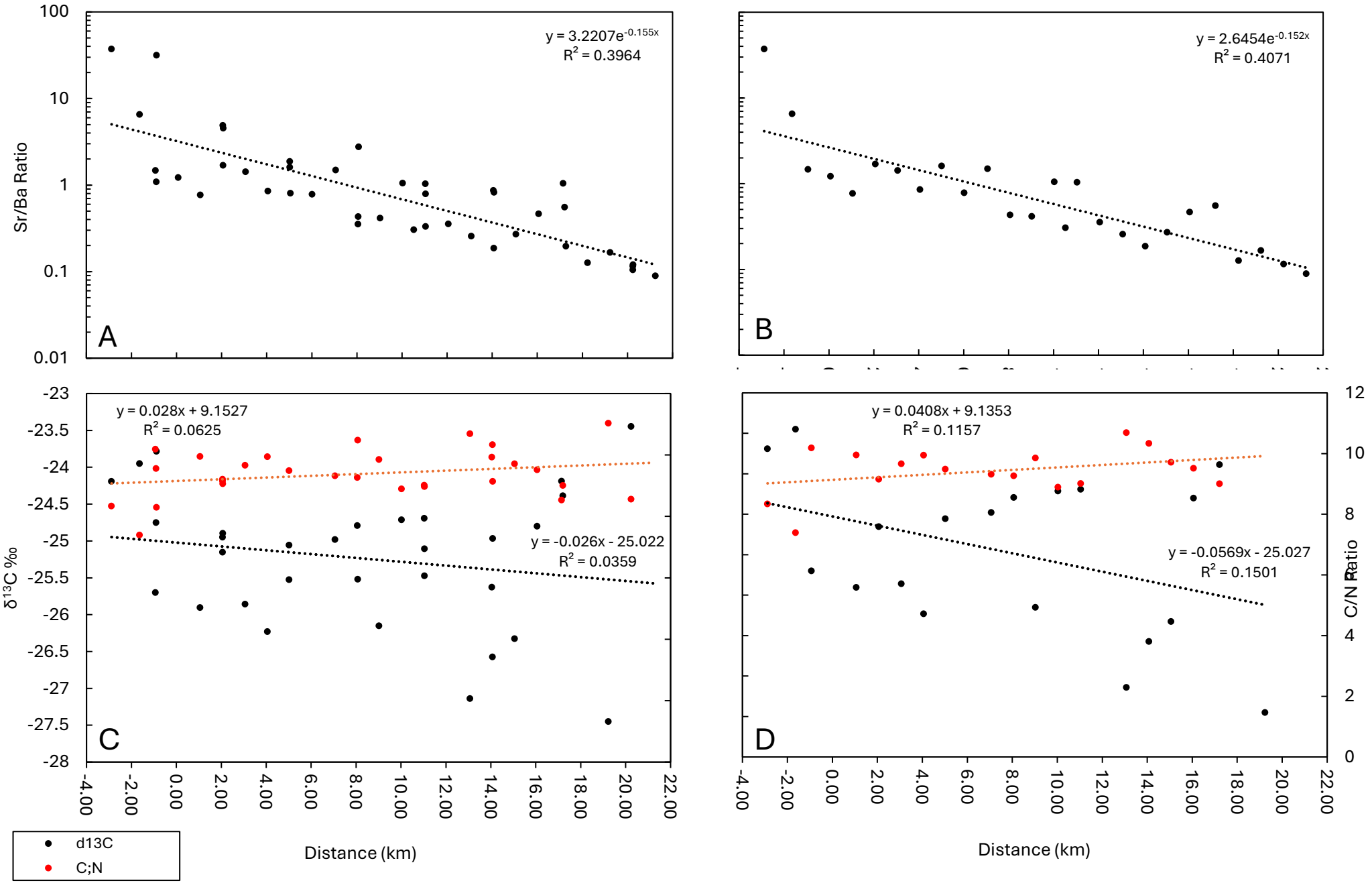

Figure 18.Graphs showing relationship between river distance and geochemical proxies. ***A****. Strontium/Barium ratio along river position of the Waihou River for sample 1-26 including samples B and C. Samples 27 (49.80) and 28 (0.08) excluded due to out of graph bounds.* ***B.*** *Strontium/Barium ratio along river position of the Waihou River for samples 1 - 26 excluding samples B and C. Samples 27 (49.80) and 28 (0.08) are excluded as are out of graph bounds.* ***C****. River position against δ13C and carbon/nitrogen ratio of samples 1 -26 including cross sections samples along the Waihou River. Samples 27 is excluded as out of graph bounds, δ13C =-21.76‰, C/N = 7.31. Samples 4, 9B, 10, 12B, 15, 17, 22B, 23, 25A, 25C, 26 and 28 are absent due to no data.* ***D****. River position against δ13C and carbon/nitrogen ratio of samples 1 -26 excluding cross sections samples B and C along the Waihou River. Sample 27 is excluded as out of graph bounds, δ13C =-21.76‰, C/N = 7.31. Samples 4, 10, 15, 17, 23, 25A, 26 and 28 are absent due to no data.*

Both $\delta^{13}C$ and C/N across all measured samples identified negligible relationships with river position, $\delta^{13}C$ posed an R^2 value of 0.0359 and C/N posed $R^2 = 0.0625$ (Figure 18C). Excluding the cross section B and C samples, $\delta^{13}C$ increases the R^2 values but the relationship remains negligible with river position (Figure 18 D). Whilst $\delta^{13}C$ and C/N values identified negligible relationships with river distance when B and C values are excluded, the variance is only explained 10-15% of the time. This lends itself to significant doubt of whether it is relevant. The $\delta^{13}C$ correlation with distance narrowly suggests a decrease as river distance increases when considering the position of the highest and lowest values. With that considered no clear pattern can be identified regarding the decrease in salinity with the values from $\delta^{13}C$ and C/N at the finer scale or larger study area. However, a comment may be made regarding the increase in $\delta^{13}C$ range towards the upstream section of the river. Land based carbon sourced from C3 plants tends to have an average $\delta^{13}C$ value of ~-27‰ and range of -23‰ to -34‰, whereas marine based algae/organic matter/phytoplankton ranges from ~-18‰ to -22‰ (Meyers, 1994; Han et al., 2020). With these values as a guide, it suggests that some upstream values have more carbon sourced from C3 land plants and shows Sample 27 as having marine sourced carbon. The large range of values between estimated carbon source values suggests a mixing of both marine and land sourced carbon throughout the majority of the study area.

Riverbanks store carbon often as CO_2 or organic matter, riverbank erosion can result in excess carbon entering the river system (Walcker et al., 2021). Meandering rivers especially cause larger amounts of channel and bank erosion therefore increasing the amount of carbon transported within the river form soil (Walcker et al., 2021). A smaller river such as the Waihou River would have the overall carbon discharged daily more significantly affected by bank erosion than a larger river. With pasture lining much of the Waihou Riverbank, erosion would be encouraged by a lack of deep roots, prompting bank collapse or erosion which increases the carbon entering the river. An increase in the discharge of carbon due to bank erosion could result in a higher detectable presence of terrestrial carbon downstream in the river due to the additional source from riverbanks. An increased abundance of terrestrial carbon may allow it to be detected in high quantities further down river than would be expected otherwise, potentially

causing increased terrestrial carbon at lower ends of the study area causing no relationship or gradient to be found.

Another consideration would be the effect of mangroves on the carbon isotopes present within the area of the river mouth; mangroves act as carbon sinks whilst also being C3 plants with a portion of the carbon stored coming from the leaf litter (Alongi, 2012). If mangroves are storing carbon in the sediment and root systems towards the marine end, it may influence the sediment potentially changing proportions of marine or terrestrial carbon towards the delta and river mouth, potentially influencing the detectable carbon sources and interfering with $\delta^{13}C$ results by skewing the ratio as mangroves are more located around the river mouth and lower river km so would influence the observed carbon in the river mouth area. This may contribute to the variation and lack of relationship observed.

The XRD results presented the mineral assemblage of all samples to be very similar with only 6 samples (Table 1) containing minerals other than quartz and plagioclase which were found in every sample. Only lower river samples contained additional minerals. Samples 27 and 6B contained halite which indicates saltwater present and matches high salinities measured by James (2024). Yet, samples in-between 27 and 6B do not contain halite. Reasoning for this is potentially that since 6B is close to the riverbank it is possible it has a pocket of low flow where river current and tides are reduced and so allows for settling or long term residence of saline/brackish water. Sample 27 is a fully marine sample within the FOT, so the presence of halite is within expectations. The calcite present in Sample 2 and aragonite in samples 1, 2, 3C and 6C can be explained by the presence of shellfish towards the marine end, the shells were physically observed in samples 1 and especially 2 during collection. All samples with additional mineralogy were located within the higher salinity range or further into the marine direction where it is assumed that salinity would remain in a similar range, or increase seaward.

The XRF results found little variation in the major and minor elements. Sb and Sn were both found to have weak and moderate relationships respectively, both increasing as river distance upstream increased. Marine values were noted as 0 PPM for both and climbed to ~5 PPM. Sample 20 has an elevated Sb of 18 PPM much higher than other

samples. Chlorine (Cl) has a weak to moderate relationship with river position with an R^2 value of 0.371, the marine samples recorded higher Cl values in the 100,000s (PPM), whilst the upstream samples measured less, in the low to mid hundreds of PPM (Figure 19).As chlorine is a major component of salt (NaCl) it could be anticipated that the proportion of chlorine would be higher towards the ocean salt water than within the fresh water. Whilst higher chlorine in rivers from road salt seems to be the most pressing source of high river chlorine (Szklarek et. al, 2022), it is less relevant for New Zealand especially within the Waihou River catchment. Fertilisers such as potassium chloride (KCl) used in agriculture, or mineral erosion in groundwater could be a plausible cause of riverine chlorine if the increased Cl is theorised to be from a riverine or mixed source. However, if those sources were of great contribution, it would be unlikely to see such an increase in the lower 8km of the Waihou river as observed in Figure 19, instead the distance upstream would also be expected to have higher Cl. Therefore, it is much more likely that the increased chlorine seaward is a product of marine water, probably as a result of the salt content, thus working as a possible representative of the saltwater intrusion upstream and a potential indicator of the concentration of saltwater to fresh water as it mixes.

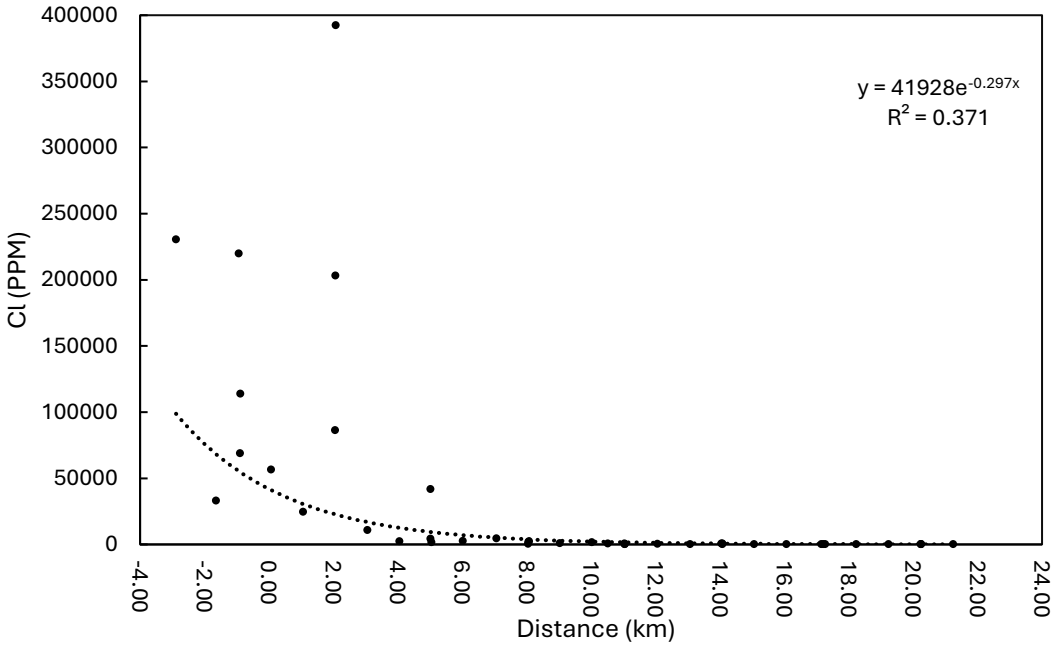

Figure 19. Chlorine along the distance up the lower Waihou River. Inclusive of samples 1-26 and cross sections of B and C.

Nickel (Ni) was another element which demonstrated a relationship with river distance upstream. Nickel was found to increase as the samples moved inland with the R^2 value being 0.595 as a moderate relationship with 59.5% of sample values explained within the relationship (Figure 20). When samples B and C are remover the R^2 value increases to 0.6619 and the highest and lowest values remain the same (Figure 21). Nickel has not identified as a metal that is likely to leach from mine tailing upstream of the Waihou River (Webster 1995), however it is still possible the nickel is upriver is sourced from mining or through exposed mine rock. The level of nickel within the environment is also slightly elevated with the expected nickel based on Waikato soils is 7mg/kg (7 PPM) (Webster, 1995). Nickel is identified to have a clear relationship with river position, but nickel was not initially considered. Nickel isotopes have indicated to being identifiable in marine environments due to phytoplankton absorbing the lighter isotopes (Bain et al. 2024). This is a possible explanation as to the observed trend with nickel reducing as it enters the marine water. The relationship for distance with nickel could also be the result of upstream weathering of nickel rich geology or an upstream source of contamination. Whilst nickel shows one of the most discernible trends in this study, it cannot be confirmed whether the source of this trend is in relation to marine water intrusion or river position, or if it is a result of mine or other contamination or weathering. As a result, whilst further study is prompted for the potential usefulness of nickel as a proxy, it cannot be said if nickel is representing saltwater intrusion up the Waihou River or if the relationship represents contaminated material.

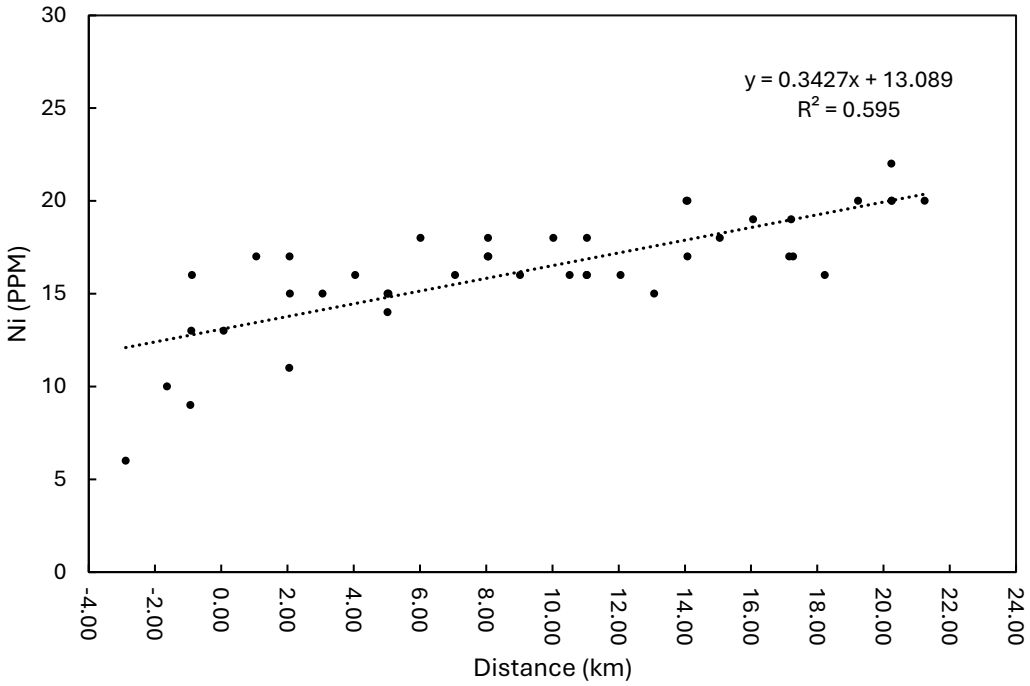

Figure 20. Nickel concentration along river distance of the lower Waihou River. Inclusive of samples 1-26 and cross sections B and C.

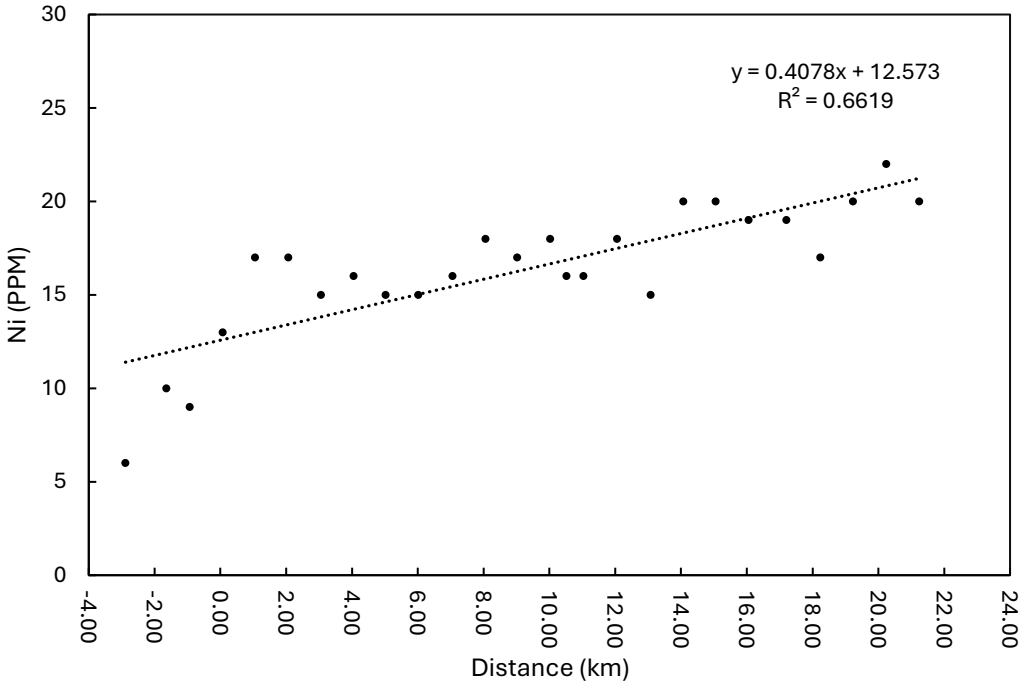

Figure 21.Nickel concentration along river distance of the lower Waihou River. Inclusive of samples 1-26, excluding cross sections samples B and C, and samples 27 and 28.

2.5.2 Comparison of proxy usage

Of the proxies tested within this study only the Sr/Ba proxy produce a definable relationship with river distance. The use of grainsize, %mud, and LOI showed no relationship across the lower Waihou River and XRD did not clearly identify any consistent pattern of mineral presence upstream. Carbon isotope data presented a negligible relationship and as a result neither $\delta^{13}C$ nor C/N could distinguish a clear trend upriver or in relation to salinity.

From this study, the proxy that best represents the marine water intrusion up the lower Waihou River is the Sr/Ba ratio however the trends observed in Sr/Ba against river distance do not represent the rapid changes in salinity range at the kilometre scale. This is likely the result of the sediment capturing the regularly changing dynamics of the river where tidal extent is dependent on river flow so the smaller more subtle changes in gradient are lost as they are not constant nor consistent enough for the sediment to settle and capture it. Since the river is a dynamic system, daily, monthly and seasonal changes will merge together to provide a range of distances for the expected values. Whilst the trend identifies, and can be used as, a proxy for salinity over a larger river scale, sample to sample variation is still high due to river fluctuations and cannot be used to identify the exact position along the river. This said, if the results are looked at a moderate scale where the lower river is divided into sections, it may be plausible to identify a range of expected Sr/Ba values as a means to indicate river position. The distance for each river studied would vary but with further investigation Sr/Ba could become a tool for identifying distinguishable sections of the FMTZ.

Although in this study no clear nor definitive answer can be derived regarding the ability of Sr/Ba as a means of whether the dynamics of the marine water intrusion are actually captured within the deposited sediment, it poses the plausibility of it on a mid-range scale. Carbon isotopes in this research provided no significant data to identify if a trend upstream occurs and for the purpose of this study is considered less than sufficient to draw a conclusion from.

2.5.3 Proxies in relation to literature

The use of proxies for marine water intrusion in past literature has provided varying results. The use of Sr/Ba-Hac from river sediments has occurred in the Fraser River Delta, Canada, the Yangtze River Delta, China (Dashtgard et al., 2022; Wang et al. 2021). Within the Fraser River it was identified that using shallow or near shallow samples only across the delta, 15km upriver to -14km out to sea, that there was a strong relationship between river distance (position) and Sr/Ba-Hac with an R^2 value of 0.75 (Dashtgard et al., 2022). A discernible and strong relationship between river position and Sr/Ba-Hac was identified by Wang et al. (2021). In comparison, results from this study identify a weak to moderate relationship with river position producing R^2 values of 0.40 (0.3965) and 0.41 (0.4071). Dashtgard et al. (2022) and Wang et al. (2021), both ranged in Sr/Ba (Sr/Ba-Hac) values between 0 - 6 and 0.42 - 24.20 respectively, while theses ranges seem to differ largely, the majority of both studies' data falls between 0 and 6. When these ranges are compared to the range found within this study it is clear there is a significant difference, the highest value was 49.8 followed by a 37.15, these two values are significantly higher than the values found within literature. Both highest values are the 2 furthest marine samples and S3C has another high value of 31.55. The strength in relationship observed in the literature and the results found in the Waihou River provide a disparity, where a strong relationship would have been anticipated based off previous findings yet one has not been identified. This could be the result of a few factors, Sr/Ba values could be affected by additional sediment processes occurring in the FMTZ, the trend could also be due to the variable flows and very tidally influenced marine water intrusion in the Waihou River, the barium starts to precipitate in various positions up the river in response to rainfall, tides, and salt wedge stratification. Since the discharge and area of flow of the Waihou River is less than many rivers used to study the proxy previously. The consistency of discharge and the overall influence of the marine intrusion will differ significantly between the river systems and as a result could be the potential explanation to why a promising proxy is shown to be lacking in the Waihou River.

Dashtgard et al, (2022), also looked at $\delta^{13}C$ as a proxy for marine water intrusion, and the shallow sample delta results had an R^2 value of 0.22 for river position. The relationship was deemed negligible between only the delta $\delta^{13}C$ and river position. It

was also found that within river (excluding the delta) there was a weak relationship with river position. The values were between -20‰ and -27‰ (Dashtgard et al, 2022), which was within range of expected values for $\delta^{13}C$ in a marine to terrestrial environment (Meyers, 1994). Dashtgard et al. (2022), found a weak relationship between salinity and $\delta^{13}C$ within the river. This varies from the lack of relationship observed in this study. Dashtgard et al. (2022), studied the Fraser River in Canada, which is located in too cold of a climate for mangroves, the river is also much larger than the Waihou so effects of bank erosion would be more diluted and of less significance in the Faser River, than in the narrow Waihou River where bank surface area and sediment to water discharge ratio is much larger. Another study also found that whilst $\delta^{13}C$ values were within the expected ranges that $\delta^{13}C$ did not represent marine water intrusion along the FMTZ (Czarnecki et al., 2014). Values were recorded between -21.08‰ and -26.55‰ within Czarnecki et al.'s (2014) study which match the ranges anticipated from marine and terrestrial sourced carbon (Meyers, 1994; Czarnecki et al., 2014).

In the results from this study the carbon isotope correlation with distance was also negligible (Figure 18C). Values found within the Waihou River match the ranges presented within Dashtgard et al. (2022) and Czarnecki et al, (2014) studies, but the relationships were weak for salinity and negligible for river distance, this implies that whilst similar patterns of $\delta^{13}C$ are found across literature, that the use of such a proxy for marine water intrusion across the fluvial to marine transition zone is inadequate for the purpose. The use of $\delta^{13}C$ is plausible but is largely affected by sediment load, erosion and deposition, and can be variable depending on the conditions, as well as the isotopic ranges for C3, C4 plants and algae or phytoplankton can overlap causing values which have an unknown nature that could be of a marine or a terrestrial carbon source (Han et al., 2021). This variability was acknowledged in Dashtgard et al. (2022) also. Perhaps the results found for $\delta^{13}C$ in this study indicate that there is strong mixing of marine and fluvial/terrestrial sourced carbon in the Waihou River or perhaps it instead flags the influence of strong depositional processes pushing carbon far beyond where it is sourced or the effect of increased soil carbon in the lower river. Whilst further implementation of $\delta^{13}C$ under different riverine conditions and systems is needed, the proxy seems to be unreliable at best or unrelated to salinity intrusion.

2.5.4 Mining impact on current day sediment

Webster (1995) investigated the presence of mining associated elements within the Tui Stream, Ohinemuri River and the Waihou River. Focusing on mainly the water chemistry, sediment and suspended sediment (85µm), they looked at lead (Pb), Iron (Fe), Manganese (Mn), Copper (Cu), Zinc (Zn), and Arsenic (As). Within the sediment fraction, high levels of trace metals were identified in the lower Waihou river, Mn, Fe, Cu, Pb, and Zn were identified as relatively high in the sediment. Lead levels were measured as 38.5 and 19.5 mg kg^{-1} (1mg kg^{-1} = 1 PPM) within the lower Waihou river between Kopu Bridge and the river mouth and Mn levels of 594 and 660 mg kg^{-1}. The equivalent location of where these values were taken is samples 6A, 6B and 6C, which when measured via XRF analysis had Pb values of 0, 0, 12 PPM and Mn in the form of MnO had values of 1973, 1026, and 1411 PPM. While the lead values are lower at that location, the Mn is significantly higher than measured by Webster (1995) at the same location. However, lead values of 212 and 227 PPM were identified within this study at S12A and S20, which are far higher than any Pb levels recorded in the Waihou River by Webster (1995), with the rest of the samples being consistent with levels found in the 1995 study. Iron values between this study and Webster's (1995) results have a similar range of values ~2-6% across the lower Waihou river and so do not seem as though there is any significant change.

It seems that in the current river setting, the Waihou River has an abundance of excess metals present within its sediment. A plausible explanation for the large increase and localised increases in trace metals identified within the sediment could be due to contaminated water that is continuously flowing into the FOT. The metals could be flocking with suspended sediment as identified by Webster (1995) and be accumulating disproportionately with the sediment deposition and perhaps not being flushed from the system with the non-flocked sediment, as a result of the past mining activity.

2.6 Conclusion

This study tested the viability of a series of proxies for marine water intrusion along river position. The first research aim provided the query of whether marine water intrusion could be recorded through grainsize, %mud, LOI, Sr/Ba, $\delta^{13}C$, C/N, XRD or XRF. Sr/Ba was the only proxy to present any evidence of marine water intrusion being represented within the sediment. At the beginning of this study $\delta^{13}C$ and Sr/Ba were the two most promising proxies to investigate. The relationships presented are negligible for the carbon isotopes and moderate at best for the Sr/Ba relationship with distance upriver. The Waihou river is a smaller river than many rivers which have been used for the past studies of these proxies, as a result small changes of bank erosion, mangroves, rainfall fluctuations and tidal forcing all have a greater influence than if it were to be a larger river in which conditions would be more stable. While no decisive answer can be given as to whether $\delta^{13}C$ or C/N are indicative of marine water intrusion up the Waihou, Sr/Ba can be said to represent a trend across the FMTZ and correlates with the large scale decrease in salinity upstream. However, in consideration of recording the complex dynamics of the FMTZ, Sr/Ba was not observed to clearly mark where salinity decreased nor where the range of salinities extended to. Future research is required to discern if the subtleties of the FMTZ are recorded in the sediment of the Waihou River.

Most proxies included within this research provided no relationship with river distance and no correlation with salinity. The proxy that did indicate a potential relation, Sr/Ba, had low values and high unexplained variability. This was theorised to be due to the variability of the Waihou River. River flow rate, tides, and stratifications may have more influence on the Waihou River compared to river systems that are larger and might be more stable and allow for continuous deposition in one location. As a result, it suggests that whilst further research is required on all proxies, future studies may benefit from further investigating carbon isotopes and Sr/Ba ratios as indicators of marine water intrusion. Further research into new proxies may also benefit the creation of a set of valuable proxies to be used within the FMTZ.

2.7 References

Alongi, D. M. (2012). Carbon sequestration in mangrove forests. *Carbon Management, 3,* 313-322.

Bian, X, Yang, S. C., Raad, R. J., Odendahl, C. E, Lanning, N. T., Sieber, M., Huang, K.F., Fitzsimmons, J. N., Conway, T. M. & John, S. G. (2024). Distribution and Cycling of Nickel and Nickel Isotopes in the Pacific Ocean. *Geophysical Research Letters*, *51*.

Blott, S. J. & Pye, K. (2001). GRADISTAT: a grain size distribution and statistics package for the analysis of unconsolidated sediments. E*arth Surface Processes and Landforms*, *26*, 1237–1248.

Chmura, G. L. and Aharon, P. (1995). Stable Carbon Isotope Signatures of Sedimentary Carbon in Coastal Wetlands as Indicators of Salinity Regime. *Journal of Coastal Research*, *11*(1), 124 -135.

Folk, R.L. and Ward, W.C. (1957). Brazos River Bar: A Study in the Significance of Grain-Size Parameters. *Journal of Sedimentary Petrology*, *27*, 3-26

Gugliotta, M., Flint, S., Hodgson, D. M., & Veiga, G. D. (2016). Recognition Criteria, Characteristics and Implications of the Fluvial to Marine Transition Zon in Ancient Deltaic Deposits (Lajas, Formation Argentina). *Sedimentology*, *63*(7)

Han, H., Hwang, J., & Kim, G. (2020). Characterizing the origin of excess dissolved organic carbon in coastal seawater using stable carbon isotope and light absorption characteristics. *Biogeosciences*, *18*(5), 1793–1801.

Haque, M., & Reza, M. (2017). Salinity intrusion affecting the ecological integrity of Sundarbans Mangrove Forests, Bangladesh. *International Journal of Conservation Science*, *8*, 131-144.

Jablonski, B.V.J. & Dalrymple, R.W. (2016). Recognition of strong seasonality and climatic cyclicity in an ancient, fluvially dominated, tidally influenced point bar: middle McMurray Formation, Lower Steepbank River, north-eastern Alberta, Canada. Sedimentology, 63, 552-585.

James, B. (2024). Measurements and modelling of the tidal salt intrusion along the Waihou River [MSc Thesis].

Land Air Water Aotearoa. (n.d-b). Waihou River. https://www.lawa.org.nz/explore-data/waikato-region/river-quality/waihou-river

Land Air Water Aotearoa. (n.d-c). *Waikato Region – Surface water zone: Waihou River at mouth*. https://www.lawa.org.nz/explore-data/waikato-region/water-quantity/surface-water-zones/waihou-river-at-mouth

Langel, R., Dyckmans, J. (2017) A closer look into the nitrogen blank in elemental analyser/isotope ratio mass spectrometry measurements. *Rapid Communications in Mass Spectrometry*, *31*(23), 2051-2055

Levin, L., Boesch, D., Covich, A., Dahm, C., Erséus, C., Ewel, K., Kneib, R., Moldenke, A., Palmer, M., Snelgrove, P., Strayer, D., & Weslawski, J. (2001). The Function of Marine Critical Transition Zones and the Importance of Sediment Biodiversity. *Ecosystems, 4*, 430-451. 10.1007/s10021-001-0021-4

Meyers, P. A. (1994) Preservation of elemental and isotopic source identification of sedimentary organic matter. *Chemical Geology, 114*(3-4), 289-302

Ohlsson, K.E. (2013) Uncertainty of blank correction in isotope ratio measurement. *Analytical Chemistry*, *85*(11), 5326-5329.

Paul, D., Skrzypek, G. and Fórizs, I., 2007. Normalization of measured stable isotopic compositions to isotope reference scales - a review. *Rapid Communications in Mass Spectrometry*, *21*, 3006-3014.

Richards, B. H., & Bhattacharya, J. P. (2018). Stratigraphy of the fluvial-to-marine transition zone associated with a forced-regressive compound incised-valley

system in the Turonian Ferron Notom Delta, Utah, U.S.A. *Journal of Sedimentary Research*, *88*(3), 311–326. https://doi.org/10.2110/jsr.2018.17

Swales, A., Bentley, S. J., Lovelock, C., & Bell, R. G. (2007). Sediment processes and mangrove-habitat expansion on a rapidly-prograding Muddy Coast, New Zealand. Coastal Sediments '07 - Proceedings of 6th International Symposium on Coastal Engineering and Science of Coastal Sediment Processes, 1441-1454

Szklarek, S., Górecka, A. & Wojtal-Frankiewicz, A. (2022). The effects of road salt on freshwater ecosystems and solutions for mitigating chloride pollution - A review. *Science of the Total Environment*, *805*.

Walcker, R., Corenblit, D., Julien, F., Martinez, J. M., & Steiger, J. (2021). Contribution of meandering rivers to natural carbon fluxes: Evidence from the Ucayali River, Peruvian Amazonia. *Science of the Total Environment, 776*.

Chapter 3

Conclusions

3.1 Conclusion of results

The goals for this study were to identify if and to what extent physical and geochemical proxies record the nuances of marine water intrusion along the fluvial to marine transition zone (FMTZ) of the Waihou River and produce a list of viable proxies to be expanded upon by future works. To achieve these goals surface sediment samples were collected using a grab sampler approximately 1km apart, up the lower Waihou River. These samples were analysed for proxies of grainsize and percent mud (%mud) as the physical proxies, and loss on ignition (LOI), $\delta^{13}C$, carbon nitrogen ratio (C/N), strontium barium ratio (Sr/Ba), XRD and XRF as geochemical proxies. With the use of salinity datasets from James (2024), this allowed me to compare the proxies to river distance upstream and correlate the relationship to the salinity found upstream as marine water intrusion.

To answer whether sediment proxies for marine water intrusion can be used to record the processes of the fluvial to marine transition, the answer is potentially. Of the proxies identified only one showed any notion of having evidence of the marine water intrusion. The Sr/Ba ratio allowed for a relation between river position and salinity to be shown. However, the gradual changes in upstream gradient for marine water intrusion displayed by Sr/Ba is faint and instead Sr/Ba shows a larger scale change from marine to fresh water. The distances upstream at which salinity was shown to decrease in range showed no significant change in values from Sr/Ba, instead the Sr/Ba values decreased at an overall constant rate at the larger scale with values varying sample to sample.

Testing the robustness of proxies as an indicator of marine water intrusion and creating a series of proxies for future studies to use provides insights into the usefulness of the proxies. It was found that though the tested proxies have been suggested and used in the past as a measure of marine intrusion or river position, in this study the significance was minimal and the only proxy that showed promise provided it in the form of weak to

moderate relationship with large levels of variance. Further consideration of the value and validity of these proxies will have to be made in future works regarding the significance and level of certainty provided by them. A list of working proxies has instead been potentially reduced, while further investigation on the usefulness of all proxies in this study is recommended, only strontium and barium ratios showed any significant indication of being valuable within the Waihou River.

3.2 Limitations

Within this study limitations which may have impacted the outcomes of the results are to be considered. One of the largest limitations present within this study was the lack of my own salinity data and only using the data collected by James (2024). Whilst the long term data serves to provide a range of values recorded over multiple months it also made a direct comparison more difficult. The utilisation of both James' (2024) data and salinity measurements made in the field at the time of sample collection may have made a direct comparison easier. As the sediment was surface sediment and the Waihou River has high variance in rainfall, discharge and high sediment load it Is also difficult to say when the sediment was deposited and whether the salinity data collected by James (2024), was representative of the salinity at the time of sediment deposition as the samples for this study were collected in August however the salinity data was collected September through March. It is unknown if the salinity ranges may have varied over the winter months with the potential of higher rainfall prior to my sample collection causing increased river flow and so it is unknown if the salinity ranges measured correspond with the salinity conditions over the timeframe of sediment deposition for this study. Ideally if this study is to be furthered, salinity measurements will have a full annual range of values detected to see how seasonal influence may change the way the sediment proxies and salinity with distance upstream can be correlated.

Another limitation of this study which may have impacted the validity of results was the use of the grab sampler. The mechanism on the grab sampler had two main issues which need to be mentioned. The first is that the mechanism would fail to trigger and

collect sediment or would trigger and miss occasionally. Whilst this delayed the collection of the sediment it may have also disturbed the sediment and sent sediment into the water column or relocated it which may have influenced the second attempt at sample collection. The second issue was that the grab sampler was not watertight once closed and on more than one occasion failed to close properly allowing the sediment to fall out during extraction. This poses a potential issue as some of the finer sediments may have been lost through the grab sampler as it was pulled from the riverbed into the boat. This therefore may have had an impact of the results, especially if fine sediment was lost more in some samples than other potentially impacting the overall conclusions of the study. It is not possible to know whether this occurred during the successful collections of the samples.

At the time of fieldwork planning and sample collection distances of approximately 1km felt appropriate. However, throughout the study I found that an increase in the number of samples closer together may have provided clarity on any trends observed and whether confirmation of smaller spatial details could have been identified.

Appendices

Appendix A. Grainsize data.

Table 1. Data from the Mastersizer showing the proportion of samples within the grainsize intervals.

	Sample Name	Sample 1	Sample 2	Sample 3A	Sample 3B
	Measurement Date Time	3/10/2023 14:57	3/10/2023 15:08	29/09/2023 9:34	29/09/2023 9:43
Grainsize (µm)	0.05	0	0	0	0
	0.06	0	0	0	0
	0.12	0	0	0	0
	0.24	0	0	0	0
	0.49	0	0	0	0
	0.98	1.82	1.33	0.48	0.32
	2	4.5	2.95	1.24	0.73
	3.9	9.52	5.6	2.49	1.5
	7.8	16.11	8.83	4.27	2.53
	15.6	21.73	11.84	6.16	3.59
	31	25.81	14.13	8.39	4.32
	37	26.86	14.64	8.96	4.46
	44	27.95	15.17	9.39	4.63
	53	29.2	15.82	9.71	4.89
	63	30.41	16.48	10.01	5.22
	74	31.59	17.11	10.54	5.56
	88	32.99	17.73	11.86	5.87
	105	34.79	18.25	14.64	6.04
	125	37.19	18.71	19.07	6.07
	149	40.79	19.4	25.65	6.13
	177	45.69	20.76	33.74	6.73
	210	51.92	23.29	42.78	8.45
	250	59.62	27.96	52.31	12.57
	300	68.29	35.11	61.82	19.79
	350	75.53	42.86	69.1	28.42
	420	83.13	53.56	76.52	41.37
	500	89.12	64.18	82.64	54.98
	590	93.49	73.75	87.61	67.74
	710	96.75	82.83	92.17	80.09
	840	98.64	89.43	95.48	88.92
	1000	99.67	94.35	97.91	95.12
	1190	99.99	97.52	99.36	98.59
	1410	100	99.37	99.96	99.93
	1680	100	100	100	100
	2000	100	100	100	100
	2380	100	100	100	100
	2830	100	100	100	100
	3360	100	100	100	100
Grainsize Statistics	Dx (10)	4.11	10.1	62.8	227
	Dx (50)	200	396	239	470
	Dx (90)	514	853	647	859
	D [4,3]	229	432	306	505
	D [3,2]	11.8	19.3	37.9	64.5
	Kurtosis [3]	0.957	0.508	2.214	0.364
	Skew [3]	1.031	0.746	1.431	0.541
	Mode	288	449	224	486
	Span	2.553	2.13	2.439	1.347
	Laser Obscuration	13.66	15.37	24.33	14.98
	Weighted Residual	0.42	0.39	0.26	0.41
	Residual	0.23	0.31	0.25	0.41

Sample 3C	Sample 4	Sample 5	Sample 6A	Sample 6B	Sample 6C
3/10/2023 15:16	29/09/2023 9:59	29/09/2023 10:10	29/09/2023 10:20	29/09/2023 10:28	29/09/2023 10:37
0	0	0	0	0	0
0	0	0	0	0	0
0	0	0	0	0	0
0	0	0	0	0	0
0	0	0	0.04	0.09	0.06
0.67	0	0	2.64	6.45	5.65
1.54	0.13	0	5.6	14.1	13.57
3.19	0.84	0.38	9.57	27.08	26
5.37	1.85	0.97	15.24	45.9	42.53
7.39	3.06	1.66	21.82	64.19	58.13
9.3	4.14	2.32	27.07	76.52	69.46
9.93	4.43	2.48	28.32	79.07	71.62
10.59	4.73	2.65	29.64	81.56	73.65
11.32	5.07	2.87	31.23	84.31	75.9
12.01	5.36	3.1	32.92	86.94	78.21
12.74	5.56	3.33	34.71	89.39	80.58
13.85	5.68	3.6	36.98	91.92	83.33
15.81	5.68	3.88	39.85	94.22	86.21
19.01	5.68	4.2	43.43	96.14	88.95
24.3	5.76	4.73	48.21	97.59	91.36
31.62	6.57	5.68	54.11	98.57	93.32
40.78	9.06	7.36	61.06	99.22	94.87
51.67	14.99	10.5	69.01	99.62	96.07
63.39	24.98	15.63	77.39	99.87	97.09
72.69	36.23	21.75	83.94	99.99	97.85
81.81	51.71	31.52	90.2	100	98.61
88.51	66.51	42.76	94.63	100	99.23
93	78.92	54.59	97.41	100	99.68
96.11	89.2	67.94	99.06	100	99.94
97.9	95.41	79.04	99.77	100	100
99	98.84	88.36	100	100	100
99.6	99.95	94.9	100	100	100
99.91	100	98.78	100	100	100
100	100	100	100	100	100
100	100	100	100	100	100
100	100	100	100	100	100
100	100	100	100	100	100
100	100	100	100	100	100
37.7	217	245	4.14	1.39	1.49
244	412	554	158	9.01	10.7
524	722	1040	417	77.1	135
279	437	598	184	26	47.1
31	106	179	10.5	4	4.32
4.194	0.414	0.065	0.897	10.851	15.044
1.535	0.445	0.573	1.017	2.932	3.499
264	421	604	256	7.57	6.43
1.997	1.227	1.435	2.62	8.401	12.427
17.01	17.9	15.56	14.85	13.02	15.29
0.28	0.45	0.49	0.44	0.97	0.91
0.26	0.41	0.47	0.25	0.41	0.45

Sample 7	Sample 8	Sample 9A	Sample 9B	Sample 9C	Sample 10
29/09/2023 10:45	29/09/2023 10:55	29/09/2023 11:05	29/09/2023 11:14	29/09/2023 11:23	29/09/2023 11:31
0	0	0	0	0	0
0	0	0	0	0	0
0	0	0	0	0	0
0	0	0	0	0	0
0.03	0	0.05	0	0.05	0
1.69	0.13	3.97	0	5.04	0.37
3.44	0.16	8.92	0.04	12.42	0.88
5.89	0.65	15.47	0.67	23.71	1.79
8.87	1.22	23.64	1.45	37.64	2.95
11.96	1.82	31.85	2.22	50.4	4.23
14.97	2.35	38.15	2.91	60.81	5.37
15.85	2.51	39.76	3.16	63.75	5.73
16.65	2.7	41.51	3.43	66.97	6.17
17.33	2.93	43.69	3.71	70.86	6.73
17.75	3.15	46.05	3.88	74.79	7.29
18.11	3.33	48.56	3.93	78.54	7.75
18.87	3.49	51.65	3.93	82.45	8.08
20.85	3.67	55.34	3.99	86.06	8.18
24.67	4.04	59.56	4.5	89.14	8.27
31.46	5.01	64.61	6.56	91.67	8.86
40.89	6.95	70.28	10.97	93.68	10.56
52.38	10.24	76.44	18.22	95.36	14
65.21	15.71	82.93	29.14	96.79	20.36
77.92	23.58	89.26	43	98.08	29.79
86.95	31.86	93.77	55.62	98.95	39.69
94.26	43.23	97.43	69.8	99.62	52.76
98.33	54.75	99.43	81.37	99.96	65.2
99.99	65.52	100	89.75	100	75.9
100	76.37	100	95.64	100	85.43
100	84.71	100	98.68	100	91.86
100	91.35	100	99.96	100	96.16
100	95.91	100	100	100	98.51
100	98.75	100	100	100	99.6
100	99.95	100	100	100	99.95
100	100	100	100	100	100
100	100	100	100	100	100
100	100	100	100	100	100
100	100	100	100	100	100
9.99	208	2.27	172	1.63	170
203	466	80.4	327	15.2	404
375	960	307	594	132	796
205	528	120	355	48	446
16.9	125	6.94	121	4.79	54.2
-0.336	0.755	0.154	0.657	8.083	1.451
0.225	0.931	0.987	0.708	2.616	0.911
234	479	223	330	67.8	417
1.798	1.616	3.787	1.292	8.583	1.548
16.12	15.92	15.25	21	16.33	20.62
0.37	0.29	0.65	0.39	0.84	0.24
0.3	0.26	0.37	0.36	0.4	0.23

Sample 11	Sample 12A	Sample 12B	Sample 12C	Sample 13	Sample 14
29/09/2023 11:43	3/10/2023 11:18	3/10/2023 11:28	3/10/2023 11:36	3/10/2023 11:44	3/10/2023 11:52
0	0	0	0	0	0
0	0	0	0	0	0
0	0	0	0	0	0
0	0	0	0	0	0
0.22	0	0	0.15	0	0.12
9.68	0.72	0	8.67	0.3	5.56
18.99	1.49	0.11	18.31	0.44	10.42
31.16	2.68	0.69	30.89	1.16	17.1
45.13	4.1	1.47	46.56	2.02	27.16
59.34	5.54	2.32	64.2	2.87	39.34
70.24	6.62	3.2	78.16	3.6	49.07
72.47	6.94	3.4	81.32	3.88	51.24
74.61	7.34	3.58	84.37	4.2	53.43
77.01	7.86	3.77	87.54	4.53	55.97
79.46	8.38	3.97	90.27	4.76	58.6
81.95	8.8	4.22	92.55	4.87	61.29
84.83	9.1	4.56	94.62	4.88	64.47
87.86	9.29	4.98	96.29	4.97	67.99
90.74	9.66	5.41	97.56	5.61	71.66
93.29	10.92	5.74	98.45	7.92	75.51
95.35	13.79	5.93	99.04	12.63	79.36
96.92	18.92	6.03	99.45	20.15	83.18
98.03	27.53	6.42	99.72	31.17	86.99
98.84	39.55	7.72	99.91	44.85	90.75
99.31	51.51	10.21	100	57.03	93.61
99.68	66.28	16.05	100	70.37	96.35
99.89	79.26	24.66	100	81.03	98.29
100	89.22	35.64	100	88.68	99.45
100	96.36	50.45	100	94.15	99.95
100	99.67	64.43	100	97.2	100
100	100	77.7	100	98.85	100
100	100	88.19	100	99.6	100
100	100	95.39	100	99.91	100
100	100	99.18	100	100	100
100	100	100	100	100	100
100	100	100	100	100	100
100	100	100	100	100	100
100	100	100	100	100	100
1	133	346	1.07	164	1.9
9.84	343	706	8.93	320	33.4
119	601	1230	61.9	614	289
38.8	354	742	22.6	358	97
3.39	36.5	141	3.45	74.8	5.67
11.695	-0.171	0.03	15.424	3.06	2.817
2.991	0.156	0.317	3.347	1.271	1.753
9.31	374	749	10.3	319	179
12.04	1.362	1.255	6.813	1.406	8.585
14.97	16.33	18.67	14.83	20.47	14.59
1.08	0.54	0.84	1.07	0.34	0.74
0.69	0.53	0.8	0.42	0.34	0.42

Sample 15	Sample 16A	Sample 16B	Sample 16C	Sample 17	Sample 18
3/10/2023 12:01	3/10/2023 12:09	3/10/2023 12:18	3/10/2023 12:26	3/10/2023 12:35	3/10/2023 12:44
0	0	0	0	0	0
0	0	0	0	0	0
0	0	0	0	0	0
0	0	0	0	0	0
0	0.06	0	0.03	0	0
0.54	3.8	0.27	1.21	0.34	0.38
1.17	7.98	0.54	2.29	0.83	0.88
2.16	13.97	1.17	3.86	1.66	1.75
3.35	22.25	1.96	5.88	2.73	2.89
4.61	31.49	2.83	8.09	3.95	4.05
5.66	39.3	3.7	10.58	5.07	5.37
5.93	41.16	3.88	11.38	5.38	5.82
6.27	42.98	4.08	12.12	5.72	6.25
6.73	44.98	4.36	12.75	6.15	6.64
7.24	46.93	4.72	13.19	6.58	6.94
7.72	48.91	5.14	13.68	6.95	7.26
8.13	51.4	5.64	14.81	7.25	7.95
8.35	54.61	6.09	17.49	7.45	9.58
8.39	58.58	6.39	22.32	7.63	12.57
8.44	63.67	6.47	30.41	8.15	17.8
8.95	69.56	6.48	41.23	9.45	25.18
10.74	75.97	6.76	53.97	12.01	34.47
15.42	82.6	8.36	67.65	16.8	45.63
23.82	88.96	12.34	80.68	24.17	57.84
33.75	93.43	18.29	89.49	32.25	67.78
48.07	97.08	29.17	96.1	43.71	77.97
62.31	99.14	42.31	99.38	55.45	85.84
74.71	100	56.16	100	66.47	91.42
85.55	100	71.15	100	77.46	95.46
92.55	100	82.83	100	85.78	97.77
96.88	100	91.78	100	92.22	99.08
98.98	100	97.35	100	96.5	99.71
99.82	100	99.84	100	99.06	99.98
100	100	100	100	100	100
100	100	100	100	100	100
100	100	100	100	100	100
100	100	100	100	100	100
100	100	100	100	100	100
198	2.58	275	27.1	186	109
430	80.1	549	199	462	267
784	310	960	354	936	564
459	122	578	204	513	307
45.5	7.34	79.9	23.6	58.5	51.2
1.019	0.249	0.084	-0.22	0.589	2.916
0.641	1.008	0.318	0.183	0.773	1.348
442	216	571	223	484	274
1.362	3.832	1.248	1.639	1.624	1.705
19.62	15.3	18.3	18.26	24.56	23.27
0.4	0.62	0.48	0.35	0.25	0.27
0.4	0.37	0.48	0.32	0.24	0.26

Sample 19A	Sample 19B	Sample 19C	Sample 20	Sample 21	Sample 22A
3/10/2023 12:51	3/10/2023 13:05	3/10/2023 13:13	3/10/2023 13:21	3/10/2023 13:29	3/10/2023 13:39
0	0	0	0	0	0
0	0	0	0	0	0
0	0	0	0	0	0
0	0	0	0	0	0
0	0.05	0.15	0.04	0.08	0.03
0.83	3.25	8.33	1.42	3.76	1.78
1.76	7.24	17.15	2.9	7.56	3.57
3.12	13.09	29.5	5.14	12.84	6.14
4.68	20.3	45.28	7.85	19.03	9.57
6.38	27.53	61.77	10.74	25.76	13.84
8.23	33.45	74.15	13.66	30.85	18.14
8.69	35.03	76.61	14.47	31.91	19.47
9.15	37	78.92	15.31	33.06	20.9
9.73	39.99	81.36	16.29	34.64	22.51
10.49	44	83.64	17.34	36.67	23.98
11.51	48.84	85.75	18.52	39.17	25.27
13.11	55.31	87.94	20.22	42.67	26.65
15.45	62.91	90.02	22.72	47.14	28.34
18.42	70.78	91.87	26.18	52.24	30.7
22.15	78.39	93.45	31.16	57.93	34.48
26.41	84.99	94.77	37.55	63.77	39.87
31.19	90.42	95.93	45.28	69.62	46.92
36.8	94.46	96.98	54.44	75.47	55.78
43.49	97.37	97.97	64.59	81.34	65.85
49.91	98.89	98.72	73.04	85.97	74.31
58.52	99.72	99.39	81.98	90.8	83.22
67.35	99.98	99.81	89.05	94.66	90.17
75.8	100	100	94.1	97.42	95.02
84.43	100	100	97.6	99.25	98.23
90.97	100	100	99.34	99.94	99.74
95.83	100	100	100	100	100
98.72	100	100	100	100	100
99.93	100	100	100	100	100
100	100	100	100	100	100
100	100	100	100	100	100
100	100	100	100	100	100
100	100	100	100	100	100
100	100	100	100	100	100
56.8	2.82	1.11	13.1	2.78	8.4
351	76.6	9.47	230	116	224
818	207	105	513	406	498
400	90.8	37.1	255	161	240
31.3	8.08	3.61	19.2	8.07	15.7
0.103	1.248	14.275	0.436	1.156	0.031
0.77	1.126	3.495	0.786	1.245	0.671
507	116	9.35	286	186	292
2.17	2.666	10.954	2.172	3.477	2.189
16.34	20.01	16.05	24.28	17.05	16.2
0.27	0.55	1.03	0.24	0.55	0.35
0.24	0.35	0.69	0.17	0.33	0.25

Sample 22B	Sample 22C	Sample 23	Sample 24	Sample 25A	Sample 25B
3/10/2023 13:49	3/10/2023 13:57	3/10/2023 14:05	3/10/2023 14:13	3/10/2023 14:21	3/10/2023 14:30
0	0	0	0	0	0
0	0	0	0	0	0
0	0	0	0	0	0
0	0	0	0	0	0
0	0.16	0	0	0	0
0.3	8.11	0.28	0.59	0	0
0.71	15.98	0.63	1.28	0.23	0.25
1.44	26.37	1.37	2.45	1.03	1.12
2.44	39.28	2.32	3.95	1.98	2.16
3.42	54	3.38	5.42	2.98	3.22
4.63	68.74	4.33	7.57	3.76	4.05
5.08	72.61	4.71	8.21	4.03	4.25
5.49	76.37	5.18	8.7	4.35	4.49
5.79	80.25	5.75	9	4.74	4.83
5.86	83.52	6.22	9.22	5.06	5.2
5.86	86.18	6.52	9.78	5.26	5.54
6.06	88.51	6.63	11.47	5.28	5.84
7.12	90.32	6.66	15.38	5.31	5.99
9.69	91.66	6.98	21.92	5.61	6.02
15	92.65	8.43	31.9	7.06	6.08
23.08	93.46	11.77	44.23	10.5	6.78
33.68	94.24	17.57	57.81	16.6	9
46.6	95.13	26.8	71.35	26.54	14.51
60.59	96.19	39.05	83.51	39.91	24.08
71.68	97.15	50.64	91.32	52.66	35.21
82.43	98.24	64.29	96.89	67.59	51.05
90.14	99.12	75.96	99.56	80.05	66.58
95.05	99.69	84.97	100	89.17	79.83
98.04	99.96	92	100	95.52	90.79
99.4	100	96.18	100	98.72	97.23
99.91	100	98.57	100	100	99.99
100	100	99.62	100	100	100
100	100	99.98	100	100	100
100	100	100	100	100	100
100	100	100	100	100	100
100	100	100	100	100	100
100	100	100	100	100	100
100	100	100	100	100	100
127	1.15	165	76.8	174	218
261	13	347	191	339	415
498	101	666	341	603	698
288	45.2	383	200	362	431
59.5	3.9	66.2	36.2	95.1	94.6
1.612	15.123	1.513	0.072	0.457	0.028
0.955	3.701	0.935	0.337	0.535	0.158
266	35.5	351	205	349	434
1.421	7.729	1.443	1.383	1.265	1.157
23.08	14.19	19.08	23.53	20.31	19.08
0.24	0.99	0.32	0.29	0.41	0.45
0.24	0.61	0.31	0.28	0.39	0.42

Sample 25C	Sample 26	Sample 27	Sample 28
3/10/2023 14:38	3/10/2023 14:48	6/10/2023 9:08	6/10/2023 9:19
0	0	0	0
0	0	0	0
0	0	0	0
0	0	0	0
0	0	0.1	0
0.49	0	6.27	0
1.24	0.12	13.81	0
2.42	0.76	23.91	0.15
3.86	1.65	34.23	0.65
5.44	2.64	43.35	1.19
6.94	3.74	52.13	1.79
7.38	4.01	54.44	1.92
7.87	4.29	56.69	2.04
8.43	4.62	59.05	2.17
8.95	5.02	61.2	2.35
9.4	5.49	63.23	2.57
9.83	6.1	65.58	2.87
10.33	6.79	68.35	3.22
11.11	7.43	71.59	3.52
12.75	7.9	75.52	3.69
15.69	8.22	79.91	3.74
20.33	8.57	84.6	3.74
27.53	9.55	89.33	3.99
37.29	12.01	93.75	5.24
47	15.94	96.71	7.95
59.4	23.9	98.88	14.68
71	34.5	99.88	24.68
80.87	46.81	100	37.25
89.47	61.81	100	53.63
95.05	74.75	100	68.44
98.46	85.89	100	81.72
99.83	93.79	100	91.5
100	98.5	100	97.63
100	100	100	99.99
100	100	100	100
100	100	100	100
100	100	100	100
100	100	100	100
94	262	1.42	373
366	614	26.3	682
719	1080	257	1150
395	641	85.2	718
41.6	123	4.69	256
0.221	-0.062	1.111	0.045
0.576	0.281	1.388	0.335
404	660	207	705
1.709	1.339	9.696	1.142
25.24	18.35	18.04	12.17
0.25	0.62	0.91	0.72
0.24	0.59	0.57	0.72

Table 2. GRADISTAT data identifying grainsize, proportion of grainsizes (%mud), and the proportion of samples within grainsize intervals.

		Sample 1	**Sample 2**	**Sample 3A**
	ANALYST AND DATE:	, 11/6/2023	, 11/7/2023	, 11/9/2023
	SAMPLE TYPE:	Bimodal, Very Poorly Sorted	Unimodal, Very Poorly Sorted	Unimodal, Poorly Sorted
	TEXTURAL GROUP:	Muddy Sand	Muddy Sand	Sand
	SEDIMENT NAME:	Fine Silty Medium Sand	Fine Silty Medium Sand	Poorly Sorted Fine Sand
FOLK AND WARD METHOD (μm)	MEAN (M_G):	87.14	252.3	240.4
	SORTING (σ_G):	6.490	4.541	2.866
	SKEWNESS (Sk_G):	-0.603	-0.593	-0.217
	KURTOSIS (K_G):	0.917	2.362	1.769
FOLK AND WARD METHOD (Description)	MEAN:	Very Fine Sand	Medium Sand	Fine Sand
	SORTING:	Very Poorly Sorted	Very Poorly Sorted	Poorly Sorted
	SKEWNESS:	Very Fine Skewed	Very Fine Skewed	Fine Skewed
	KURTOSIS:	Mesokurtic	Very Leptokurtic	Very Leptokurtic
	MODE 1 (μm):	275.0	460.0	230.0
	D_{10} (μm):	4.102	10.21	62.64
	D_{50} (μm):	199.2	395.3	239.7
	D_{90} (μm):	516.9	857.1	650.1
	(D_{90} / D_{10}) (μm):	126.0	83.94	10.38
	(D_{90} - D_{10}) (μm):	512.8	846.9	587.5
	(D_{75} / D_{25}) (μm):	12.79	2.704	2.763
	(D_{75} - D_{25}) (μm):	319.0	381.4	258.2
	D_{10} (ϕ):	0.952	0.222	0.621
	D_{50} (ϕ):	2.328	1.339	2.061
	D_{90} (ϕ):	7.929	6.614	3.997
	(D_{90} / D_{10}) (ϕ):	8.330	29.74	6.434
	(D_{90} - D_{10}) (ϕ):	6.978	6.391	3.376
	(D_{75} / D_{25}) (ϕ):	3.402	2.981	2.123
	(D_{75} - D_{25}) (ϕ):	3.677	1.435	1.466
	% GRAVEL:	0.0%	0.0%	0.0%
	% SAND:	69.6%	83.6%	90.0%
	% MUD:	30.4%	16.4%	10.0%
	% V COARSE GRAVEL:	0.0%	0.0%	0.0%
	% COARSE GRAVEL:	0.0%	0.0%	0.0%
	% MEDIUM GRAVEL:	0.0%	0.0%	0.0%
	% FINE GRAVEL:	0.0%	0.0%	0.0%
	% V FINE GRAVEL:	0.0%	0.0%	0.0%
	% V COARSE SAND:	0.3%	5.7%	2.1%
	% COARSE SAND:	10.6%	30.2%	15.3%
	% MEDIUM SAND:	29.5%	36.2%	30.3%
	% FINE SAND:	22.4%	9.3%	33.2%
	% V FINE SAND:	6.8%	2.3%	9.1%
	% V COARSE SILT:	4.5%	2.3%	1.6%
	% COARSE SILT:	4.1%	2.3%	2.3%
	% MEDIUM SILT:	5.6%	3.0%	1.9%
	% FINE SILT:	6.6%	3.2%	1.8%
	% V FINE SILT:	5.1%	2.7%	1.3%
	% CLAY:	4.4%	2.9%	1.2%

Sample 3B	Sample 3C	Sample 4	Sample 5
, 9/29/2023	, 11/8/2023	, 9/30/2023	, 10/1/2023
Unimodal, Poorly Sorted	Unimodal, Poorly Sorted	Unimodal, Moderately Sorted	Unimodal, Moderately Sorted
Sand	Muddy Sand	Sand	Sand
Poorly Sorted Medium Sand	Very Coarse Silty Medium Sand	Moderately Sorted Medium Sand	Moderately Sorted Coarse Sand
460.8	225.6	407.7	536.5
2.001	2.856	1.927	1.797
-0.264	-0.359	-0.264	-0.163
1.703	2.116	1.833	1.106
Medium Sand	Fine Sand	Medium Sand	Coarse Sand
Poorly Sorted	Poorly Sorted	Moderately Sorted	Moderately Sorted
Fine Skewed	Very Fine Skewed	Fine Skewed	Fine Skewed
Very Leptokurtic	Very Leptokurtic	Very Leptokurtic	Mesokurtic
460.0	275.0	385.0	650.0
224.2	37.69	215.9	243.2
469.1	243.4	411.6	553.3
865.9	528.2	725.5	1044.6
3.862	14.02	3.361	4.296
641.7	490.5	509.7	801.4
1.998	2.420	1.866	2.125
328.6	215.1	259.9	418.3
0.208	0.921	0.463	-0.063
1.092	2.039	1.281	0.854
2.157	4.730	2.212	2.040
10.38	5.137	4.778	-32.417
1.949	3.809	1.749	2.103
2.653	1.880	2.076	4.199
0.999	1.275	0.900	1.087
0.0%	0.0%	0.0%	0.0%
94.8%	88.0%	94.7%	96.9%
5.2%	12.0%	5.3%	3.1%
0.0%	0.0%	0.0%	0.0%
0.0%	0.0%	0.0%	0.0%
0.0%	0.0%	0.0%	0.0%
0.0%	0.0%	0.0%	0.0%
0.0%	0.0%	0.0%	0.0%
4.9%	1.0%	1.2%	11.6%
40.1%	10.5%	32.3%	45.6%
42.4%	36.8%	51.5%	32.3%
6.5%	32.7%	9.3%	6.3%
0.9%	7.0%	0.3%	1.1%
0.9%	2.6%	1.2%	0.8%
0.7%	1.9%	1.1%	0.7%
1.1%	2.0%	1.2%	0.7%
1.0%	2.2%	1.0%	0.6%
0.8%	1.7%	0.7%	0.4%
0.7%	1.5%	0.1%	0.0%

Sample 6A	Sample 6B	Sample 6C	Sample 7
, 10/2/2023	, 10/3/2023	, 10/4/2023 9	, 10/5/2023
Bimodal, Very Poorly Sorted	Bimodal, Very Poorly Sorted	Bimodal, Very Poorly Sorted	Unimodal, Poorly Sorted
Muddy Sand	Sandy Mud	Sandy Mud	Muddy Sand
Medium Silty Medium Sand	Very Fine Sandy Fine Silt	Very Fine Sandy Fine Silt	Medium Silty Fine Sand
77.48	10.14	13.15	137.1
6.009	4.630	5.766	3.639
-0.577	0.064	0.122	-0.617
0.937	0.959	0.866	2.461
Very Fine Sand	Medium Silt	Medium Silt	Fine Sand
Very Poorly Sorted	Very Poorly Sorted	Very Poorly Sorted	Poorly Sorted
Very Fine Skewed	Symmetrical	Coarse Skewed	Very Fine Skewed
Mesokurtic	Mesokurtic	Platykurtic	Very Leptokurtic
275.0	5.850	5.850	230.0
4.110	1.365	1.450	10.05
157.0	9.111	10.87	202.7
417.6	77.16	134.9	377.7
101.6	56.54	93.06	37.58
413.5	75.79	133.5	367.6
12.04	8.128	13.31	2.282
261.2	24.98	45.50	161.6
1.260	3.696	2.890	1.405
2.671	6.778	6.523	2.303
7.926	9.517	9.430	6.637
6.291	2.575	3.263	4.724
6.667	5.821	6.540	5.232
2.981	1.589	1.859	1.662
3.590	3.023	3.735	1.190
0.0%	0.0%	0.0%	0.0%
67.2%	13.2%	21.9%	82.3%
32.8%	86.8%	78.1%	17.7%
0.0%	0.0%	0.0%	0.0%
0.0%	0.0%	0.0%	0.0%
0.0%	0.0%	0.0%	0.0%
0.0%	0.0%	0.0%	0.0%
0.0%	0.0%	0.0%	0.0%
0.0%	0.0%	0.0%	0.0%
5.4%	0.0%	0.8%	1.7%
25.6%	0.4%	3.2%	33.1%
25.6%	3.5%	7.1%	40.5%
10.6%	9.3%	10.8%	6.9%
5.7%	10.2%	8.5%	2.7%
5.3%	12.4%	11.4%	3.0%
6.6%	18.3%	15.6%	3.1%
5.7%	18.8%	16.5%	3.0%
4.1%	13.3%	12.7%	2.5%
5.5%	13.8%	13.3%	3.4%

Sample 8	Sample 9A	Sample 9B	Sample 9C
, 10/6/2023	, 10/11/2023	, 10/7/2023	, 10/8/2023
Unimodal, Moderately Sorted	Bimodal, Very Poorly Sorted	Unimodal, Moderately Sorted	Bimodal, Very Poorly Sorted
Sand	Muddy Sand	Sand	Sandy Mud
Moderately Sorted Medium Sand	Medium Silty Fine Sand	Moderately Sorted Medium Sand	Very Fine Sandy Fine Silt
459.4	43.86	324.9	15.30
1.836	6.780	1.643	5.588
-0.074	-0.453	-0.057	-0.015
1.033	0.756	1.035	0.802
Medium Sand	Very Coarse Silt	Medium Sand	Medium Silt
Moderately Sorted	Very Poorly Sorted	Moderately Sorted	Very Poorly Sorted
Symmetrical	Very Fine Skewed	Symmetrical	Symmetrical
Mesokurtic	Platykurtic	Mesokurtic	Platykurtic
460.0	230.0	325.0	68.50
207.4	2.233	170.4	1.583
465.3	80.22	326.8	15.26
965.2	307.7	594.7	132.7
4.654	137.8	3.489	83.83
757.8	305.5	424.2	131.1
2.252	23.06	1.941	15.29
385.6	193.0	220.2	59.41
0.051	1.700	0.750	2.914
1.104	3.640	1.614	6.034
2.270	8.807	2.553	9.303
44.38	5.179	3.404	3.193
2.218	7.106	1.803	6.389
3.218	2.961	1.840	1.990
1.171	4.527	0.957	3.934
0.0%	0.0%	0.0%	0.0%
96.9%	54.1%	96.1%	25.4%
3.1%	45.9%	3.9%	74.6%
0.0%	0.0%	0.0%	0.0%
0.0%	0.0%	0.0%	0.0%
0.0%	0.0%	0.0%	0.0%
0.0%	0.0%	0.0%	0.0%
0.0%	0.0%	0.0%	0.0%
8.7%	0.0%	0.0%	0.0%
36.6%	0.6%	18.6%	0.0%
39.0%	16.5%	52.2%	3.2%
11.7%	23.4%	24.6%	7.7%
0.9%	13.6%	0.6%	14.5%
0.8%	7.7%	1.0%	13.7%
0.5%	6.4%	0.7%	10.5%
0.6%	8.2%	0.8%	12.8%
0.6%	8.2%	0.8%	13.9%
0.5%	6.7%	0.6%	11.6%
0.2%	8.8%	0.0%	12.2%

Sample 10	Sample 11	Sample 12A	Sample 12B
, 10/9/2023	, 10/10/2023	, 10/12/2023	, 10/13/2023
Unimodal, Poorly Sorted	Trimodal, Very Poorly Sorted	Unimodal, Poorly Sorted	Unimodal, Moderately Sorted
Sand	Sandy Mud	Sand	Sand
Poorly Sorted Medium Sand	Very Fine Sandy Medium Silt	Poorly Sorted Medium Sand	Moderately Sorted Coarse Sand
395.6	10.96	328.3	690.1
2.309	6.207	2.395	1.886
-0.293	0.057	-0.393	-0.271
1.981	0.809	2.411	1.620
Medium Sand	Medium Silt	Medium Sand	Coarse Sand
Poorly Sorted	Very Poorly Sorted	Poorly Sorted	Moderately Sorted
Fine Skewed	Symmetrical	Very Fine Skewed	Fine Skewed
Very Leptokurtic	Platykurtic	Very Leptokurtic	Very Leptokurtic
385.0	11.70	385.0	775.0
167.2	1.004	131.1	345.5
404.1	9.892	343.3	706.0
800.1	119.5	602.1	1241.8
4.784	119.0	4.593	3.595
632.9	118.5	471.0	896.4
2.128	16.31	1.988	1.920
308.4	42.57	234.7	462.6
0.322	3.065	0.732	-0.312
1.307	6.660	1.543	0.502
2.580	9.960	2.932	1.533
8.020	3.250	4.005	-4.907
2.258	6.895	2.200	1.846
2.394	1.902	1.916	19.39
1.089	4.027	0.991	0.941
0.0%	0.0%	0.0%	0.0%
92.7%	20.7%	91.6%	96.0%
7.3%	79.3%	8.4%	4.0%
0.0%	0.0%	0.0%	0.0%
0.0%	0.0%	0.0%	0.0%
0.0%	0.0%	0.0%	0.0%
0.0%	0.0%	0.0%	0.0%
0.0%	0.0%	0.0%	0.0%
3.8%	0.0%	0.0%	22.3%
31.0%	0.1%	20.7%	53.0%
44.8%	1.9%	51.7%	18.2%
12.1%	7.3%	17.9%	1.0%
1.0%	11.4%	1.3%	1.4%
1.9%	9.0%	1.7%	0.8%
1.2%	11.0%	1.1%	0.9%
1.3%	14.2%	1.4%	0.9%
1.2%	14.0%	1.4%	0.8%
0.9%	12.5%	1.2%	0.6%
0.9%	18.7%	1.5%	0.1%

Sample 12C	Sample 13	Sample 14	Sample 15
, 10/14/2023	, 10/15/2023	, 10/16/2023	, 10/17/2023
Unimodal, Very Poorly Sorted	Unimodal, Moderately Sorted	Trimodal, Very Poorly Sorted	Unimodal, Poorly Sorted
Mud	Sand	Sandy Mud	Sand
Medium Silt	Moderately Sorted Medium Sand	Fine Sandy Medium Silt	Poorly Sorted Medium Sand
8.656	319.5	29.42	422.2
4.679	1.737	7.021	2.297
-0.033	-0.071	-0.143	-0.327
0.889	1.155	0.805	2.367
Medium Silt	Medium Sand	Coarse Silt	Medium Sand
Very Poorly Sorted	Moderately Sorted	Very Poorly Sorted	Poorly Sorted
Symmetrical	Symmetrical	Fine Skewed	Very Fine Skewed
Platykurtic	Leptokurtic	Platykurtic	Very Leptokurtic
11.70	325.0	163.0	460.0
1.081	160.8	1.880	195.7
8.929	320.2	33.44	430.0
61.93	617.0	289.3	790.1
57.27	3.837	153.8	4.038
60.85	456.2	287.4	594.4
9.302	1.998	21.66	1.941
23.68	226.3	138.9	287.4
4.013	0.697	1.789	0.340
6.807	1.643	4.902	1.217
9.853	2.637	9.055	2.354
2.455	3.785	5.060	6.924
5.840	1.940	7.265	2.014
1.615	1.874	2.596	2.268
3.218	0.999	4.437	0.956
0.0%	0.0%	0.0%	0.0%
9.9%	95.3%	41.5%	92.8%
90.1%	4.7%	58.5%	7.2%
0.0%	0.0%	0.0%	0.0%
0.0%	0.0%	0.0%	0.0%
0.0%	0.0%	0.0%	0.0%
0.0%	0.0%	0.0%	0.0%
0.0%	0.0%	0.0%	0.0%
0.0%	1.2%	0.0%	3.1%
0.0%	17.8%	1.7%	34.6%
0.3%	49.9%	11.3%	46.9%
2.2%	25.6%	15.3%	7.0%
7.4%	0.9%	13.2%	1.2%
11.8%	1.1%	9.3%	1.5%
14.1%	0.7%	9.8%	1.1%
17.6%	0.8%	12.2%	1.3%
15.7%	0.9%	10.1%	1.2%
12.9%	0.7%	6.9%	1.0%
18.0%	0.4%	10.3%	1.1%

Sample 16A	Sample 16B	Sample 16C	Sample 17
, 10/18/2023	, 10/19/2023	, 10/20/2023	, 10/21/2023
Bimodal, Very Poorly Sorted	Unimodal, Moderately Sorted	Unimodal, Poorly Sorted	Unimodal, Poorly Sorted
Muddy Sand	Sand	Muddy Sand	Sand
Medium Silty Fine Sand	Moderately Sorted Coarse Sand	Very Coarse Silty Fine Sand	Poorly Sorted Medium Sand
45.79	537.6	182.0	449.4
6.548	1.929	2.577	2.343
-0.436	-0.276	-0.444	-0.288
0.770	1.738	2.365	1.850
Very Coarse Silt	Coarse Sand	Fine Sand	Medium Sand
Very Poorly Sorted	Moderately Sorted	Poorly Sorted	Poorly Sorted
Very Fine Skewed	Fine Skewed	Very Fine Skewed	Fine Skewed
Platykurtic	Very Leptokurtic	Very Leptokurtic	Very Leptokurtic
230.0	545.0	230.0	460.0
2.505	269.5	26.42	183.6
79.83	548.1	199.1	461.1
311.0	965.9	355.0	941.7
124.1	3.584	13.44	5.128
308.4	696.4	328.5	758.0
21.35	1.916	2.091	2.235
195.0	358.8	144.6	376.4
1.685	0.050	1.494	0.087
3.647	0.867	2.328	1.117
8.641	1.892	5.242	2.445
5.127	37.81	3.508	28.20
6.956	1.842	3.748	2.358
2.929	3.265	1.575	3.095
4.416	0.938	1.064	1.160
0.0%	0.0%	0.0%	0.0%
53.2%	95.3%	86.8%	93.4%
46.8%	4.7%	13.2%	6.6%
0.0%	0.0%	0.0%	0.0%
0.0%	0.0%	0.0%	0.0%
0.0%	0.0%	0.0%	0.0%
0.0%	0.0%	0.0%	0.0%
0.0%	0.0%	0.0%	0.0%
0.0%	8.2%	0.0%	7.8%
0.9%	49.5%	0.6%	36.8%
16.5%	34.0%	31.7%	38.7%
24.0%	2.0%	45.3%	9.2%
11.7%	1.7%	9.2%	1.1%
7.5%	1.0%	2.6%	1.5%
7.9%	0.9%	2.5%	1.1%
9.2%	0.9%	2.2%	1.2%
8.3%	0.8%	2.0%	1.1%
6.1%	0.6%	1.6%	0.8%
7.8%	0.5%	2.3%	0.8%

Sample 18	Sample 19A	Sample 19B	Sample 19C
, 10/22/2023	, 10/23/2023	, 10/24/2023	, 10/25/2023
Unimodal, Poorly Sorted	Unimodal, Poorly Sorted	Bimodal, Very Poorly Sorted	Bimodal, Very Poorly Sorted
Sand	Muddy Sand	Muddy Sand	Sandy Mud
Poorly Sorted Medium Sand	Very Coarse Silty Medium Sand	Very Coarse Silty Very Fine Sand	Very Fine Sandy Medium Silt
261.9	299.1	40.80	10.39
2.243	3.250	5.338	5.628
-0.233	-0.411	-0.536	0.074
1.660	1.545	0.891	0.950
Medium Sand	Medium Sand	Very Coarse Silt	Medium Silt
Poorly Sorted	Poorly Sorted	Very Poorly Sorted	Very Poorly Sorted
Fine Skewed	Very Fine Skewed	Very Fine Skewed	Symmetrical
Very Leptokurtic	Very Leptokurtic	Platykurtic	Mesokurtic
275.0	545.0	115.0	11.70
107.6	56.36	2.741	1.122
266.9	350.7	76.33	9.512
565.7	819.3	207.2	104.8
5.257	14.54	75.62	93.45
458.1	763.0	204.5	103.7
2.260	3.474	11.26	10.78
222.0	413.6	125.5	29.90
0.822	0.288	2.271	3.254
1.906	1.512	3.712	6.716
3.216	4.149	8.511	9.800
3.913	14.43	3.748	3.012
2.394	3.862	6.241	6.546
1.885	3.292	2.221	1.697
1.176	1.797	3.493	3.430
0.0%	0.0%	0.0%	0.0%
93.1%	89.5%	56.2%	16.5%
6.9%	10.5%	43.8%	83.5%
0.0%	0.0%	0.0%	0.0%
0.0%	0.0%	0.0%	0.0%
0.0%	0.0%	0.0%	0.0%
0.0%	0.0%	0.0%	0.0%
0.0%	0.0%	0.0%	0.0%
0.9%	4.2%	0.0%	0.0%
13.2%	28.5%	0.0%	0.2%
40.2%	30.6%	5.5%	2.8%
33.1%	18.4%	23.7%	5.1%
5.6%	8.0%	27.0%	8.3%
1.5%	2.2%	10.3%	9.3%
1.3%	1.9%	6.0%	12.5%
1.2%	1.7%	7.2%	16.5%
1.1%	1.6%	7.2%	15.8%
0.9%	1.4%	6.0%	12.7%
0.9%	1.7%	7.1%	16.9%

Sample 20	Sample 21	Sample 22A	Sample 22B
, 10/26/2023	, 10/27/2023	, 10/28/2023	, 10/29/2023
Unimodal, Poorly Sorted	Bimodal, Very Poorly Sorted	Bimodal, Very Poorly Sorted	Unimodal, Moderately Sorted
Muddy Sand	Muddy Sand	Muddy Sand	Sand
Very Coarse Silty Medium Sand	Medium Silty Fine Sand	Very Coarse Silty Medium Sand	Moderately Sorted Medium Sand
172.0	59.52	128.2	258.7
3.735	6.902	4.698	1.987
-0.506	-0.499	-0.597	-0.224
1.854	0.870	1.360	1.622
Fine Sand	Very Coarse Silt	Fine Sand	Medium Sand
Poorly Sorted	Very Poorly Sorted	Very Poorly Sorted	Moderately Sorted
Very Fine Skewed	Very Fine Skewed	Very Fine Skewed	Fine Skewed
Very Leptokurtic	Platykurtic	Leptokurtic	Very Leptokurtic
275.0	193.5	275.0	275.0
13.06	2.723	8.364	126.3
229.7	115.8	223.1	261.3
515.8	407.5	497.9	498.4
39.49	149.6	59.53	3.947
502.8	404.8	489.5	372.1
3.093	17.09	4.961	2.028
246.5	232.1	283.4	187.7
0.955	1.295	1.006	1.005
2.122	3.110	2.164	1.936
6.258	8.521	6.902	2.985
6.553	6.579	6.859	2.972
5.303	7.225	5.895	1.981
2.118	3.027	2.546	1.712
1.629	4.095	2.311	1.020
0.0%	0.0%	0.0%	0.0%
82.7%	63.4%	76.1%	94.1%
17.3%	36.6%	23.9%	5.9%
0.0%	0.0%	0.0%	0.0%
0.0%	0.0%	0.0%	0.0%
0.0%	0.0%	0.0%	0.0%
0.0%	0.0%	0.0%	0.0%
0.0%	0.0%	0.0%	0.0%
0.0%	0.0%	0.0%	0.1%
11.0%	5.3%	9.8%	9.8%
34.6%	19.2%	34.4%	43.5%
28.3%	23.2%	25.1%	36.9%
8.9%	15.7%	6.8%	3.8%
3.6%	5.7%	5.7%	1.2%
2.9%	5.1%	4.4%	1.2%
2.9%	6.7%	4.3%	1.0%
2.7%	6.2%	3.4%	1.0%
2.3%	5.4%	2.6%	0.7%
2.9%	7.4%	3.5%	0.7%

Sample 22C	Sample 23	Sample 24	Sample 25A
, 10/30/2023	, 10/31/2023	, 11/1/2023	, 11/2/2023
Trimodal, Very Poorly Sorted	Unimodal, Poorly Sorted	Unimodal, Poorly Sorted	Unimodal, Moderately Sorted
Sandy Mud	Sand	Sand	Sand
Very Fine Sandy Coarse Silt	Poorly Sorted Medium Sand	Poorly Sorted Fine Sand	Moderately Sorted Medium Sand
11.88	342.9	183.3	335.0
5.733	2.044	2.182	1.838
-0.029	-0.235	-0.342	-0.221
0.969	1.707	2.026	1.539
Medium Silt	Medium Sand	Fine Sand	Medium Sand
Very Poorly Sorted	Poorly Sorted	Poorly Sorted	Moderately Sorted
Symmetrical	Fine Skewed	Very Fine Skewed	Fine Skewed
Mesokurtic	Very Leptokurtic	Very Leptokurtic	Very Leptokurtic
34.00	325.0	193.5	325.0
1.163	161.6	75.69	172.6
12.92	347.0	190.3	338.9
101.8	673.6	341.0	604.5
87.50	4.169	4.505	3.502
100.6	512.0	265.3	431.8
11.57	2.040	2.001	1.915
37.74	251.2	132.1	222.5
3.297	0.570	1.552	0.726
6.274	1.527	2.393	1.561
9.748	2.630	3.724	2.534
2.957	4.613	2.399	3.489
6.451	2.060	2.172	1.808
1.768	2.008	1.521	1.850
3.532	1.028	1.001	0.937
0.0%	0.0%	0.0%	0.0%
16.6%	93.8%	90.8%	95.0%
83.4%	6.2%	9.2%	5.0%
0.0%	0.0%	0.0%	0.0%
0.0%	0.0%	0.0%	0.0%
0.0%	0.0%	0.0%	0.0%
0.0%	0.0%	0.0%	0.0%
0.0%	0.0%	0.0%	0.0%
0.0%	1.4%	0.0%	0.0%
0.9%	22.6%	0.4%	20.0%
4.0%	49.2%	28.2%	53.5%
3.5%	19.8%	49.4%	20.9%
8.3%	0.8%	12.7%	0.6%
14.5%	1.9%	1.6%	1.3%
14.9%	1.0%	2.2%	0.8%
14.7%	1.1%	1.5%	1.0%
12.9%	1.0%	1.5%	1.0%
10.7%	0.8%	1.2%	0.8%
15.7%	0.6%	1.3%	0.2%

Sample 25B	Sample 25C	Sample 26	Sample 27
, 11/3/2023	, 11/4/2023	, 11/5/2023	, 11/10/2023
Unimodal, Moderately Sorted	Unimodal, Poorly Sorted	Unimodal, Poorly Sorted	Trimodal, Very Poorly Sorted
Sand	Sand	Sand	Sandy Mud
Moderately Sorted Medium Sand	Poorly Sorted Medium Sand	Poorly Sorted Coarse Sand	Fine Sandy Very Fine Silt
407.3	345.7	593.3	23.19
1.864	2.580	2.030	7.543
-0.285	-0.368	-0.314	-0.120
1.784	2.084	1.805	0.685
Medium Sand	Medium Sand	Coarse Sand	Coarse Silt
Moderately Sorted	Poorly Sorted	Poorly Sorted	Very Poorly Sorted
Fine Skewed	Very Fine Skewed	Very Fine Skewed	Fine Skewed
Very Leptokurtic	Very Leptokurtic	Very Leptokurtic	Platykurtic
460.0	385.0	650.0	193.5
216.8	93.45	258.5	1.395
415.0	365.8	613.7	26.24
700.6	721.4	1094.7	257.0
3.232	7.720	4.235	184.3
483.8	628.0	836.2	255.6
1.828	2.274	1.972	34.69
251.6	299.5	415.6	141.4
0.513	0.471	-0.131	1.960
1.269	1.451	0.704	5.252
2.206	3.420	1.952	9.486
4.297	7.259	-14.950	4.839
1.693	2.949	2.082	7.526
2.026	2.312	4.984	2.840
0.870	1.185	0.980	5.117
0.0%	0.0%	0.0%	0.0%
94.8%	91.1%	95.0%	38.9%
5.2%	8.9%	5.0%	61.1%
0.0%	0.0%	0.0%	0.0%
0.0%	0.0%	0.0%	0.0%
0.0%	0.0%	0.0%	0.0%
0.0%	0.0%	0.0%	0.0%
0.0%	0.0%	0.0%	0.0%
0.0%	1.5%	14.1%	0.0%
33.4%	27.5%	51.4%	0.1%
52.1%	43.5%	25.0%	10.6%
8.5%	16.4%	2.1%	17.7%
0.8%	2.2%	2.4%	10.5%
1.1%	2.0%	1.2%	8.9%
0.8%	1.5%	1.1%	8.9%
1.1%	1.6%	1.0%	9.1%
1.0%	1.4%	0.9%	10.3%
0.9%	1.2%	0.6%	10.4%
0.2%	1.2%	0.1%	13.6%

Sample 28
, 11/11/2023
Unimodal, Moderately Well Sorted
Sand
Moderately Well Sorted Coarse Sand
673.1
1.568
-0.087
1.030
Coarse Sand
Moderately Well Sorted
Symmetrical
Mesokurtic
650.0
370.0
681.5
1158.7
3.132
788.7
1.823
413.4
-0.212
0.553
1.434
-6.751
1.647
7.809
0.867
0.0%
97.7%
2.3%
0.0%
0.0%
0.0%
0.0%
0.0%
18.3%
57.0%
20.7%
0.5%
1.2%
0.5%
0.6%
0.5%
0.5%
0.2%
0.0%

Appendix B. Loss on Ignition (LOI)

Table 3. Data for measurements taken to calculate loss on ignition.

Container weight	0.55g					
Sample Name	Weight (g) at 105	Minus container	weight (g) at 550	Minus Container	% LOI	weight loss (g)
1	6.96	6.41	6.71	6.16	3.90	0.25
2	6.53	5.98	6.32	5.77	3.51	0.21
3A	5.6	5.05	5.38	4.83	4.36	0.22
3B	7.22	6.67	7.06	6.51	2.40	0.16
3C	6.26	5.71	5.97	5.42	5.08	0.29
4	8.99	8.44	8.8	8.25	2.25	0.19
5	7.34	6.79	7.19	6.64	2.21	0.15
6A	5.99	5.44	5.65	5.1	6.25	0.34
6B	4.58	4.03	4.19	3.64	9.68	0.39
6C	5.33	4.78	4.99	4.44	7.11	0.34
7	5.38	4.83	5.17	4.62	4.35	0.21
8	6.54	5.99	6.39	5.84	2.50	0.15
9A	7.91	7.36	7.65	7.1	3.53	0.26
9B	6.57	6.02	6.38	5.83	3.16	0.19
9C	5.42	4.87	5.02	4.47	8.21	0.4
10	8.12	7.57	7.94	7.39	2.38	0.18
11	3.78	3.23	3.53	2.98	7.74	0.25
12A	8.03	7.48	7.85	7.3	2.41	0.18
12B	7.54	6.99	7.41	6.86	1.86	0.13
12C	4.87	4.32	4.59	4.04	6.48	0.28
13	5.69	5.14	5.52	4.97	3.31	0.17
14	6.75	6.2	6.49	5.94	4.19	0.26
15	8.35	7.8	8.16	7.61	2.44	0.19
16A	5.79	5.24	5.53	4.98	4.96	0.26
16B	8.43	7.88	8.28	7.73	1.90	0.15
16C	7.18	6.63	6.99	6.44	2.87	0.19
17	8.93	8.38	8.73	8.18	2.39	0.2
18	8.04	7.49	7.87	7.32	2.27	0.17
19A	4.87	4.32	4.76	4.21	2.55	0.11
19B	4.6	4.05	4.44	3.89	3.95	0.16
19C	4.95	4.4	4.58	4.03	8.41	0.37
20	8.05	7.5	7.77	7.22	3.73	0.28
21	4.79	4.24	4.59	4.04	4.72	0.2
22A	5.3	4.75	5.11	4.56	4.00	0.19
22B	7.38	6.83	7.2	6.65	2.64	0.18
22C	6.11	5.56	5.79	5.24	5.76	0.32
23	8.51	7.96	8.3	7.75	2.64	0.21
24	7.5	6.95	7.27	6.72	3.31	0.23
25A	8.31	7.76	8.15	7.6	2.06	0.16
25B	9.9	9.35	9.69	9.14	2.25	0.21
25C	8.94	8.39	8.67	8.12	3.22	0.27
26	8.57	8.02	8.33	7.78	2.99	0.24
27	4.93	4.38	4.57	4.02	8.22	0.36
28	7.6	7.05	7.51	6.96	1.28	0.09
Repeart Samples						
6B(2)	5.9	5.35	5.33	4.78	10.65	0.57
9C(2)	5.09	4.54	4.65	4.1	9.69	0.44
6C(2)	4.31	3.76	4	3.45	8.24	0.31
11(2)	4.78	4.23	4.35	3.8	10.17	0.43
19C(2)	5.77	5.22	5.35	4.8	8.05	0.42
27(2)	4.94	4.39	4.55	4	8.88	0.39
8(2)	5.79	5.24	5.6	5.05	3.63	0.19
15(2)	7.18	6.63	6.99	6.44	2.87	0.19

Appendix C. Strontium and Barium Ratio

Table 4. Data for showing strontium and barium values for all 44 samples.

Analysis No.	Sample No.	Sr	Ba
HC23120101	1	146	3.93
HC23120102	2	135	20.7
HC23120103	3A	27.3	18.6
HC23120104	3B	23.8	21.9
HC23120105	3c	130	4.12
HC23120106	4	21.0	17.2
HC23120107	5	26.9	35.1
HC23120108	6A	28.2	16.7
HC23120109	6B	39.5	8.73
HC23120110	6C	38.5	7.89
HC23120111	7	17.9	12.6
HC23120112	8	25.4	29.8
HC23120113	9A	18.6	11.6
HC23120114	9B	18.9	23.6
HC23120115	9C	30.5	16.3
HC23120116	10	19.0	24.3
HC23120117	11	35.8	24.1
HC23120118	12A	17.2	39.9
HC23120119	12B	23.6	66.7
HC23120120	12C	44.5	16.2

Analysis No.	Sample No.	Sr	Ba
HC23120121	13	17.1	41.2
HC23120122	14	20.8	19.8
HC23120123	15	16.0	52.5
HC23120124	16A	26.8	25.9
HC23120125	16B	18.8	56.6
HC23120126	16C	22.0	27.8
HC23120127	17	19.0	53.6
HC23120128	18	14.7	57.3
HC23120129	19A	14.5	77.8
HC23120130	19B	23.4	27.1
HC23120131	19C	30.0	36.6
HC23120132	20	15.3	56.6
HC23120133	21	18.6	40.0
HC23120134	22A	16.5	29.8
HC23120135	22B	11.3	57.8
HC23120136	22C	28.4	27.2
HC23120137	23	12.9	102
HC23120138	24	12.4	74.7
HC23120139	25A	11.5	99.5
HC23120140	25B	15.7	150

Analysis No.	Sample No.	Sr	Ba
HC23120141	25C	13.1	109
HC23120142	26	13.9	156
HC23120143	27	125	2.51
HC23120144	28	6.83	83.3

Appendix D. Carbon isotopic data

Table 5. Carbon Isotope data, carbon/nitrogen, and nitrogen isotope data of the fine grained fraction for 33 of 44 samples.

Corrected Identifier 1	Corrected Amount (mg)
Sample 1_Sed_Acid	58.294
Sample 1_Sed_Acid_test	20.178
Sample 11_Sed_Sieved 63um_Acid	21.489
Sample 12A_Sed_Acid	52.831
Sample 12C_Sed_Sieved 63um_Acid	21.288
Sample 13_Sed_Acid	59.938
Sample 14_Sed_Sieved 63um_Acid	19.607
Sample 16A_Sed_Sieved 63um_Acid	20.226
Sample 16B_Sed_Acid	57.963
Sample 16C_Sed_Acid	58.719
Sample 18_Sed_Acid	61.648
Sample 19A_Sed_Acid	57.247
Sample 19B_Sed_Acid_test	31.27
Sample 19B_Sed_Sieved 63um_Acid	20.442
Sample 19C_Sed_Sieved 63um_Acid	19.216
Sample 2_Sed_Acid_lw	20.212
Sample 20_Sed_Acid	55.294
Sample 21_Sed_Sieved 63um_Acid	19.994
Sample 22A_Sed_Acid_w	20.818
Sample 22C_Sed_Sieved 63um_Acid	21.42
Sample 24_Sed_Acid_lw	20.342
Sample 25B_Sed_Acid_lw	20.256
Sample 27_Sed_Sieved 63um_Acid	20.227
Sample 3A_Sed_Acid	54.17
Sample 3B_Sed_Acid	51.998
Sample 3C_Sed_Acid	55.757
Sample 5_Sed_Acid	60.757
Sample 6A_Sed_Acid	59.816
Sample 6B_Sed_Sieved 63um_Acid	19.282
Sample 6C_Sed_Sieved 63um_Acid	21.501
Sample 7_Sed_Acid	50.746
Sample 8_Sed_Acid	54.487
Sample 9A_Sed_Sieved 63um_Acid	19.621
Sample 9C_Sed_Sieved 63um_Acid	20.724

SIA Sample ID	Sample Type	Ampl Flash TCD (mV)	All Correct Amt% N Flash TCD	Ampl 28 (mV)	normalised d15N	Blank corrected?
Sample 1	Sediment - marine	6828	0.21	3601	8.65	N
Sample 1_Acid_Test		2758	0.21	1426	8.71	Y
Sample 11_Sed_Sieved 63µm_Acid	Sediment - marine	4282	0.30	2096	7.73	N
Sample 12A	Sediment - marine	6824	0.19	3415	7.62	N
Sample 12C_Sed_Sieved 63µm_Acid	Sediment - marine	2382	0.17	1176	8.06	Y
Sample 13	Sediment - marine	5634	0.14	2831	8.43	N
Sample 14_Sed_Sieved 63µm_Acid	Sediment - marine	2674	0.21	1317	8.33	Y
Sample 16A_Sed_Sieved 63µm_Acid	Sediment - marine	2942	0.22	1447	8.32	Y
Sample 16B	Sediment - marine	7030	0.19	3496	15.18	N
Sample 16C	Sediment - marine	7625	0.19	3809	8.55	N
Sample 18	Sediment - marine	3455	0.09	1808	6.71	N
Sample 19A	Sediment - marine	6266	0.16	3239	6.54	N
Sample 19B_Acid_Test	Sediment - marine	3500	0.17	1806	6.85	N
Sample 19B_Sed_Sieved 63µm_Acid	Sediment - marine	2645	0.20	1301	7.44	Y
Sample 19C_Sed_Sieved 63µm_Acid	Sediment - marine	2707	0.22	1327	7.86	Y
Sample 2	Sediment - marine	3162	0.24	1579	9.29	Y
Sample 20	Sediment - marine	7118	0.19	3658	7.25	N
Sample 21_Sed_Sieved 63µm_Acid	Sediment - marine	2310	0.18	1137	7.83	Y
Sample 22A	Sediment - marine	1618	0.12	817	7.67	Y
Sample 22C_Sed_Sieved 63µm_Acid	Sediment - marine	2989	0.21	1463	8.74	Y
Sample 24	Sediment - marine	1162	0.09	592	5.88	Y
Sample 25B	Sediment - marine	2289	0.17	1149	8.55	Y
Sample 27_Sed_Sieved 63µm_Acid	Sediment - marine	4164	0.31	2036	8.80	N
Sample 3A	Sediment - marine	3899	0.13	2059	7.51	N
Sample 3B	Sediment - marine	4730	0.16	2503	7.73	N
Sample 3C	Sediment - marine	6705	0.22	3527	8.22	N
Sample 5	Sediment - marine	4187	0.13	2222	6.80	N
Sample 6A	Sediment - marine	6442	0.21	3417	7.17	N
Sample 6B_Sed_Sieved 63µm_Acid	Sediment - marine	3190	0.25	1571	8.03	Y
Sample 6C_Sed_Sieved 63µm_Acid	Sediment - marine	3271	0.23	1605	8.05	Y
Sample 7	Sediment - marine	6855	0.27	3646	7.00	N
Sample 8	Sediment - marine	3025	0.11	1620	8.13	Y
Sample 9A_Sed_Sieved 63µm_Acid	Sediment - marine	2639	0.21	1296	7.94	Y
Sample 9C_Sed_Sieved 63µm_Acid	Sediment - marine	2789	0.21	1373	7.54	Y

SIA Sample ID	Sample Type	Ampl Flash TCD (mV)	All Correct Amt% C Flash TCD	Ampl 44 (mV)	normalised d13C	Sample Dilution (%)	C:N mass ratio
Sample 1	Sediment - marine	137077.0	1.7	6001.0	-24.2	92.0	8.3
Sample 1_Acid_Test		57499.0	1.7	2361.0	-24.3	92.0	8.3
Sample 11_Sed_Sieved 63µm_Acid	Sediment - marine	96296.0	2.8	15100.0	-25.0	72.0	9.3
Sample 12A	Sediment - marine	142293.0	1.8	6071.0	-24.8	92.0	9.3
Sample 12C_Sed_Sieved 63µm_Acid	Sediment - marine	61852.0	1.8	9584.0	-25.5	72.0	10.5
Sample 13	Sediment - marine	125386.0	1.4	5276.0	-26.2	92.0	9.9
Sample 14_Sed_Sieved 63µm_Acid	Sediment - marine	59160.0	1.9	9109.0	-24.7	72.0	8.9
Sample 16A_Sed_Sieved 63µm_Acid	Sediment - marine	66156.0	2.0	10231.0	-24.7	72.0	9.0
Sample 16B	Sediment - marine	145878.0	1.7	6263.0	-25.5	92.0	9.0
Sample 16C	Sediment - marine	151348.0	1.7	6446.0	-25.1	92.0	9.0
Sample 18	Sediment - marine	88600.0	0.9	3837.0	-27.1	92.0	10.7
Sample 19A	Sediment - marine	146141.0	1.7	6534.0	-26.6	92.0	10.3
Sample 19B_Acid_Test	Sediment - marine	93598.0	1.9	3964.0	-25.9	92.0	11.0
Sample 19B_Sed_Sieved 63µm_Acid	Sediment - marine	65159.0	2.0	10066.0	-25.6	72.0	9.9
Sample 19C_Sed_Sieved 63µm_Acid	Sediment - marine	61604.0	2.0	9487.0	-25.0	72.0	9.1
Sample 2	Sediment - marine	58381.0	1.8	9181.0	-23.9	72.0	7.4
Sample 20	Sediment - marine	153627.0	1.9	6842.0	-26.3	92.0	9.7
Sample 21_Sed_Sieved 63µm_Acid	Sediment - marine	55059.0	1.7	8442.0	-24.8	72.0	9.5
Sample 22A	Sediment - marine	37879.0	1.1	5885.0	-24.4	72.0	9.0
Sample 22C_Sed_Sieved 63µm_Acid	Sediment - marine	63532.0	1.8	9774.0	-24.2	72.0	8.5
Sample 24	Sediment - marine	33147.0	1.0	5102.0	-27.5	72.0	11.0
Sample 25B	Sediment - marine	49866.0	1.5	7795.0	-23.4	72.0	8.6
Sample 27_Sed_Sieved 63µm_Acid	Sediment - marine	74899.0	2.3	11576.0	-21.8	72.0	7.3
Sample 3A	Sediment - marine	98759.0	1.3	4220.0	-25.7	92.0	10.2
Sample 3B	Sediment - marine	111180.0	1.6	4792.0	-24.8	92.0	9.6
Sample 3C	Sediment - marine	134924.0	1.8	5931.0	-23.8	92.0	8.3
Sample 5	Sediment - marine	103684.0	1.3	4461.0	-25.9	92.0	10.0
Sample 6A	Sediment - marine	141437.0	1.9	6314.0	-25.2	92.0	9.2
Sample 6B_Sed_Sieved 63µm_Acid	Sediment - marine	71681.0	2.3	11137.0	-24.9	72.0	9.1
Sample 6C_Sed_Sieved 63µm_Acid	Sediment - marine	74463.0	2.1	11562.0	-24.9	72.0	9.2
Sample 7	Sediment - marine	154508.0	2.6	7085.0	-25.9	92.0	9.7
Sample 8	Sediment - marine	75434.0	1.1	3244.0	-26.2	92.0	9.9
Sample 9A_Sed_Sieved 63µm_Acid	Sediment - marine	62455.0	2.0	9651.0	-25.1	72.0	9.5
Sample 9C_Sed_Sieved 63µm_Acid	Sediment - marine	67006.0	2.0	10393.0	-25.5	72.0	

Appendix E. X-Ray Diffraction

Graphs showing XRD results for peaks for all samples.

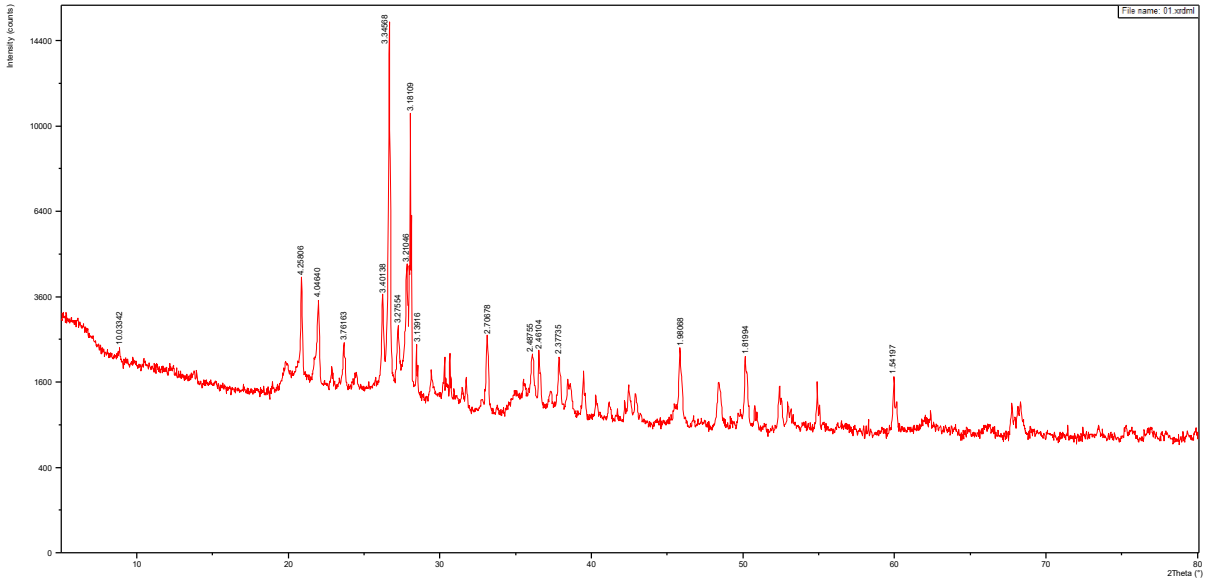

Figure 1. XRD graph showing peaks of minerals within the sample. Sample 1

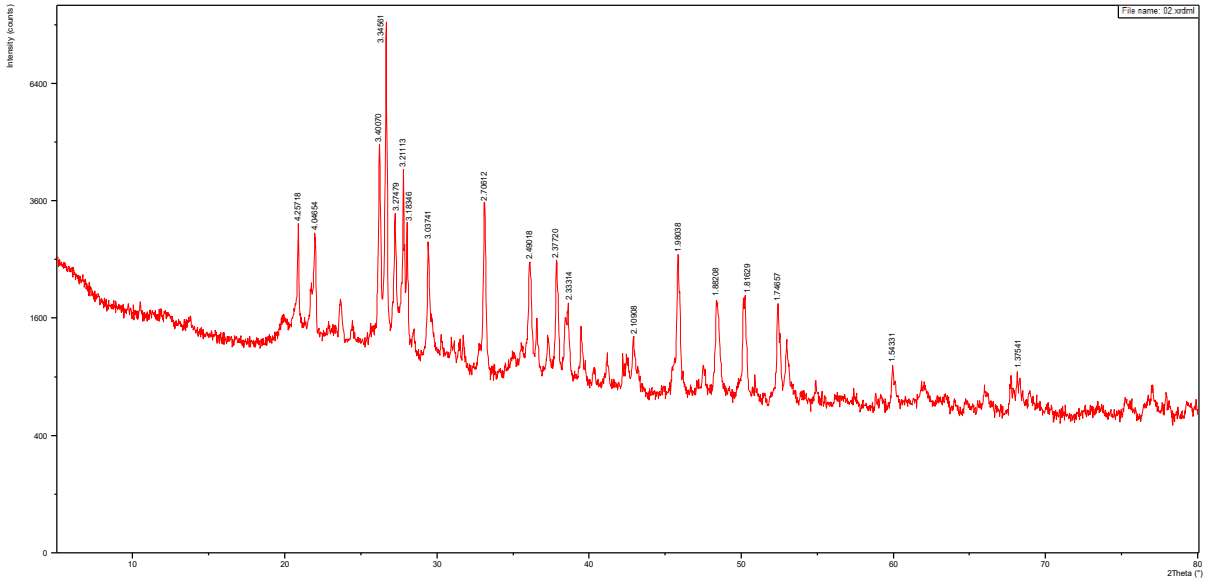

Figure 2.XRD graph showing peaks of minerals within the sample. Sample 2.

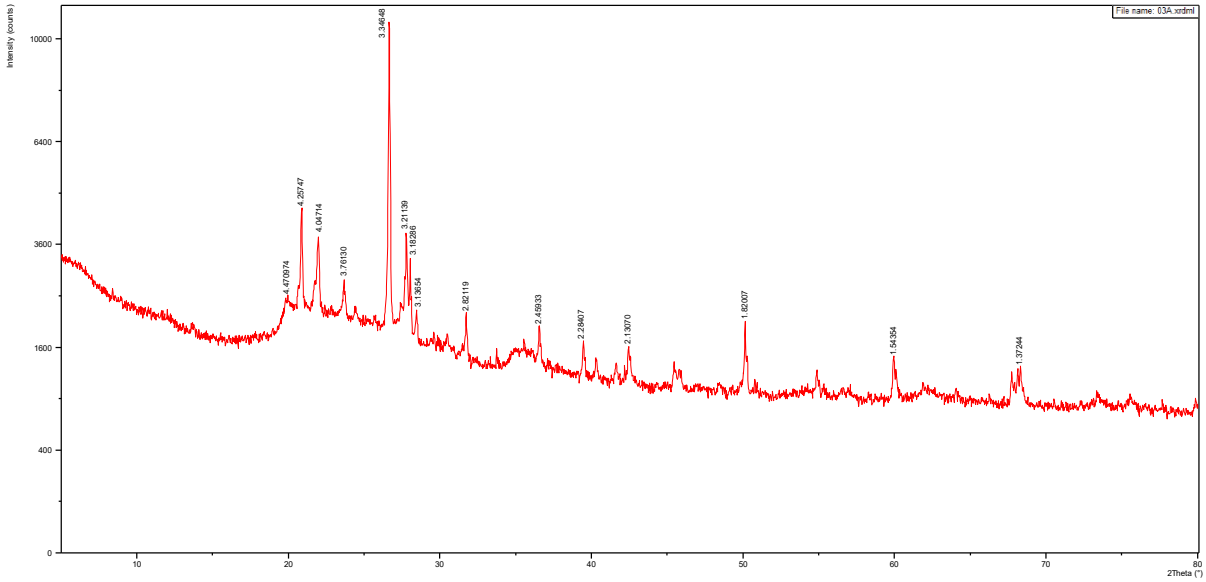

Figure 3.XRD graph showing peaks of minerals within the sample. Sample 3A.

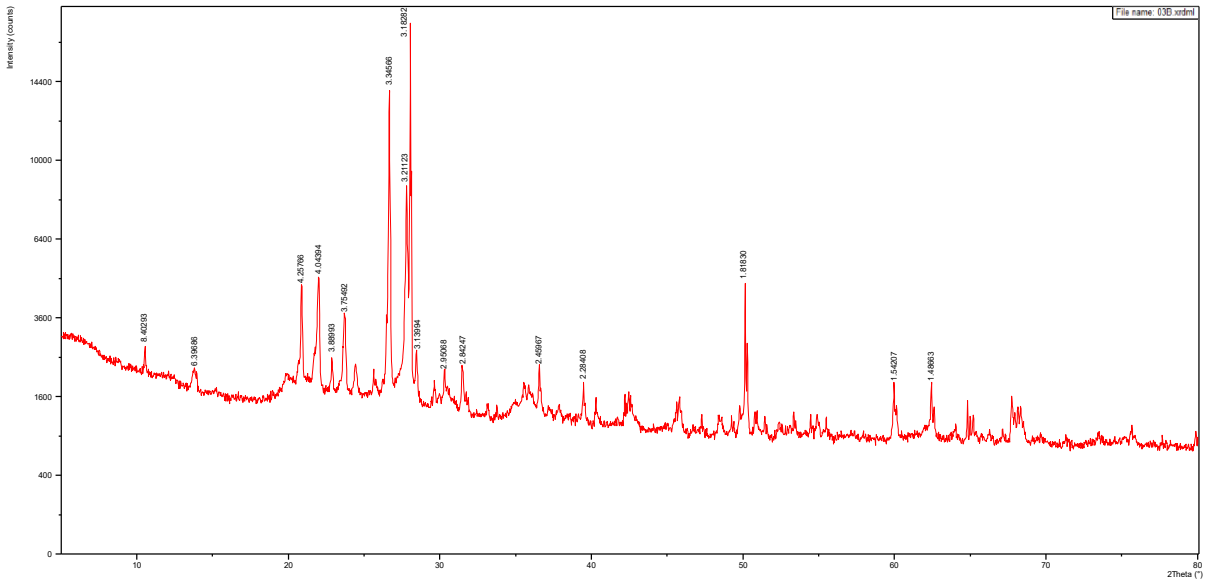

Figure 4. XRD graph showing peaks of minerals within the sample. Sample 3B.

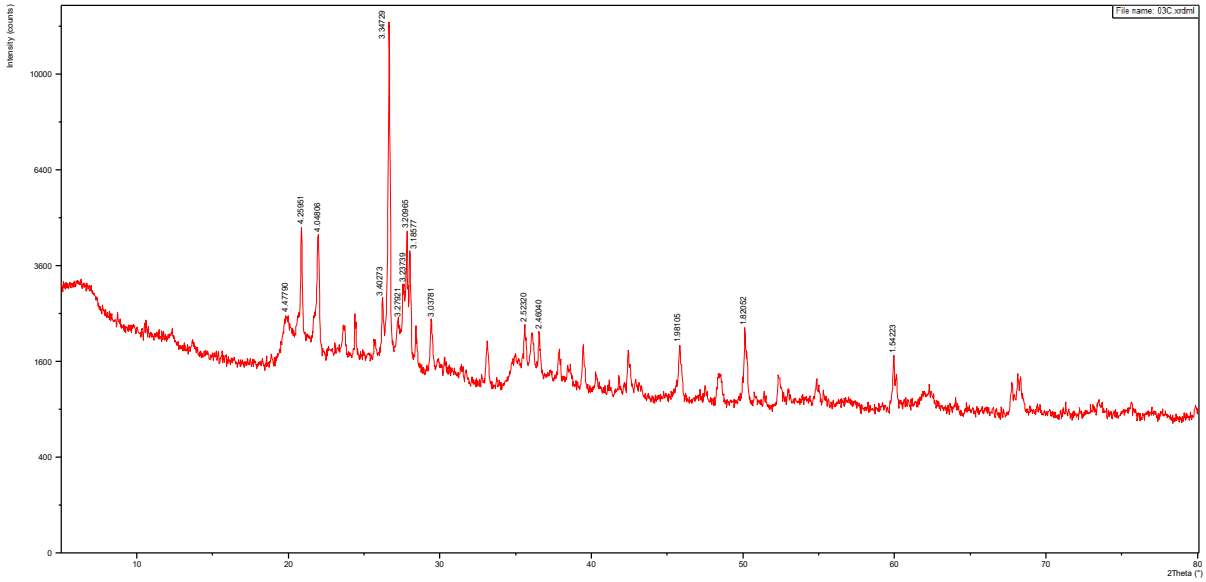

Figure 5.XRD graph showing peaks of minerals within the sample. Sample 3C.

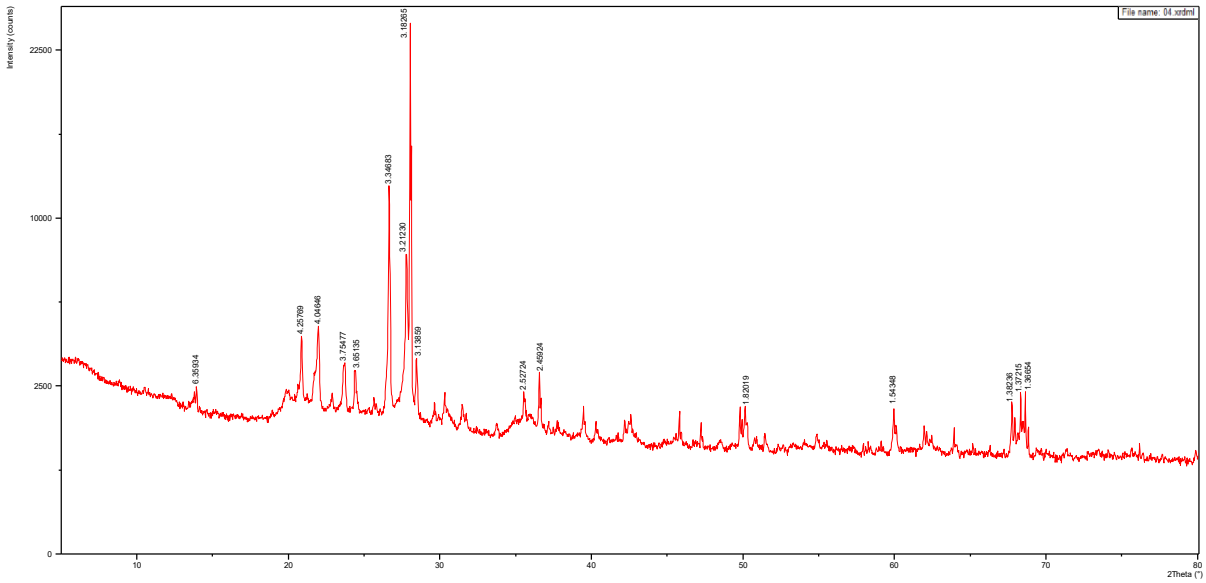

Figure 6. XRD graph showing peaks of minerals within the sample. Sample 4.

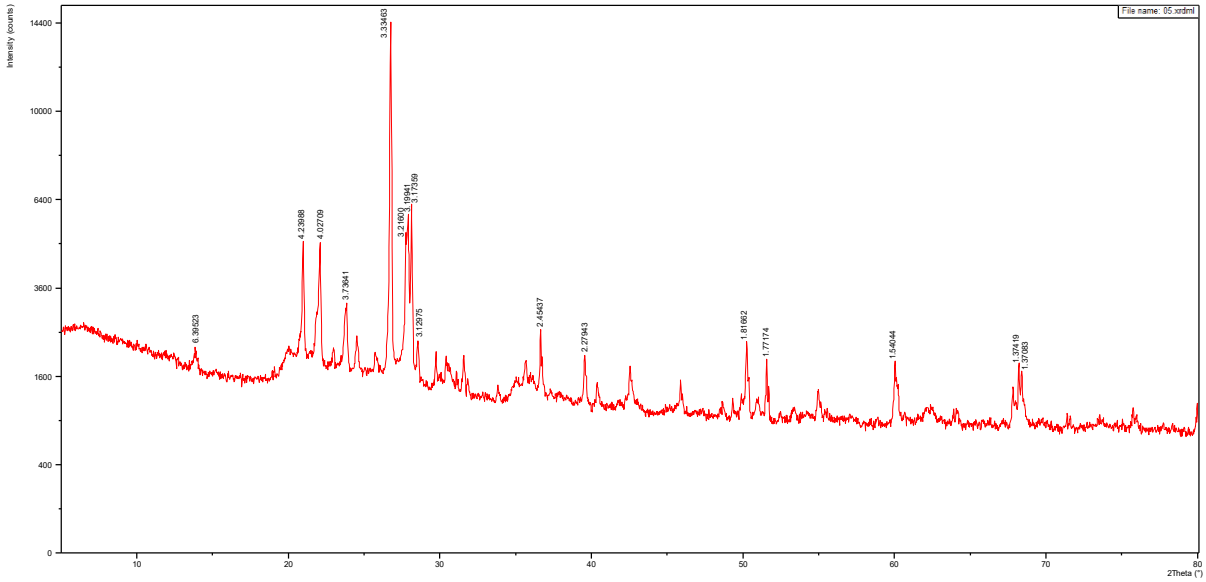

Figure 7. XRD graph showing peaks of minerals within the sample. Sample 5.

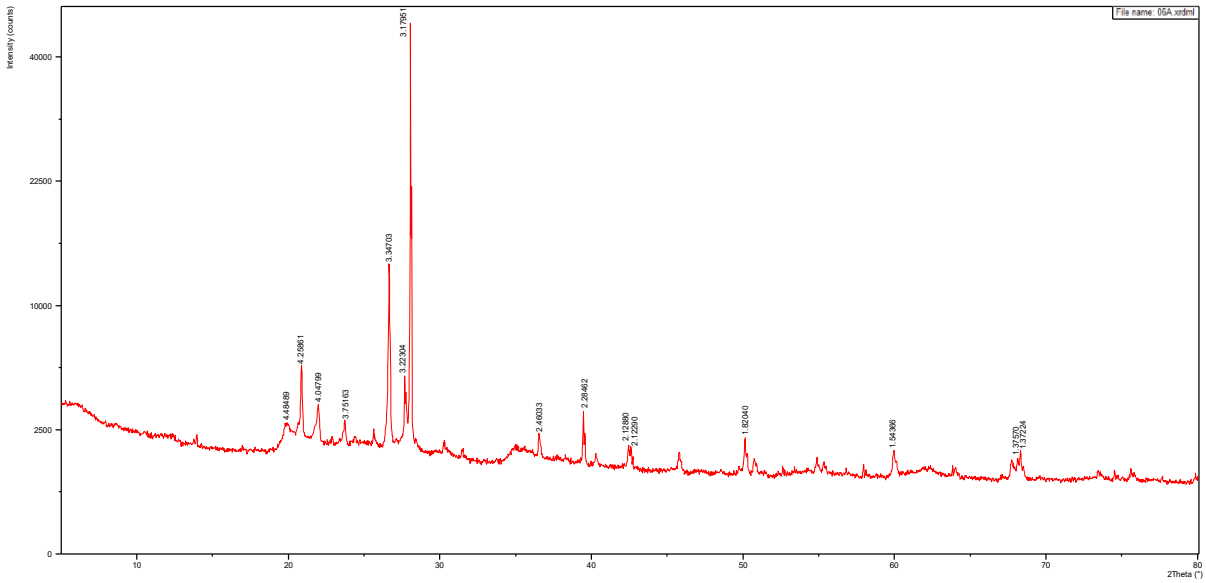

Figure 8. XRD graph showing peaks of minerals within the sample. Sample 6A.

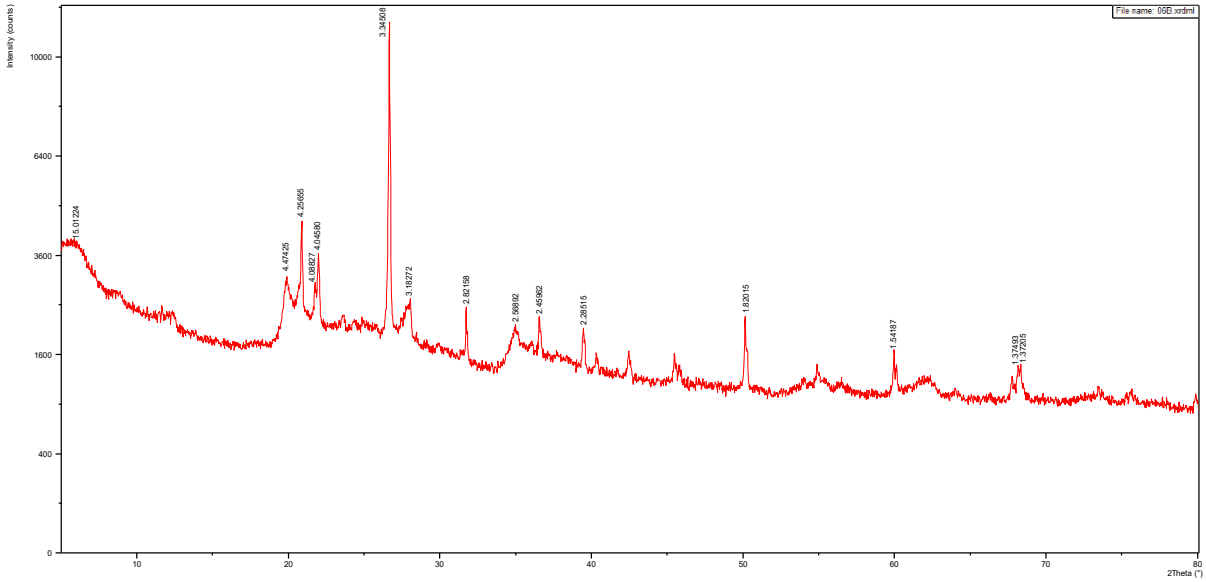

Figure 9. XRD graph showing peaks of minerals within the sample. Sample 6B

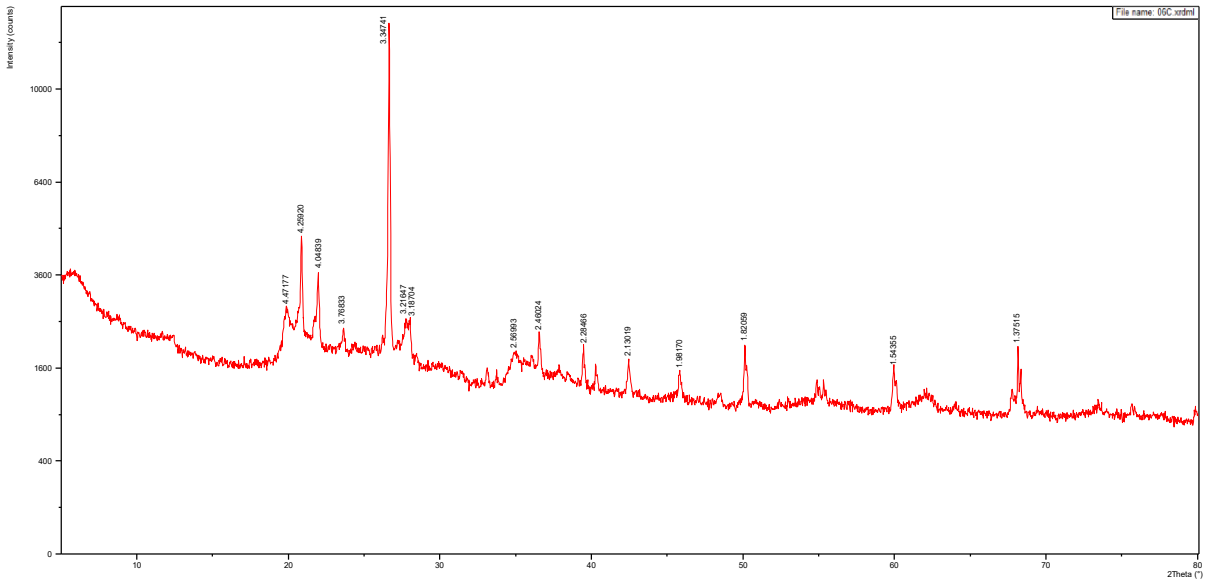

Figure 10. XRD graph showing peaks of minerals within the sample. Sample 6C.

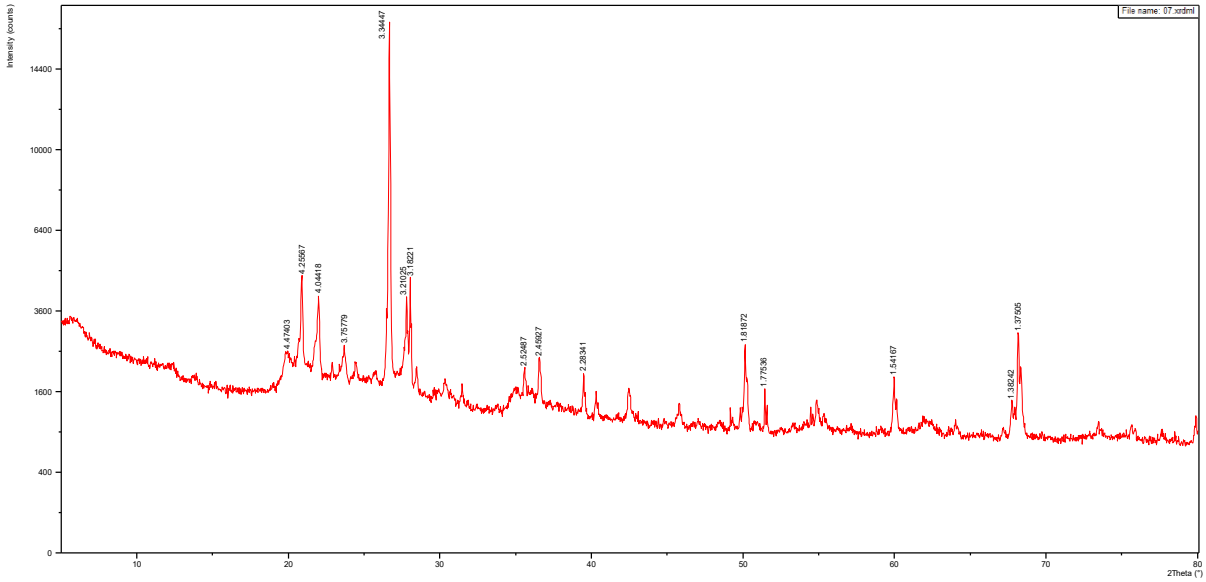

Figure 11. XRD graph showing peaks of minerals within the sample. Sample 7.

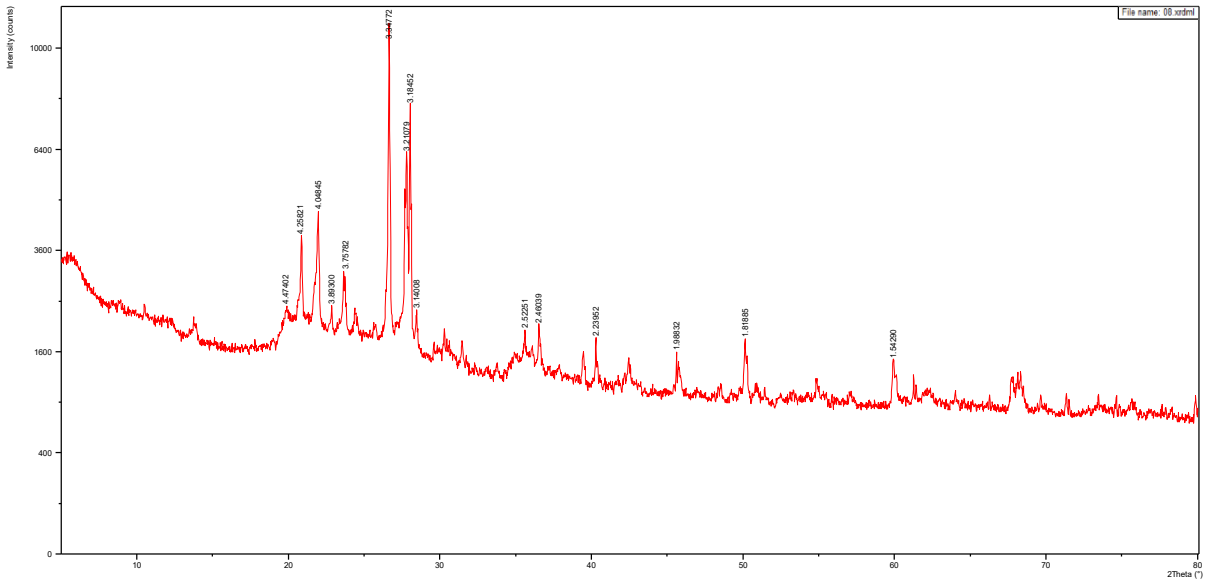

Figure 12. XRD graph showing peaks of minerals within the sample. Sample 8.

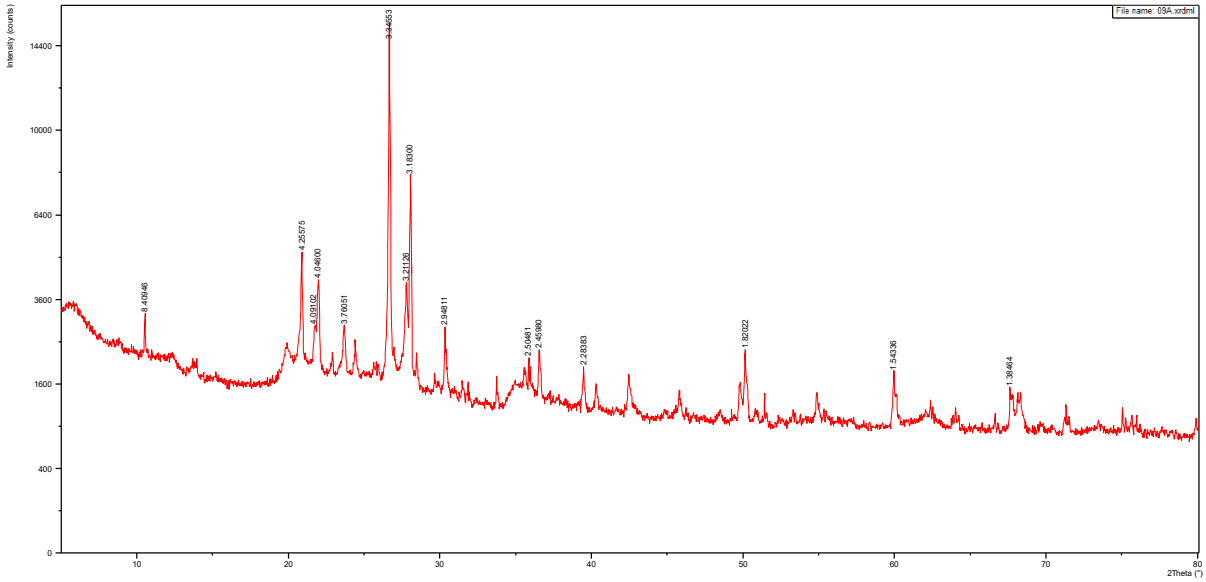

Figure 13.XRD graph showing peaks of minerals within the sample. Sample 9A.

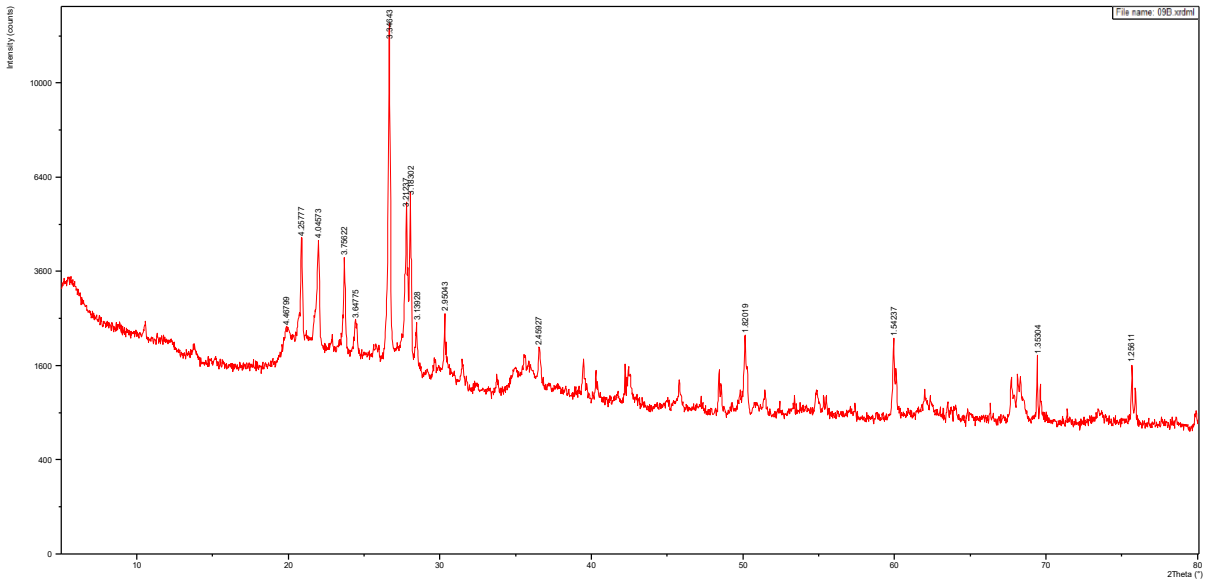

Figure 14.XRD graph showing peaks of minerals within the sample. Sample 9B.

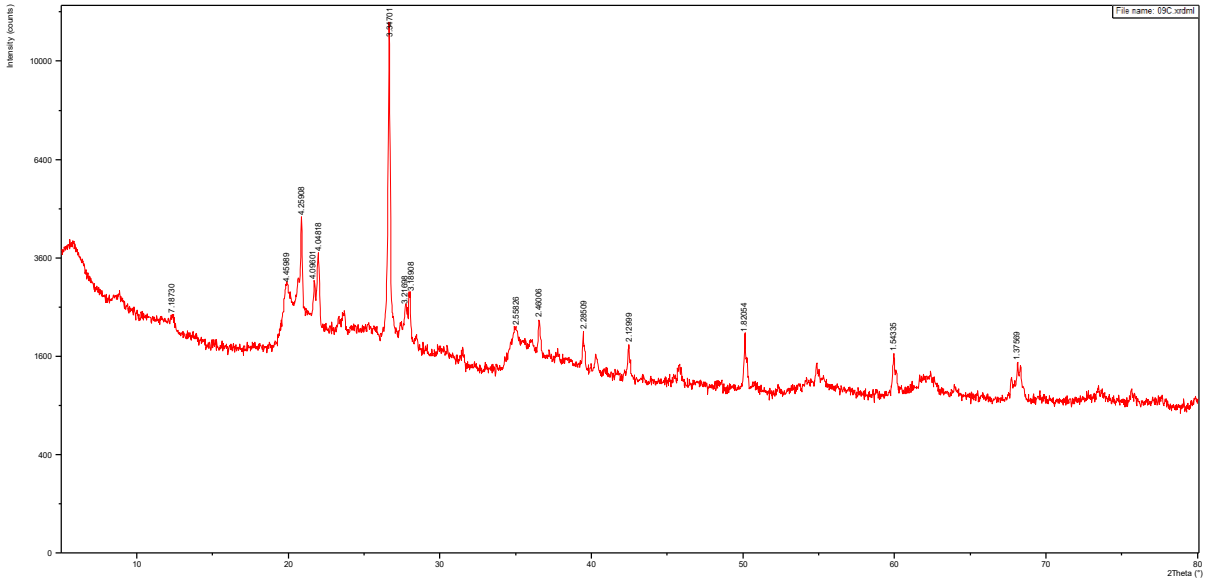

Figure 15.XRD graph showing peaks of minerals within the sample. Sample 9C.

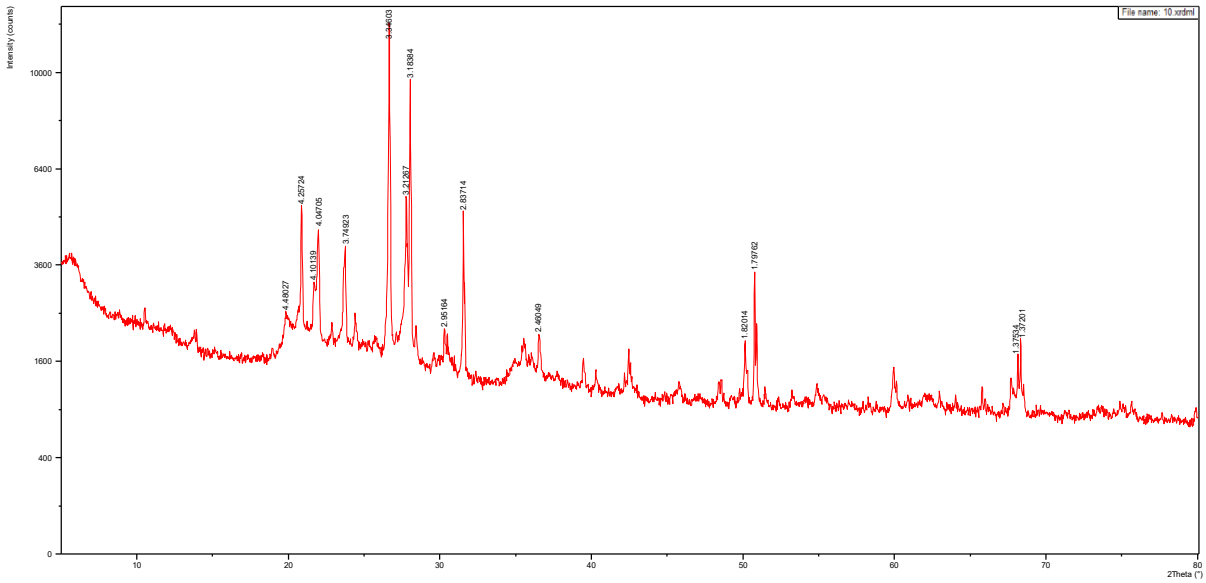

Figure 16. XRD graph showing peaks of minerals within the sample. Sample 10.

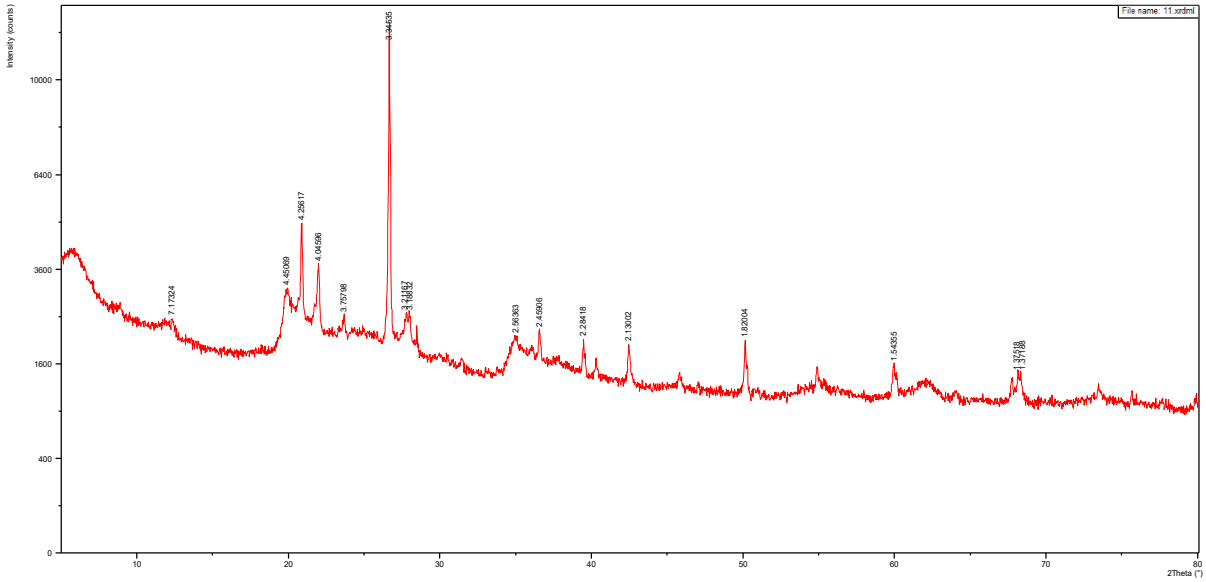

Figure 17. XRD graph showing peaks of minerals within the sample. Sample 11.

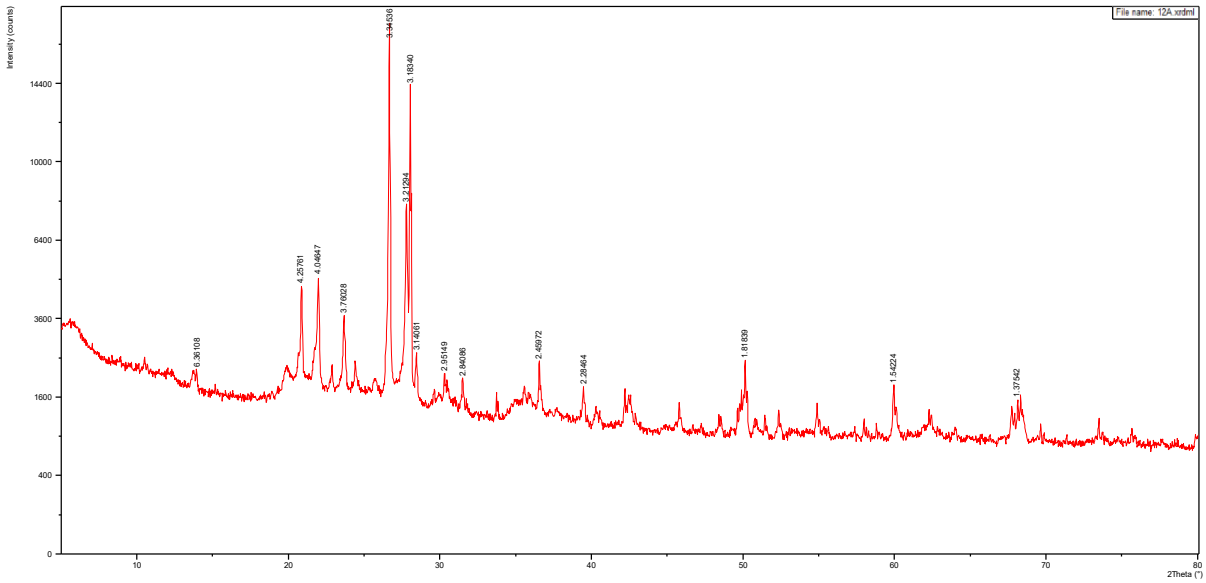

Figure 18. XRD graph showing peaks of minerals within the sample. Sample 12A.

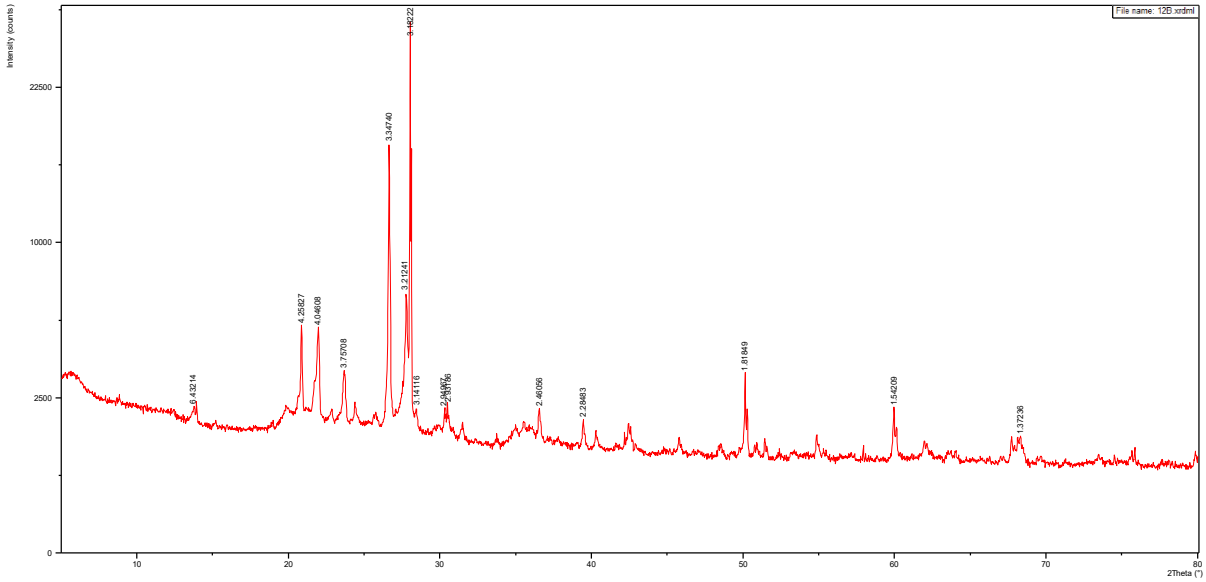

Figure 19.XRD graph showing peaks of minerals within the sample. Sample 12B.

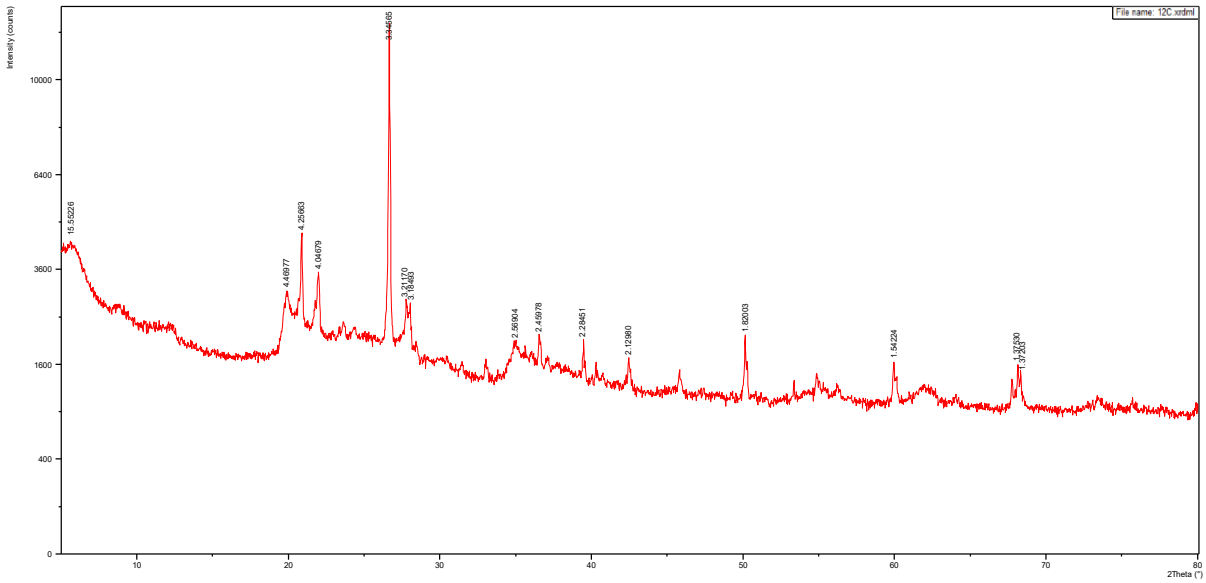

Figure 20.XRD graph showing peaks of minerals within the sample. Sample 12C.

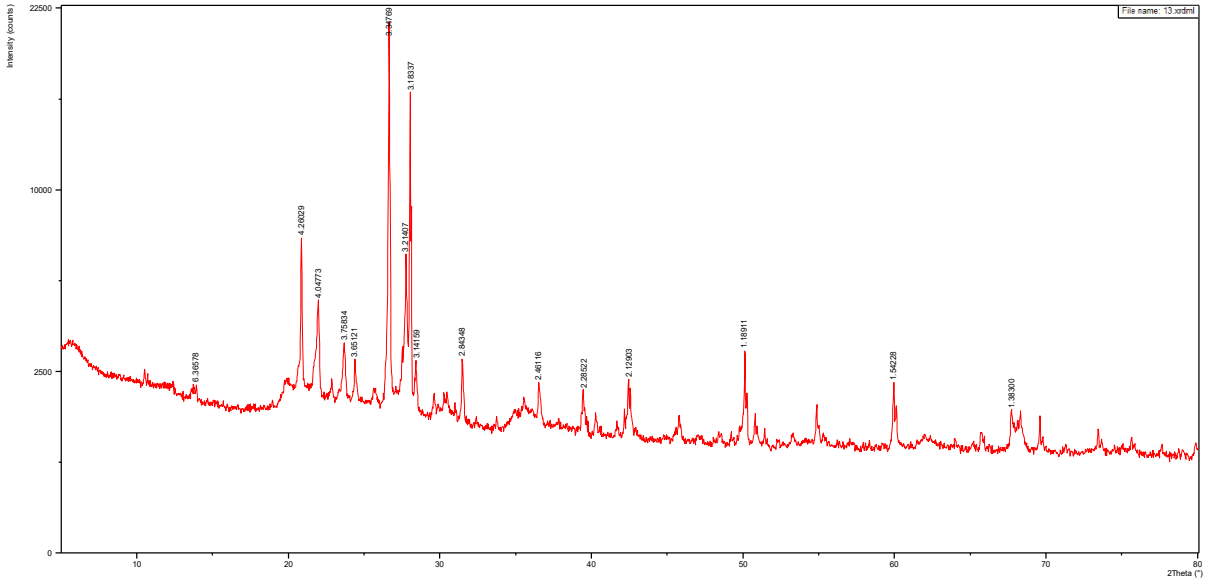

Figure 21.XRD graph showing peaks of minerals within the sample. Sample 13.

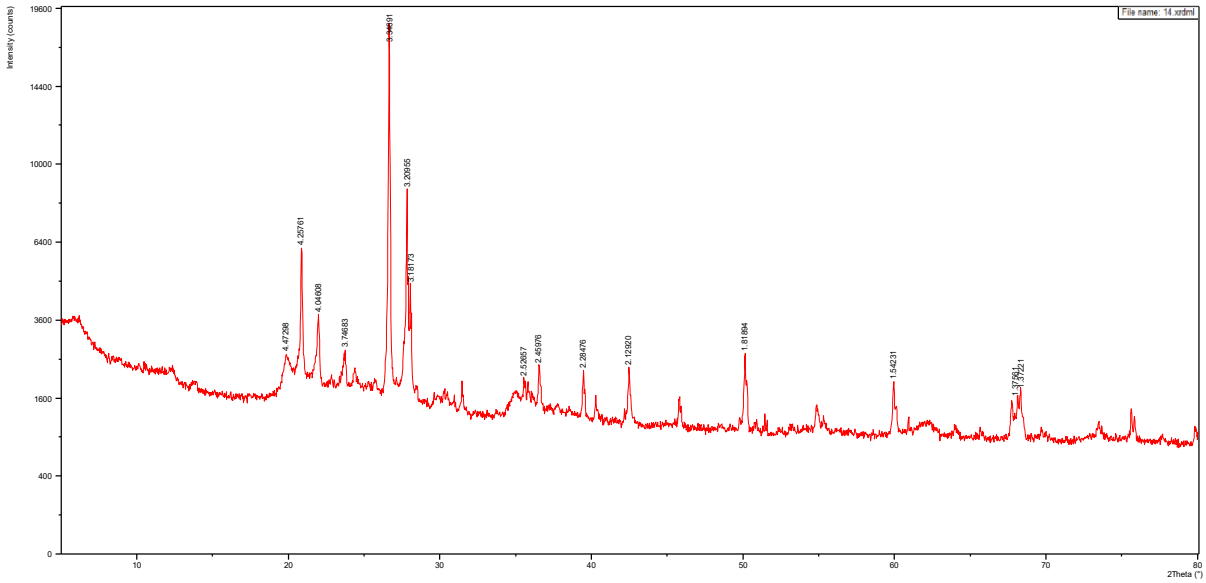

Figure 22.XRD graph showing peaks of minerals within the sample. Sample 14.

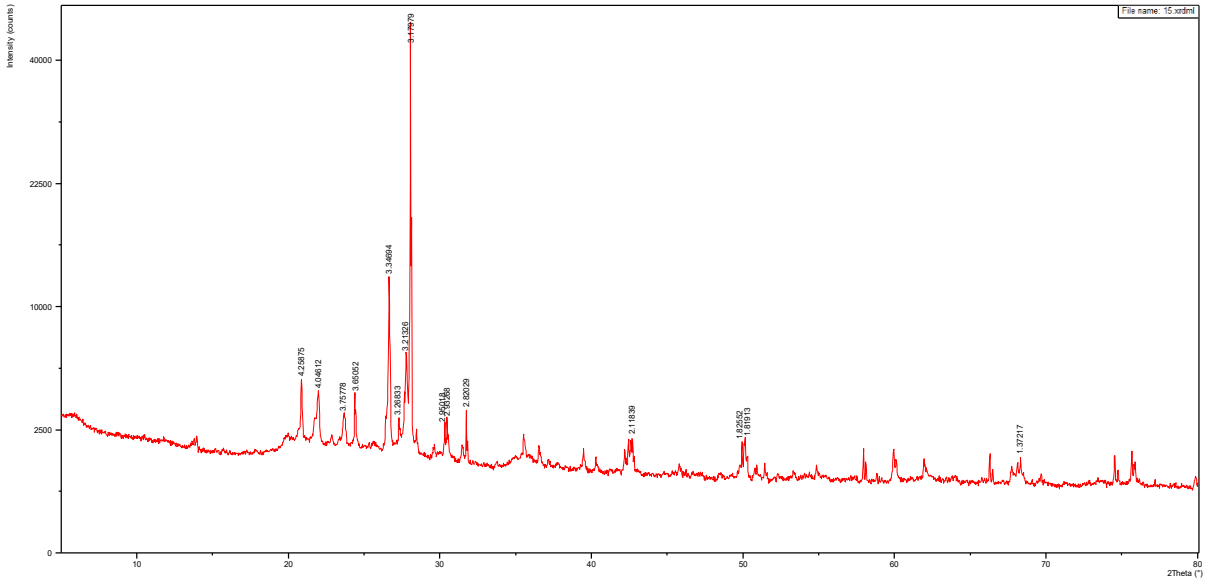

Figure 23. XRD graph showing peaks of minerals within the sample. Sample 15.

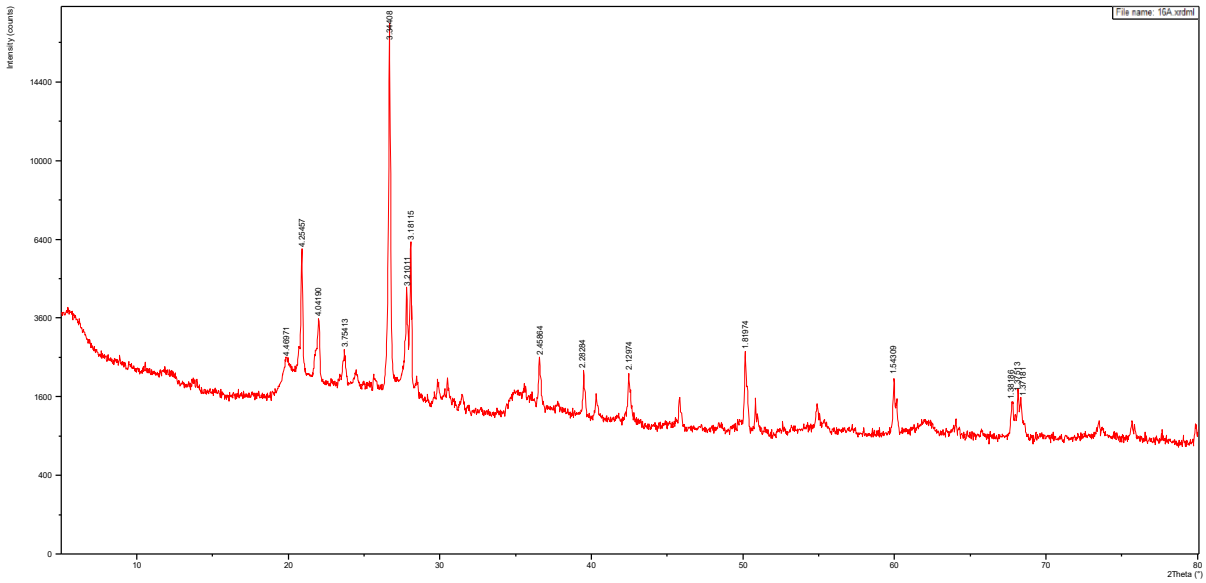

Figure 24.XRD graph showing peaks of minerals within the sample. Sample 16A.

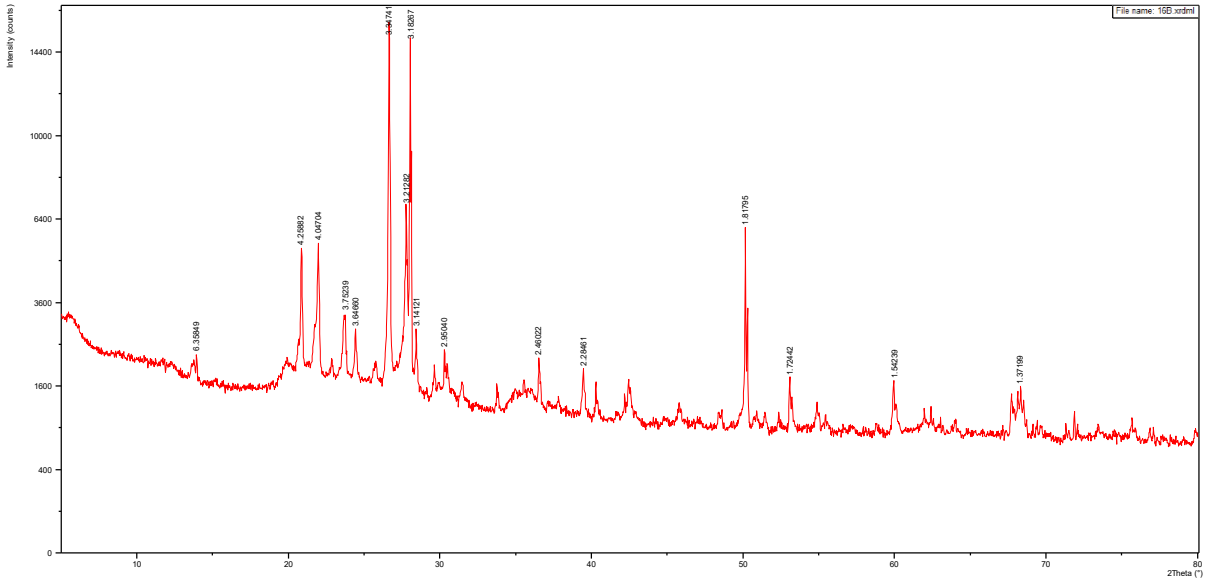

Figure 25.XRD graph showing peaks of minerals within the sample. Sample 16B.

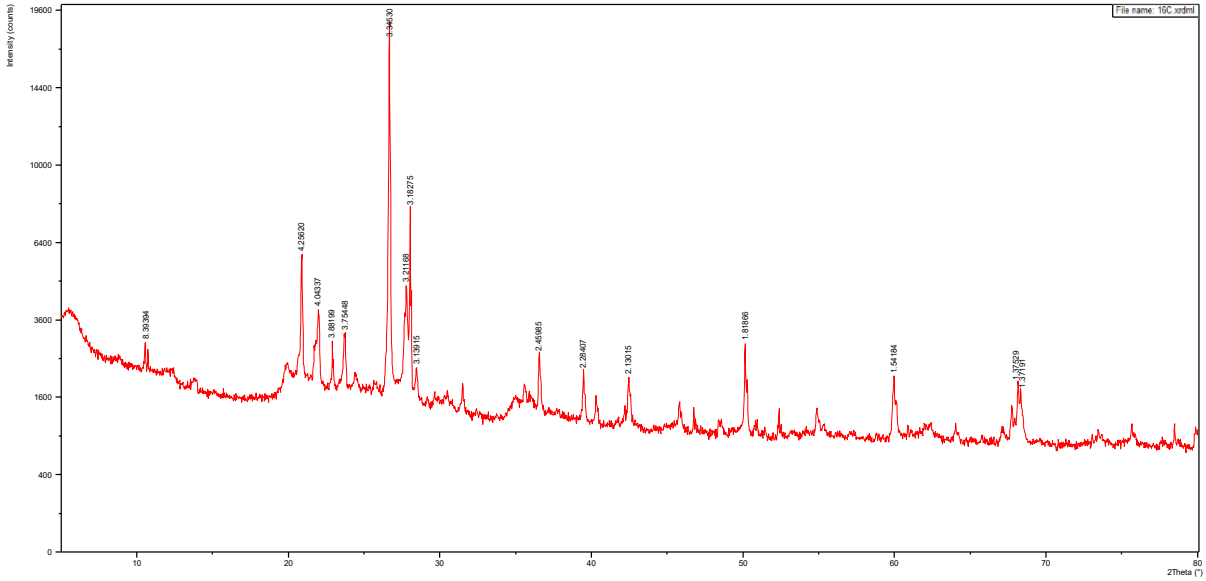

Figure 26. XRD graph showing peaks of minerals within the sample. Sample 16C.

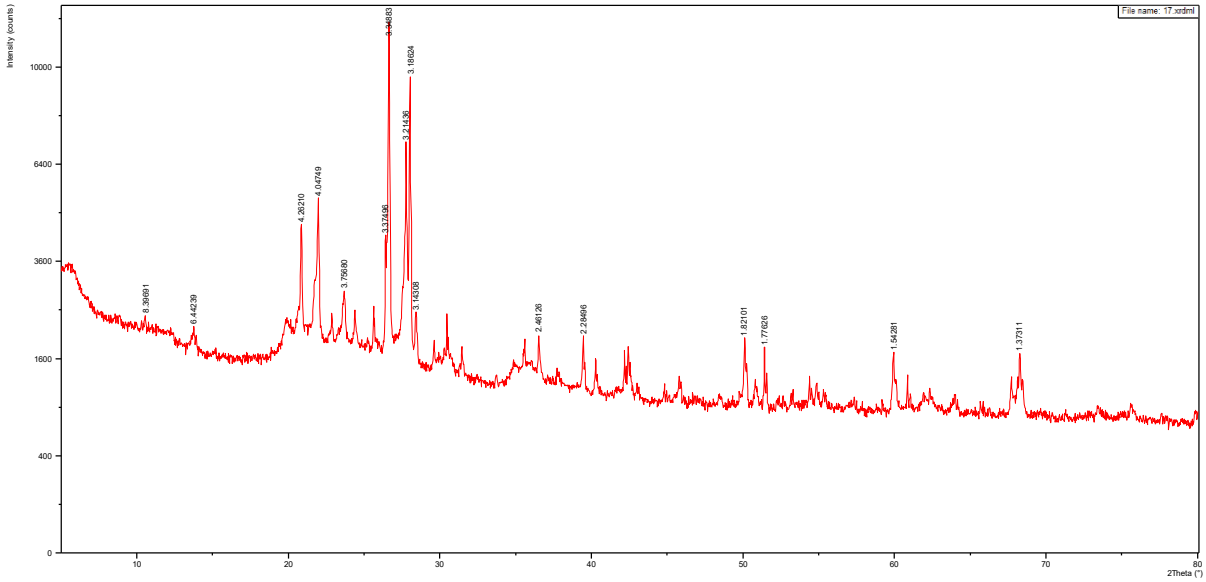

Figure 27.XRD graph showing peaks of minerals within the sample. Sample 17.

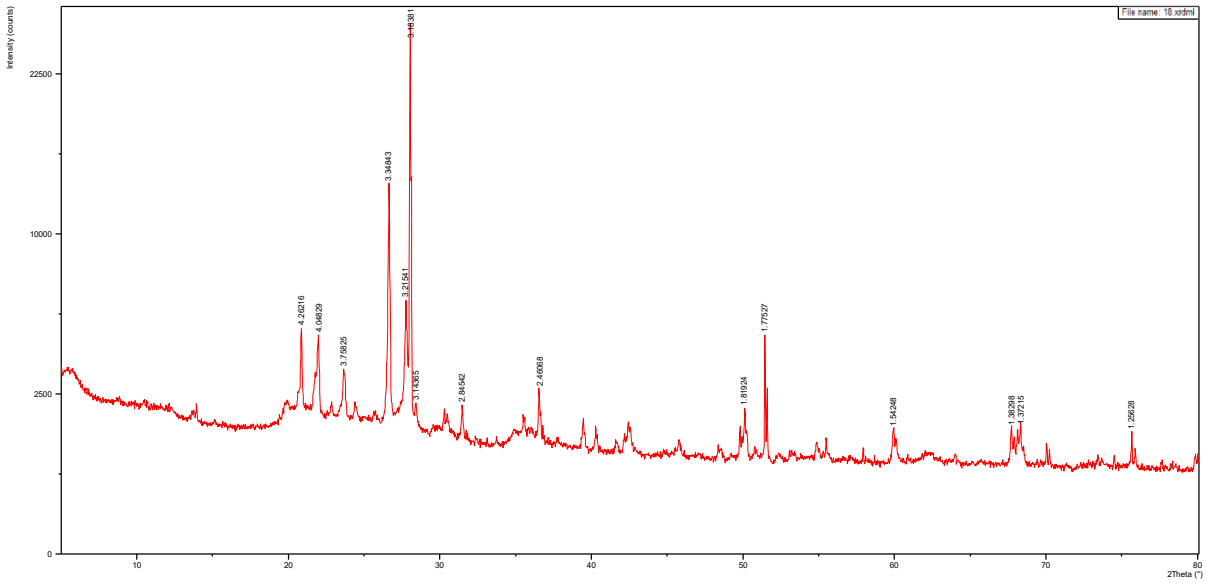

Figure 28.XRD graph showing peaks of minerals within the sample. Sample 18.

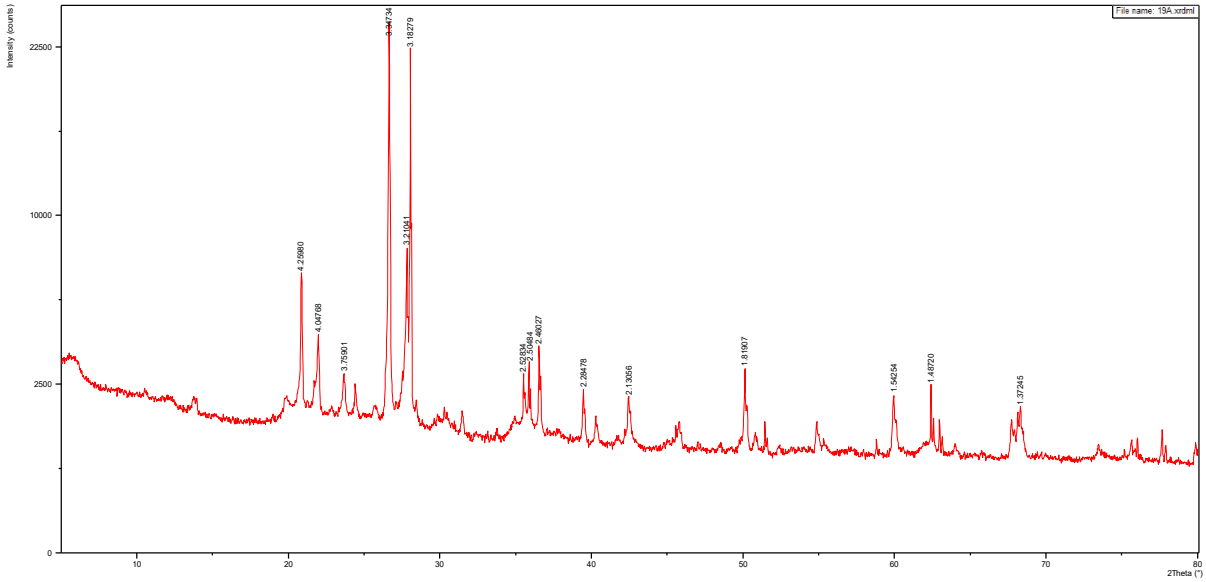

Figure 29.XRD graph showing peaks of minerals within the sample. Sample 19A.

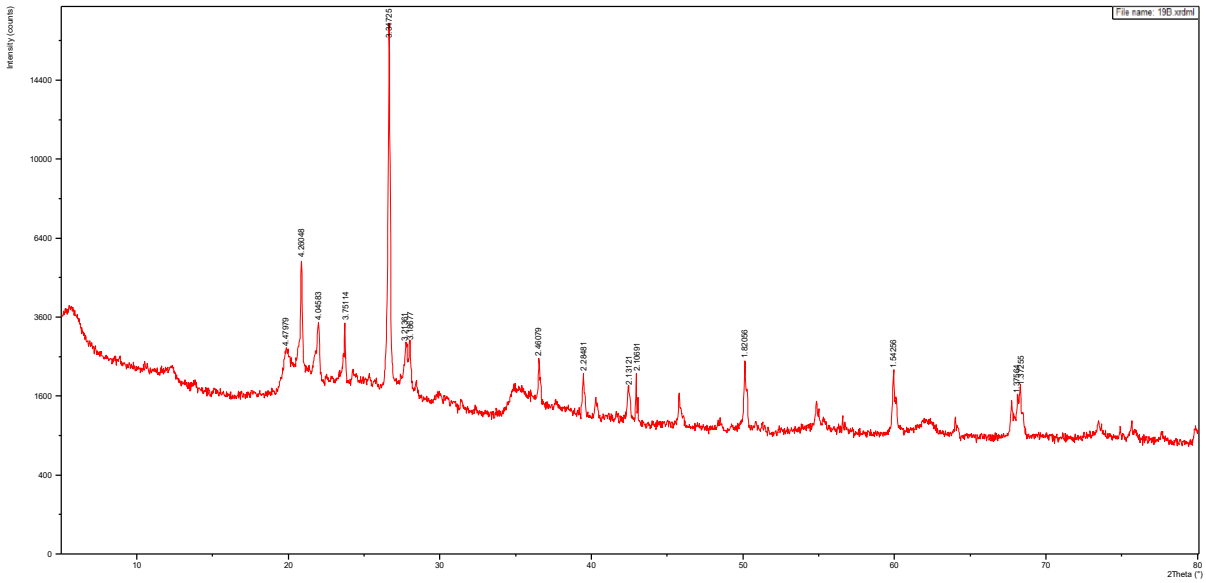

Figure 30.XRD graph showing peaks of minerals within the sample. Sample 19B.

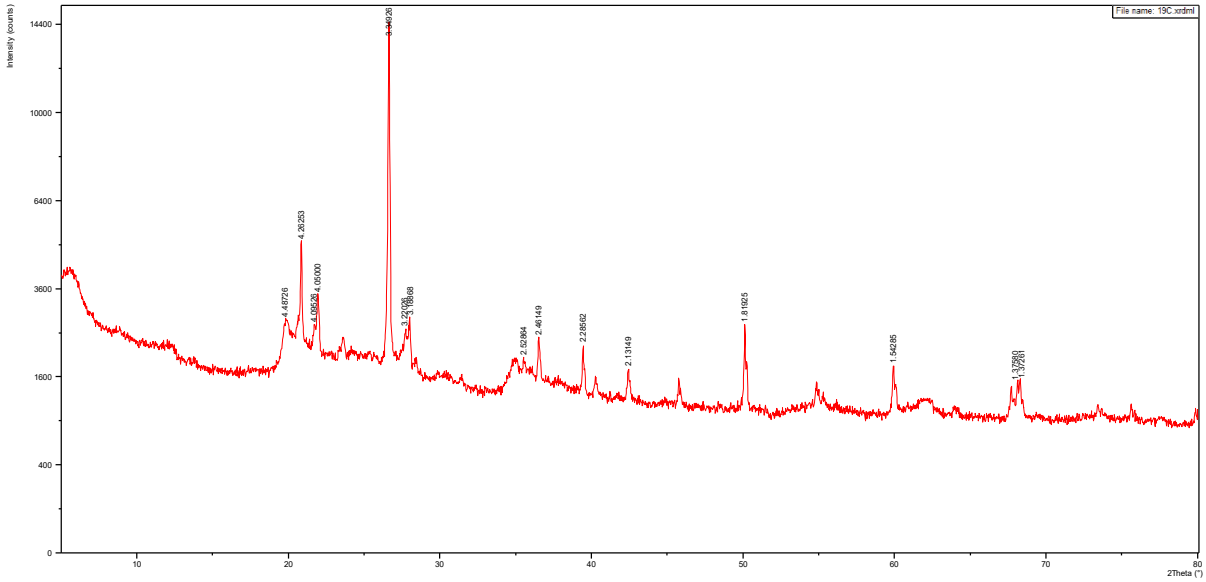

Figure 31. XRD graph showing peaks of minerals within the sample. Sample 19C.

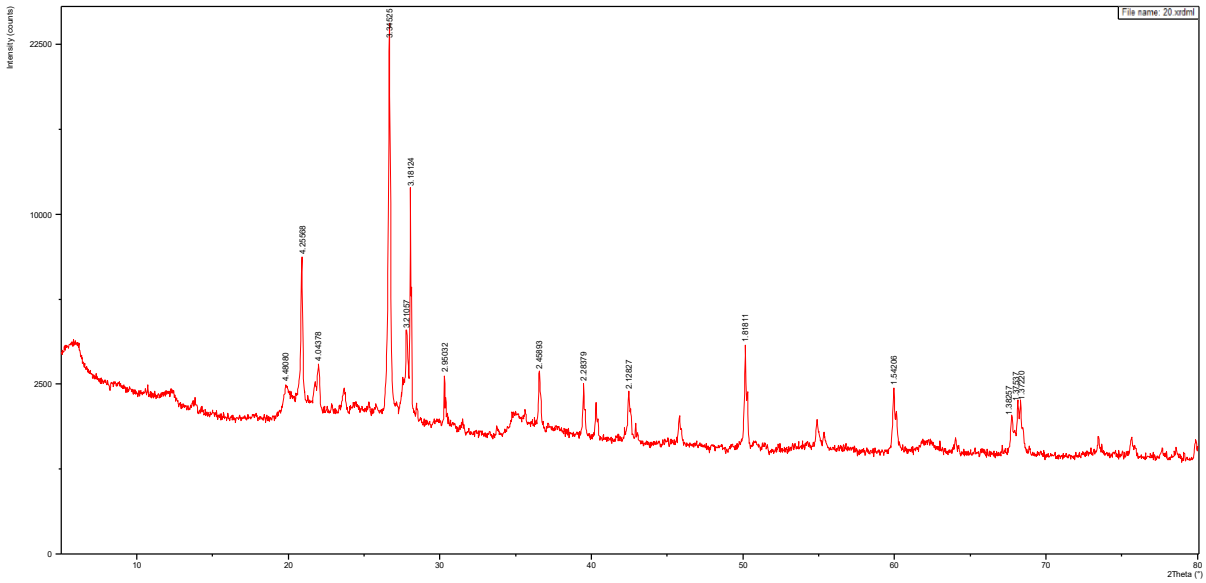

Figure 32.XRD graph showing peaks of minerals within the sample. Sample 20.

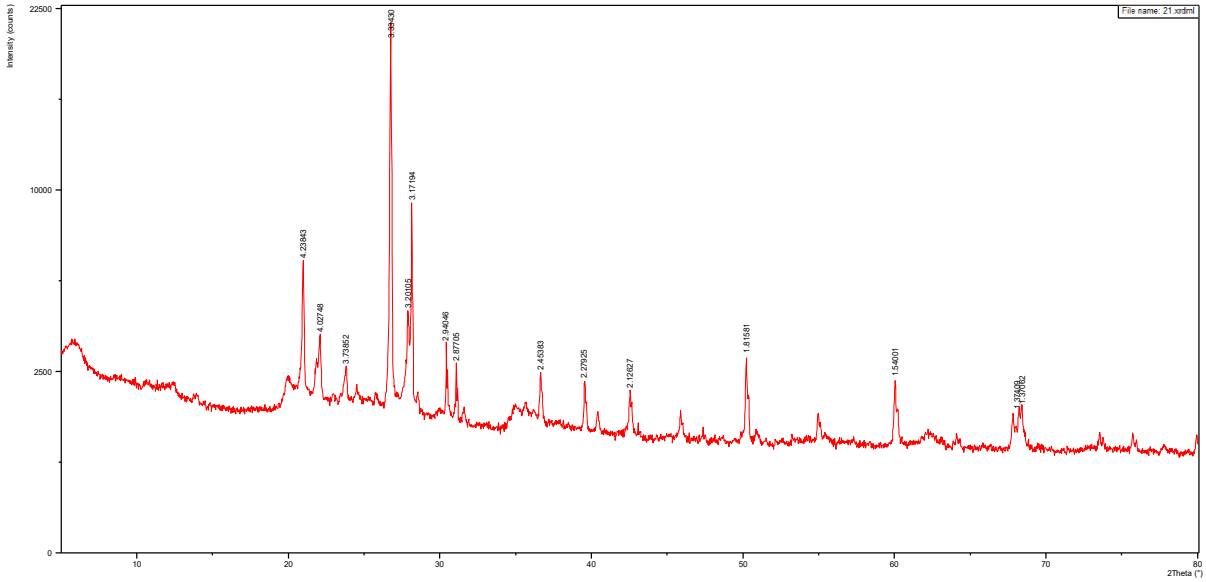

Figure 33.XRD graph showing peaks of minerals within the sample. Sample 21.

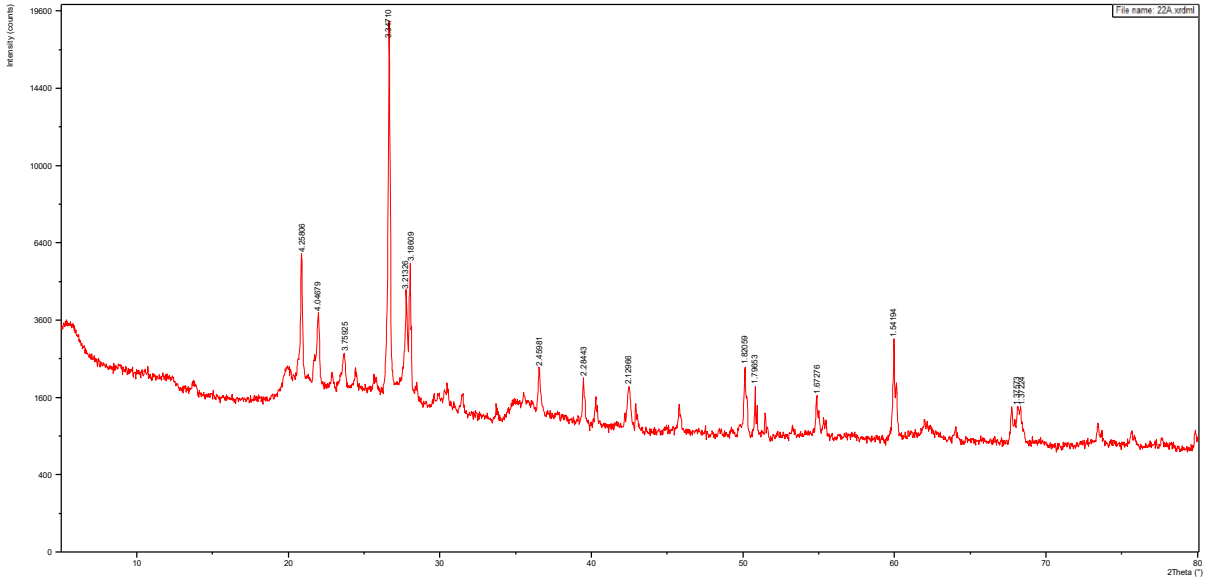

Figure 34. XRD graph showing peaks of minerals within the sample. Sample 22A.

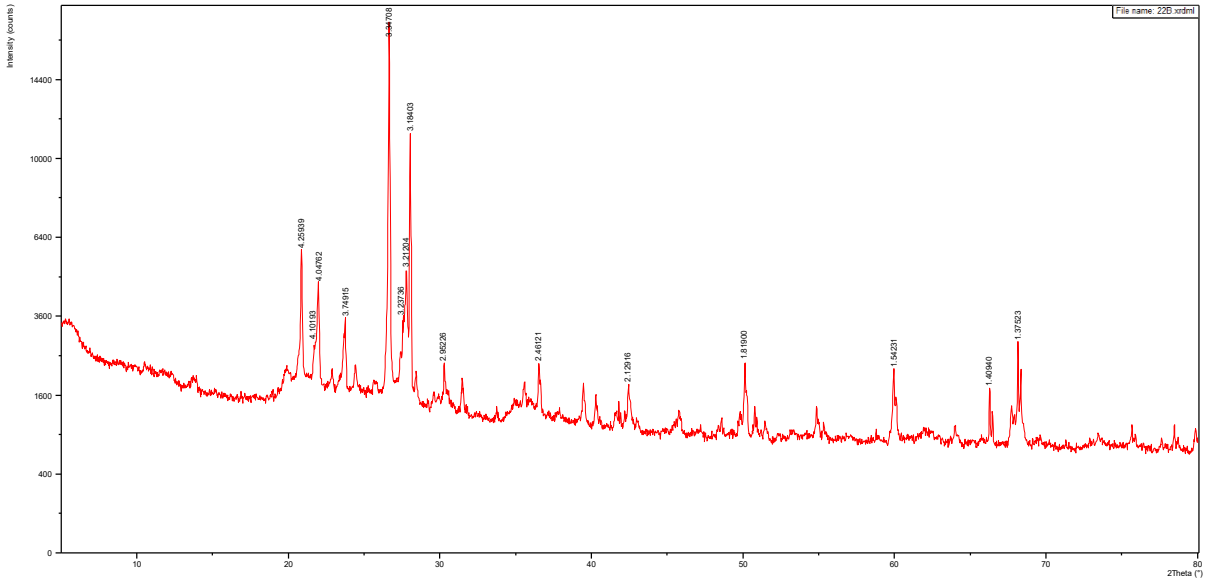

Figure 35.XRD graph showing peaks of minerals within the sample. Sample 22B.

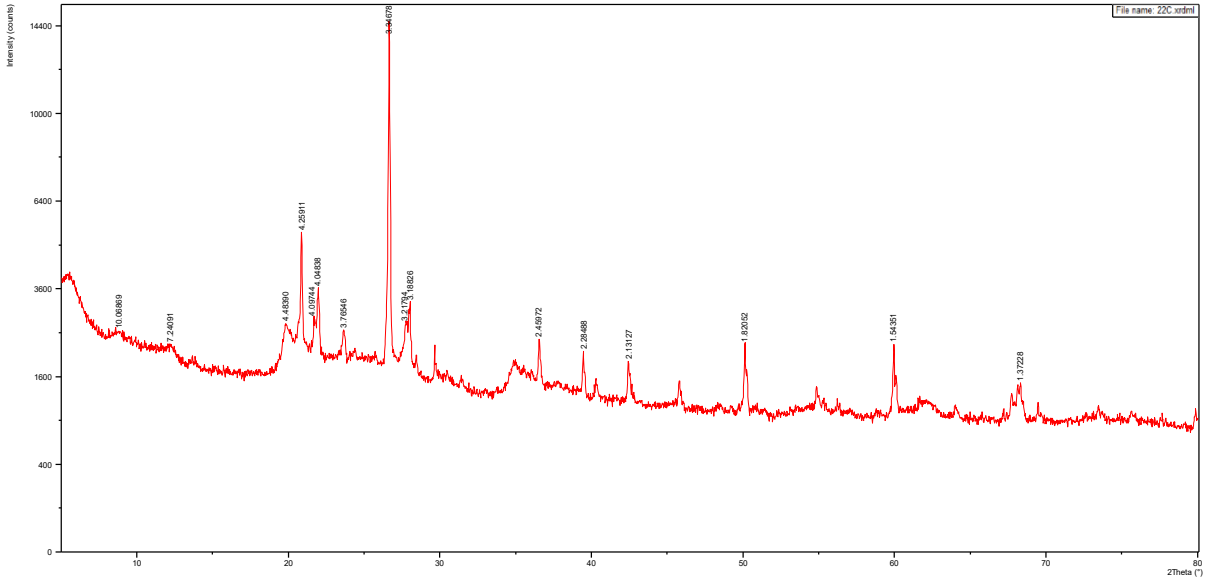

Figure 36.XRD graph showing peaks of minerals within the sample. Sample 22C.

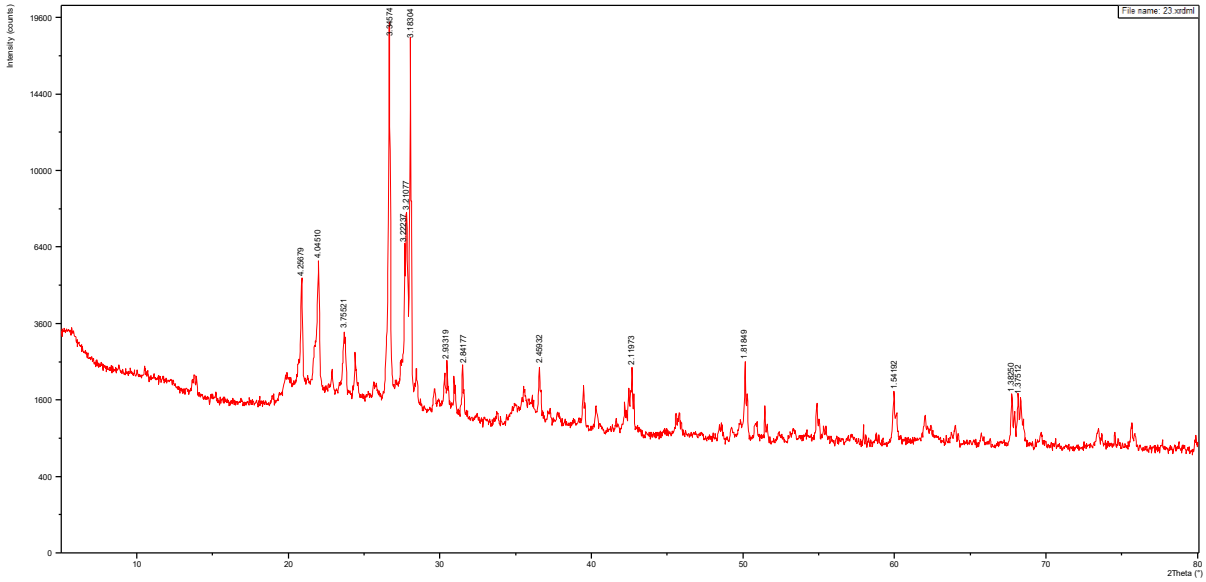

Figure 37.XRD graph showing peaks of minerals within the sample. Sample 23.

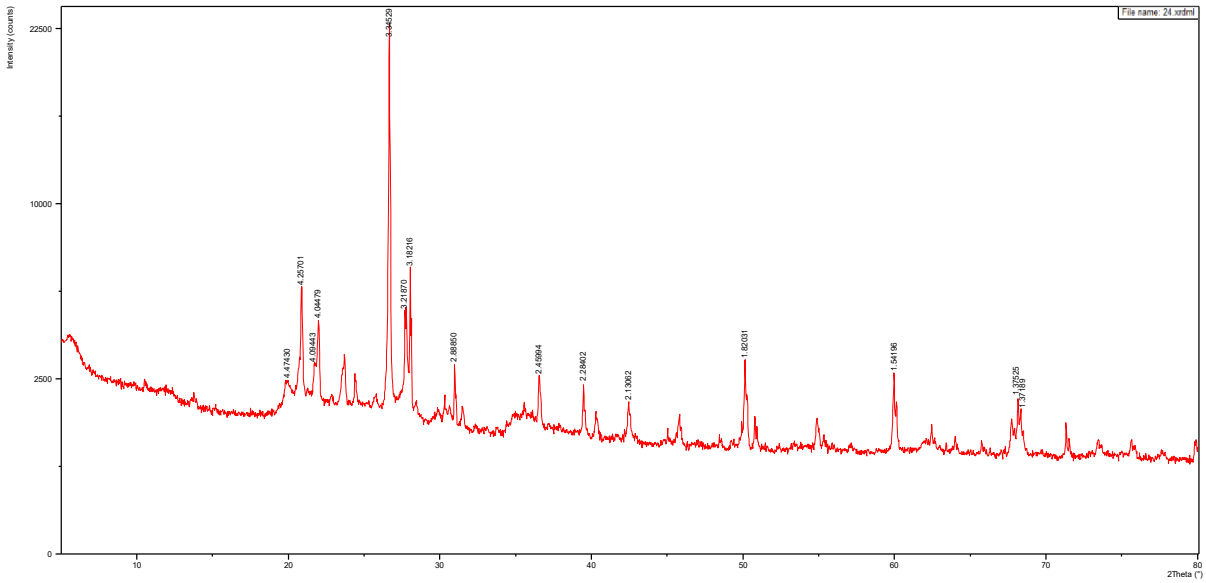

Figure 38. XRD graph showing peaks of minerals within the sample. Sample 24.

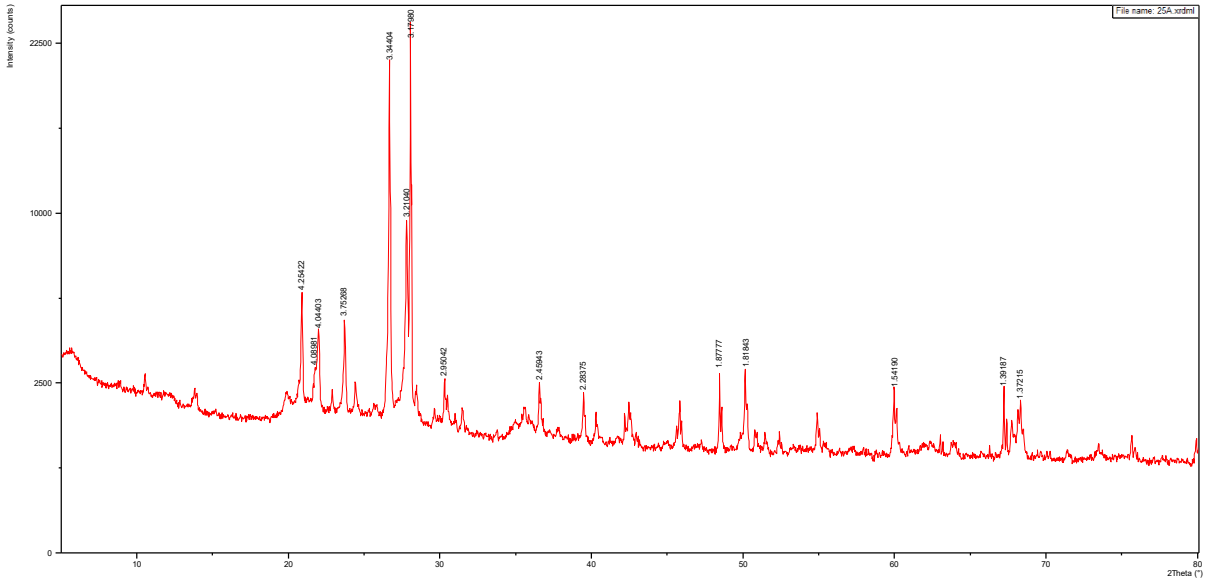

Figure 39. XRD graph showing peaks of minerals within the sample. Sample 25A.

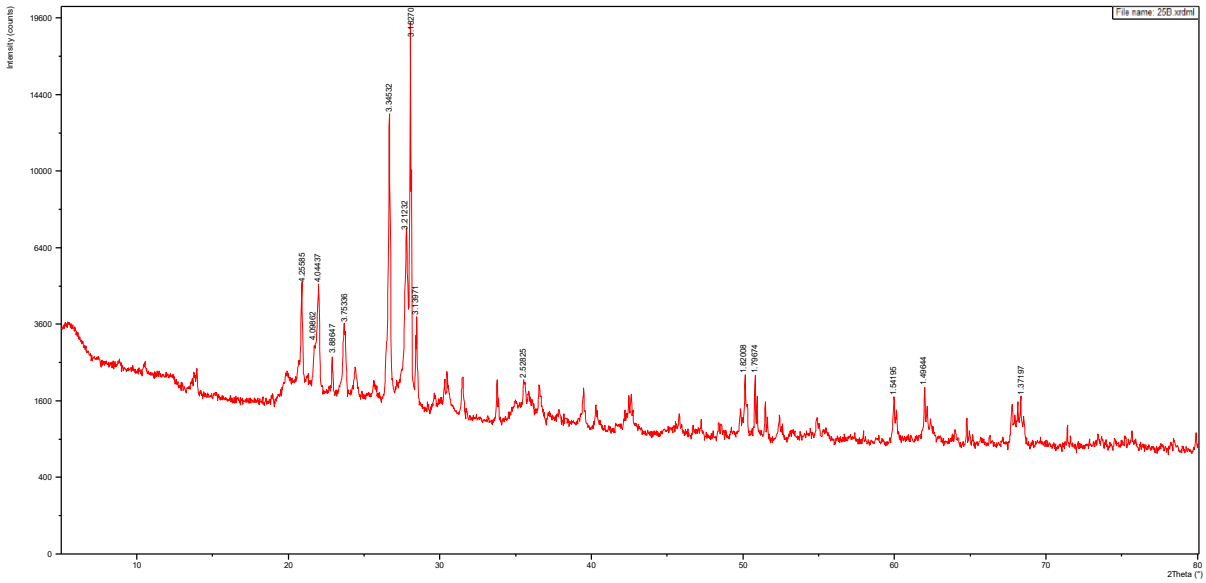

Figure 40. XRD graph showing peaks of minerals within the sample. Sample 25B.

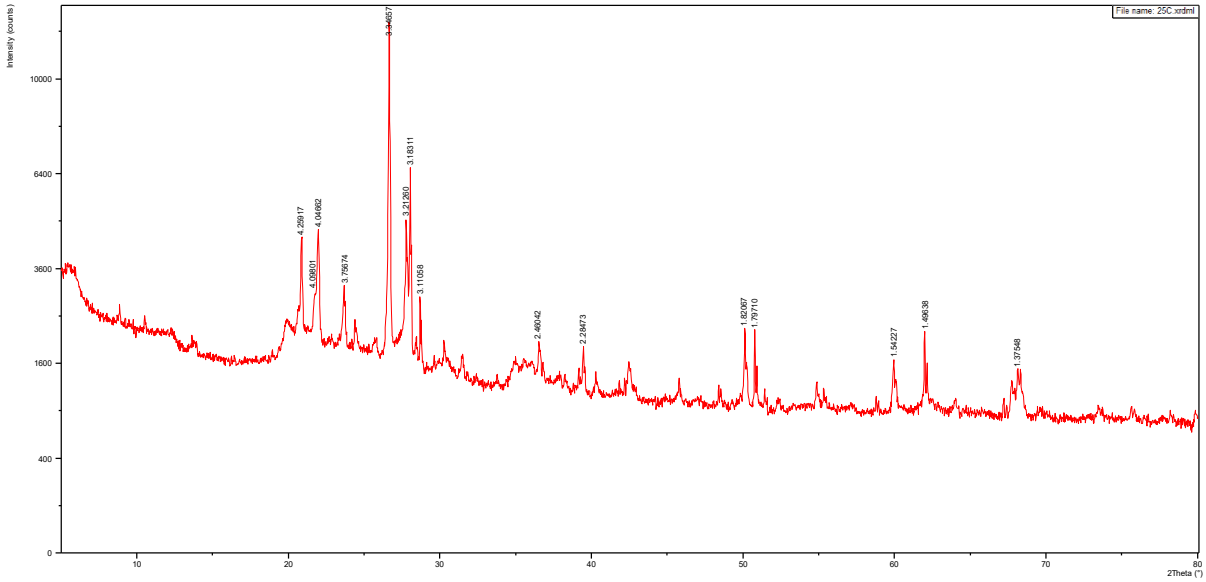

Figure 41.XRD graph showing peaks of minerals within the sample. Sample 25C.

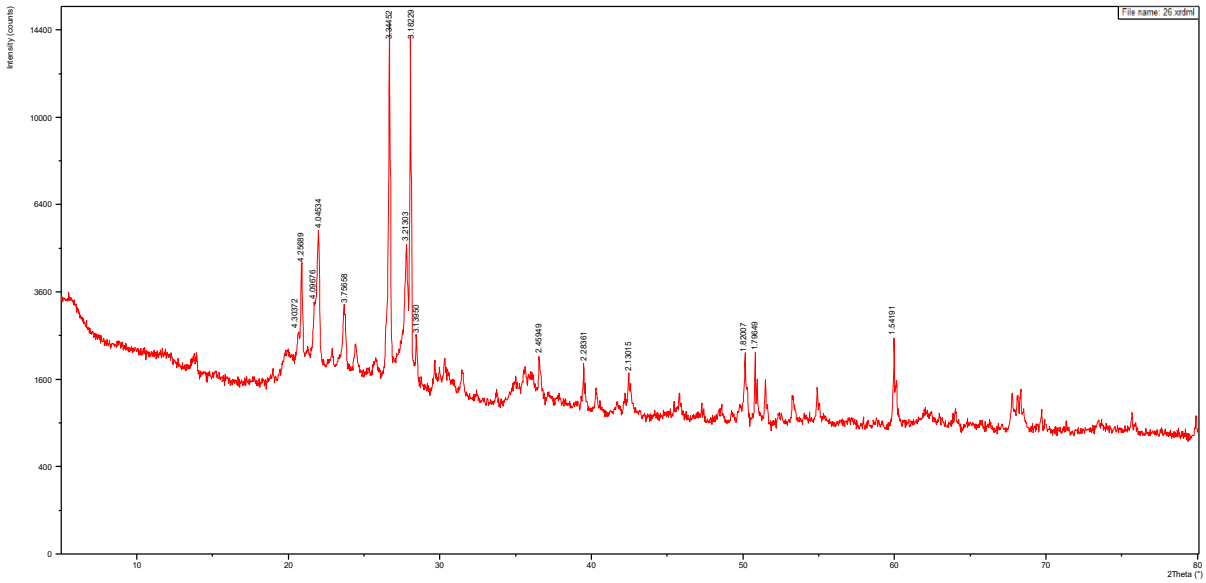

Figure 42. XRD graph showing peaks of minerals within the sample. Sample 26.

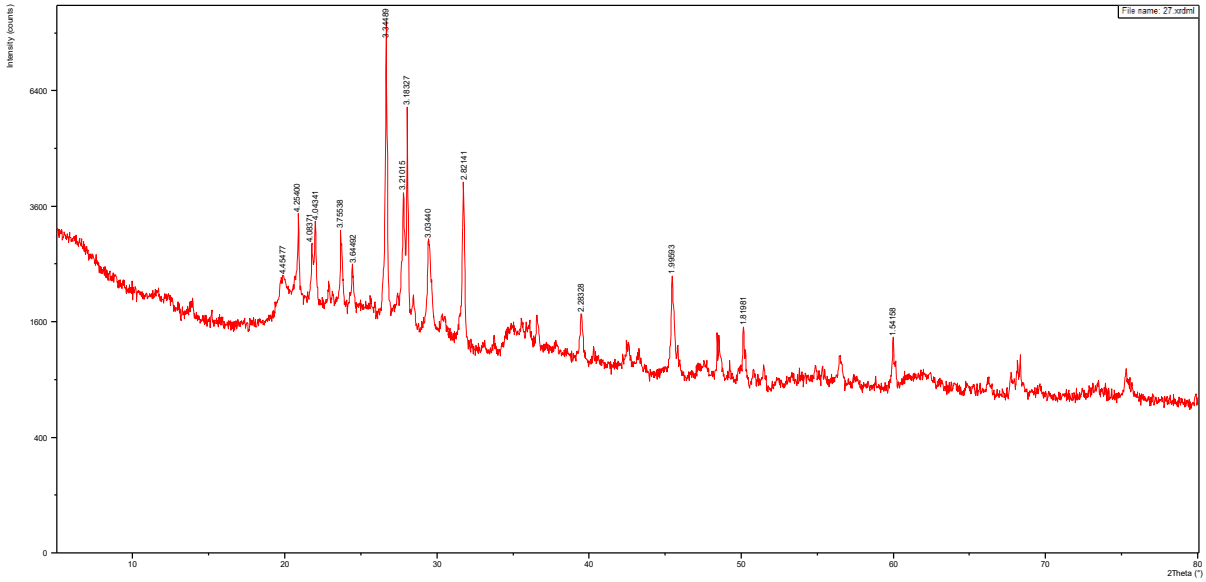

Figure 43. XRD graph showing peaks of minerals within the sample. Sample 27.

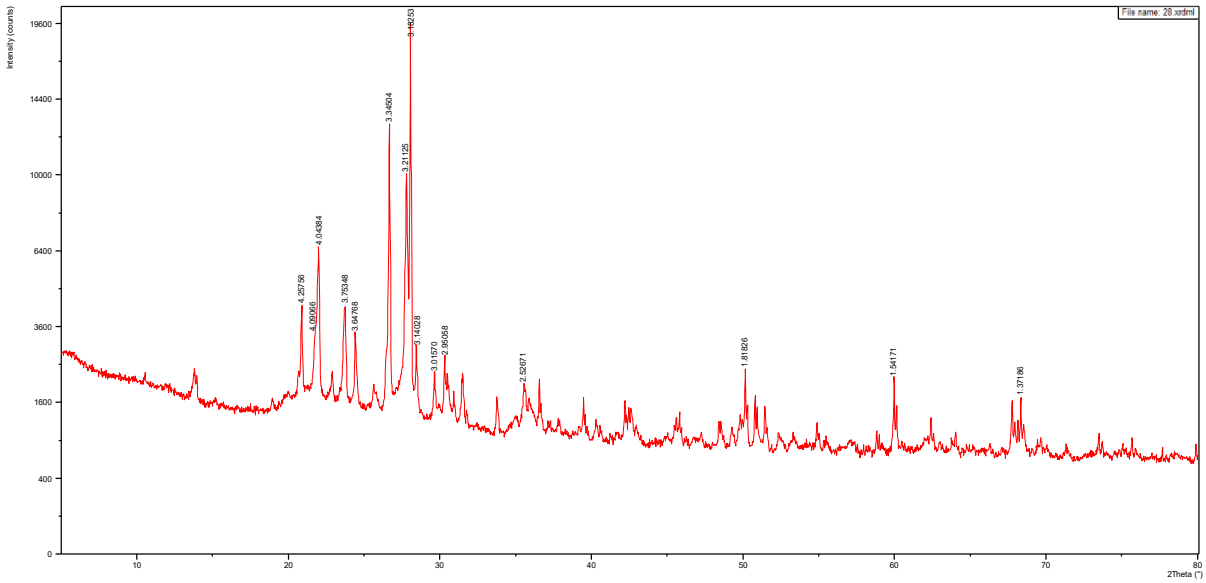

Figure 44.XRD graph showing peaks of minerals within the sample. Sample 28.

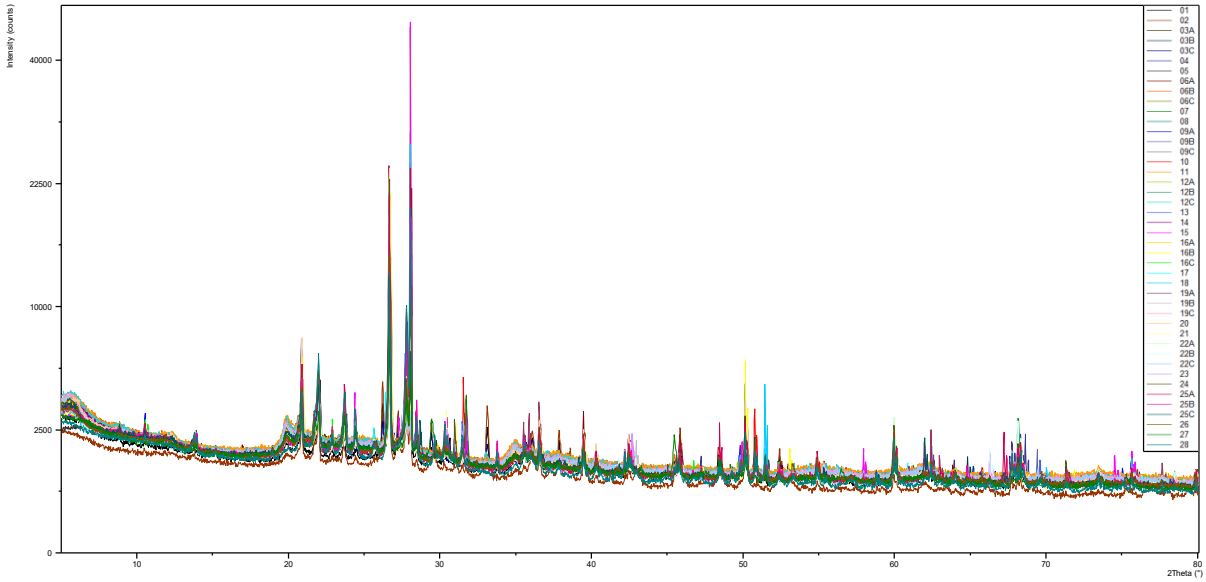

Figure 45. Shows all data from all samples on a single graph.

Appendix F. XRF trace and major elements

Table 6. XRF data for both trace and major elements for all samples.

	Measurement Finished	Evaluation Date	Calibratior Customer	Sc (PPM)	V (PPM)	Cr (PPM)
NG 1	15/06/2024 8:23	15/06/2024 8:23	Geotraces Nicole Greaves	13	84	128
NG 2	15/06/2024 5:30	15/06/2024 5:30	Geotraces Nicole Greaves	20	60	14
NG 3A	15/06/2024 19:57	15/06/2024 19:57	Geotraces Nicole Greaves	8	42	26
NG 3B	15/06/2024 17:03	15/06/2024 17:03	Geotraces Nicole Greaves	11	57	50
NG 3C	14/06/2024 23:43	14/06/2024 23:43	Geotraces Nicole Greaves	19	110	72
NG 4	15/06/2024 2:36	15/06/2024 2:36	Geotraces Nicole Greaves	12	66	59
NG 5	14/06/2024 20:49	14/06/2024 20:49	Geotraces Nicole Greaves	11	70	46
NG 6A	14/06/2024 17:56	14/06/2024 17:56	Geotraces Nicole Greaves	13	89	79
NG 6B	15/06/2024 22:50	15/06/2024 22:50	Geotraces Nicole Greaves	6	38	39
NG 6C	16/06/2024 19:04	16/06/2024 19:04	Geotraces Nicole Greaves	15	110	89
NG 7	16/06/2024 1:44	16/06/2024 1:44	Geotraces Nicole Greaves	15	82	125
NG 8	16/06/2024 16:11	16/06/2024 16:11	Geotraces Nicole Greaves	11	61	32
NG 9A	16/06/2024 4:37	16/06/2024 4:37	Geotraces Nicole Greaves	15	106	93
NG 9B	16/06/2024 13:17	16/06/2024 13:17	Geotraces Nicole Greaves	12	69	58
NG 9C	16/06/2024 7:30	16/06/2024 7:30	Geotraces Nicole Greaves	16	113	62
NG 10	16/06/2024 10:24	16/06/2024 10:24	Geotraces Nicole Greaves	13	79	43
NG 11	17/06/2024 10:43	17/06/2024 10:43	Geotraces Nicole Greaves	16	115	50
NG 12A	17/06/2024 0:51	17/06/2024 0:51	Geotraces Nicole Greaves	11	78	53
NG 12B	17/06/2024 7:49	17/06/2024 7:49	Geotraces Nicole Greaves	11	63	46
NG 12C	15/06/2024 11:17	15/06/2024 11:17	Geotraces Nicole Greaves	15	108	45
NG 13	16/06/2024 21:57	16/06/2024 21:58	Geotraces Nicole Greaves	12	64	52
NG 14	15/06/2024 14:10	15/06/2024 14:10	Geotraces Nicole Greaves	15	103	60
NG 15	22/06/2024 11:49	22/06/2024 11:49	Geotraces Nicole Greaves	11	57	36
NG 16A	17/07/2024 14:31	17/07/2024 14:31	Geotraces Nicole Greaves	15	102	85
NG 16B	23/06/2024 5:09	23/06/2024 5:09	Geotraces Nicole Greaves	11	59	41
NG 16C	22/06/2024 8:55	22/06/2024 8:55	Geotraces Nicole Greaves	14	90	108
NG 17	22/06/2024 6:02	22/06/2024 6:02	Geotraces Nicole Greaves	13	62	36
NG 18	23/06/2024 2:16	23/06/2024 2:16	Geotraces Nicole Greaves	12	78	57
NG 19A	22/06/2024 14:42	22/06/2024 14:42	Geotraces Nicole Greaves	13	103	110
NG 19B	22/06/2024 23:22	22/06/2024 23:22	Geotraces Nicole Greaves	17	125	92
NG 19C	22/06/2024 3:08	22/06/2024 3:08	Geotraces Nicole Greaves	15	110	59
NG 20	22/06/2024 17:35	22/06/2024 17:36	Geotraces Nicole Greaves	16	120	121
NG 21	22/06/2024 20:29	22/06/2024 20:29	Geotraces Nicole Greaves	16	125	126
NG 22A	23/06/2024 16:43	23/06/2024 16:43	Geotraces Nicole Greaves	13	83	65
NG 22B	22/06/2024 0:15	22/06/2024 0:15	Geotraces Nicole Greaves	12	65	53
NG 22C	24/06/2024 14:08	24/06/2024 14:08	Geotraces Nicole Greaves	15	100	55
NG 23	23/06/2024 19:36	23/06/2024 19:36	Geotraces Nicole Greaves	13	73	59
NG 24	23/06/2024 13:49	23/06/2024 13:49	Geotraces Nicole Greaves	13	80	104
NG 25A	24/06/2024 11:15	24/06/2024 11:15	Geotraces Nicole Greaves	12	71	50
NG 25B	23/06/2024 22:30	23/06/2024 22:30	Geotraces Nicole Greaves	13	72	60
NG 25C	23/06/2024 10:56	23/06/2024 10:56	Geotraces Nicole Greaves	13	77	67
NG 26	24/06/2024 8:21	24/06/2024 8:21	Geotraces Nicole Greaves	12	60	45
NG 27	24/06/2024 3:25	24/06/2024 3:25	Geotraces Nicole Greaves	3	6	7
NG 28	23/06/2024 8:03	23/06/2024 8:03	Geotraces Nicole Greaves	9	37	14

Co (PPM)	Ni (PPM)	Cu (PPM)	Zn (PPM)	Ga (PPM)	As (PPM)	Rb (PPM)	Sr (PPM)	Y (PPM)	Zr (PPM)
21	10	9	80	10	10	16	82	0	0
20	9	8	62	10	12	39	579	10	95
26	13	9	90	12	8	20	14	0	0
26	16	6	86	15	11	42	156	10	118
19	13	12	86	13	16	33	183	7	49
23	17	8	105	15	11	43	152	11	114
29	17	10	110	16	15	57	171	16	126
30	15	16	128	13	9	18	20	0	0
14	11	14	114	9	6	0	0	0	0
23	15	18	130	16	13	41	92	10	152
22	16	14	114	16	10	59	115	16	148
25	15	7	105	16	12	64	182	17	128
20	15	13	120	16	11	52	150	14	207
25	14	10	107	17	11	64	152	17	125
24	18	21	137	17	14	47	64	16	161
26	16	11	100	18	11	59	164	17	126
27	18	21	164	19	16	63	88	24	155
28	17	10	120	17	2	56	171	15	150
27	17	10	118	16	17	66	167	17	125
24	16	16	116	18	15	62	103	20	168
27	18	9	115	17	12	61	176	14	109
27	16	16	144	15	12	61	118	17	192
29	16	8	118	17	13	65	173	17	122
33	18	16	148	17	12	61	113	18	202
38	16	11	114	17	13	68	169	16	120
22	16	13	107	16	11	61	140	15	210
34	15	10	124	17	13	69	159	17	129
30	20	11	127	16	12	67	155	16	160
29	20	14	122	16	14	62	145	15	194
31	17	21	143	17	15	66	99	19	300
32	18	24	183	18	17	67	89	22	166
26	19	17	113	16	17	69	108	18	199
25	19	16	142	16	15	61	119	17	222
26	17	17	157	15	11	65	130	15	193
32	17	12	132	16	10	66	154	14	127
24	16	17	147	17	11	64	112	19	154
34	20	10	138	17	13	64	169	15	125
27	22	13	127	15	12	69	118	15	146
30	20	10	130	17	11	57	190	12	108
32	20	9	142	17	11	56	199	14	106
30	20	13	140	16	11	70	146	16	141
41	23	11	153	16	14	71	159	17	130
9	6	6	38	6	4	0	0	0	0
38	9	8	61	17	6	62	225	13	105

Nb (PPM)	Mo (PPM)	Sn (PPM)	Sb (PPM)	Cs (PPM)	Ba (PPM)	La (PPM)	Ce (PPM)	Nd (PPM)	Tl (PPM)	Pb (PPM)	Th (PPM)	U (PPM)
0	3	0	0	1	145	2	17	13	0	0	0	3
2	4	0	0	4	246	2	33	16	0	10	5	3
0	3	0	0	0	265	8	33	13	0	0	0	3
1	4	0	0	2	373	9	35	14	1	14	4	3
0	4	0	0	6	206	5	31	15	0	7	3	3
2	4	0	0	4	387	11	32	19	1	25	5	3
5	4	0	0	0	461	9	47	20	1	32	7	3
0	3	0	0	0	183	2	30	16	0	0	0	3
0	2	0	0	0	38	0	9	7	0	0	0	3
1	4	0	0	2	190	8	38	17	1	12	3	3
5	4	1	0	0	329	12	42	19	1	27	7	3
5	4	3	1	4	480	14	45	24	1	33	8	3
6	4	1	1	2	329	9	39	13	1	28	7	3
5	4	3	1	4	441	11	36	19	1	33	8	3
3	4	0	0	3	206	8	45	19	1	20	6	3
5	4	1	2	2	422	12	49	20	1	32	9	3
7	4	3	1	0	236	15	56	25	1	42	11	3
6	4	1	3	0	425	7	42	14	5	212	10	3
5	4	6	2	2	563	14	51	21	1	36	7	3
6	4	0	0	1	252	13	58	23	1	26	10	3
5	4	3	3	1	463	7	42	15	1	35	7	3
6	4	2	2	0	301	10	41	18	1	34	8	3
5	4	3	2	1	527	9	46	20	1	36	8	3
7	4	2	2	2	303	9	44	17	1	34	8	3
5	4	5	3	1	538	8	41	17	1	36	8	3
6	4	2	2	5	365	7	31	17	1	26	7	3
6	4	4	3	4	512	13	40	19	1	38	9	3
7	4	3	4	3	505	7	41	19	1	32	8	3
7	4	2	2	4	445	1	30	16	1	26	7	3
9	5	2	3	5	308	10	39	15	1	35	9	3
7	4	3	1	0	287	11	53	24	1	53	11	3
6	4	3	18	4	385	0	31	14	5	227	11	3
8	4	2	1	6	350	8	37	17	1	29	7	3
6	4	2	3	0	398	5	43	19	1	51	7	3
5	4	4	4	3	505	5	30	13	1	36	8	3
6	4	3	2	2	288	11	51	19	1	38	9	3
6	4	2	3	1	578	4	38	18	1	34	8	3
6	4	3	5	1	498	2	31	13	1	26	6	3
4	4	3	3	0	569	4	31	12	1	29	6	3
4	4	4	3	0	627	7	37	16	1	35	7	3
6	4	2	3	0	608	9	45	18	1	32	9	3
5	4	3	2	0	735	10	54	19	1	41	9	3
0	3	0	0	0	12	0	4	7	0	0	0	3
4	4	4	2	2	696	6	40	19	1	12	8	3

SiO2 (%)	Al2O3 (%)	TiO2 (%)	MnO (PPM)	Fe2O3 (%)	Na2O (%)	MgO (%)	K2O (%)	CaO (%)	P2O5 (%)
50.13	11.08	0.533	1067	5.50795	2.443	2.134	1.133	11.543	0.099
39.01	8.57	0.364	2100	3.10493	2.174	0.973	1.149	21.984	0.09
65.42	13.58	0.278	3538	3.82188	3.327	0.888	2.229	1.367	0.096
64.14	14.95	0.379	2948	4.32571	3.498	1.153	1.542	3.625	0.088
53.94	13.27	0.594	1046	5.57051	2.159	1.586	1.333	8.154	0.106
64.54	15.94	0.418	2784	4.51757	3.567	1.159	1.522	2.487	0.086
64.53	14.74	0.428	5097	4.4566	3.167	1.097	1.573	2.129	0.101
58.43	14.7	0.566	1973	5.15201	2.453	1.649	1.39	1.335	0.165
52.26	14.35	0.185	1026	5.35187	2.942	1.79	1.4	0.65	0.185
53.42	14.09	0.661	1411	5.38597	2.203	1.677	1.36	3.294	0.175
64.91	14.5	0.562	1484	4.27907	2.414	1.266	1.634	1.511	0.117
65.28	14.77	0.392	3287	4.11801	2.983	0.919	1.8	3.051	0.092
64.46	14.68	0.862	1293	5.39695	2.601	1.789	1.454	2.039	0.099
66.48	15.4	0.452	2393	4.12437	2.756	1.087	1.747	1.974	0.085
53.41	15.41	0.653	1378	5.594	1.779	1.634	1.291	0.666	0.177
65.27	15.91	0.476	2272	4.48893	2.848	1.097	1.617	2.093	0.087
54.54	15.48	0.688	2837	6.13228	1.282	1.742	1.35	0.684	0.237
65.82	15.15	0.607	2058	4.84905	2.814	1.357	1.506	2.274	0.097
67.55	14.61	0.4	4332	4.56828	2.785	0.9	1.755	2.007	0.117
55.91	15.41	0.673	2633	5.54392	1.154	1.538	1.395	1.366	0.167
67.67	15.37	0.411	2397	3.79489	2.796	0.901	1.594	2.24	0.09
63.43	13.98	0.773	1023	5.44221	1.714	1.808	1.432	1.425	0.138
65.85	15.15	0.386	2611	3.90896	3.031	0.963	1.732	2.228	0.091
62.88	14.03	0.833	1947	5.56654	1.643	1.718	1.455	1.361	0.139
68.04	14.73	0.387	2377	4.05659	2.835	0.905	1.761	2.15	0.098
66.59	14.32	0.73	1187	4.5635	2.15	1.443	1.557	1.867	0.107
66.82	15.31	0.406	2365	4.01767	2.824	0.849	1.815	1.988	0.093
67.47	14.61	0.678	2786	4.3403	2.633	1.105	1.694	2.051	0.085
67.62	14.13	0.769	2217	5.02937	2.204	1.459	1.507	2.066	0.096
61.26	14.66	0.93	1727	5.80296	1.276	1.567	1.483	1.085	0.147
58.4	14.71	0.69	2644	5.59699	0.987	1.575	1.396	0.856	0.198
66.4	14.43	0.801	2064	5.28817	1.502	1.442	1.506	1.45	0.13
64.55	13.87	1.009	1787	5.82361	1.699	1.715	1.453	1.642	0.12
67.62	13.93	0.68	1781	4.3234	2.133	1.171	1.684	1.631	0.103
69.14	14.43	0.488	1995	3.75569	2.487	1.046	1.661	2.077	0.078
59.93	14.57	0.677	2370	5.32246	1.368	1.59	1.413	1.131	0.16
66.86	15.31	0.537	2312	4.39265	2.789	1.158	1.626	2.318	0.088
68.35	14.39	0.543	1888	4.00568	1.942	1.144	1.72	1.663	0.086
67.83	15.31	0.485	2819	3.88062	2.855	1.167	1.457	2.595	0.077
66.03	15.67	0.466	3465	4.16716	2.992	1.223	1.407	2.646	0.081
66.48	15.09	0.541	2951	4.30589	2.489	1.032	1.762	1.917	0.092
66.53	15.27	0.357	4379	4.15751	2.899	0.781	1.853	2.068	0.088
54.41	13.04	0.033	142	3.71214	4.731	1.648	1.769	4.058	0.186
68.47	16.1	0.269	1393	2.84842	3.865	0.606	1.644	2.851	0.069

S (PPM)	F (PPM)	Cl (PPM)	CO2 (%)	Sum (%)	Compton (
6251	171	230563	15.92	124.4	89.015
4323	202	33157	22.95	104.47	101.478
3148	111	220030	9.06	122.81	85.323
3415	168	68988	6.68	108.04	96.696
5767	234	114119	13.71	112.64	93.984
3778	204	56650	6.19	106.87	97.468
3845	14	24689	6.52	102.24	100.735
9961	37	203238	14.56	121.99	86.43
7197	66	392411	20.5	139.72	78.098
7794	274	86481	18.23	110.19	96.918
9303	349	11039	9.34	102.88	101.888
4464	33	2579	6.99	101.56	102.316
12310	321	4353	7.29	102.63	102.48
3962	214	1877	6.34	101.42	102.387
14298	252	41824	19.68	106.17	102.145
1522	233	2627	6.59	101.27	102.85
4752	212	4663	18.01	101.51	103.146
5878	240	2096	6.11	101.76	103.153
565	82	596	5.71	101.1	102.734
20534	142	2549	16.93	102.78	102.988
725	205	1137	5.54	100.99	102.119
11993	348	1834	9.97	101.75	102.045
2271	178	703	7.05	101.1	102.9
13366	294	766	10.79	102.18	101.512
521	190	378	5.42	100.87	102.844
10860	400	361	7.19	101.93	101.305
275	193	482	6.28	100.87	103.064
391	106	412	5.78	100.96	102.41
833	195	201	5.58	100.95	103.035
5780	372	710	12.14	101.36	102.964
5642	251	757	15.98	101.45	104.256
877	367	197	7.59	101.04	102.229
15287	237	245	8.42	102.2	101.511
8929	191	345	7.22	101.76	101.506
271	292	405	5.32	100.92	102.826
6564	341	311	14.24	101.48	103.458
307	178	315	5.42	100.95	102.551
632	290	309	6.67	100.96	102.862
264	146	264	4.83	100.97	101.967
1003	180	265	5.41	100.73	102.542
626	175	413	6.62	100.89	102.115
435	30	394	6.33	101.02	102.949
286	229	327131	16.05	132.42	85.331
61	178	405	3.55	100.61	103.297